A NEW BIDIRECTIONAL AC-DC CONVERTER WITH LOW HARMONIC INPUT CURRENTS AND AN ADJUSTABLE POWER FACTOR

By

VEERAPOL MONYAKUL

Bachelor of Science
King Mongkut's Institute of Technology
Bangkok, Thailand
1982

Master of Engineering
Kasetsart University
Bangkok, Thailand
1986

Submitted to the Faculty of the
Graduate College of the
Oklahoma State University
in partial fulfillment of
the requirements for
the Degree of
DOCTOR OF PHILOSOPHY
December, 1993

A NEW BIDIRECTIONAL AC-DC CONVERTER

WITH LOW HARMONIC INPUT CURRENTS

AND AN ADJUSTABLE POWER FACTOR

Thesis Approved:

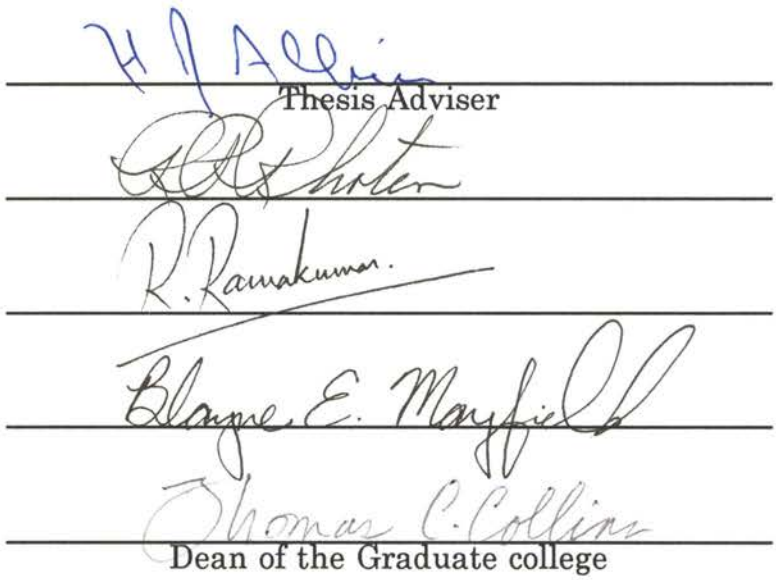

Thesis Adviser

Dean of the Graduate college

PREFACE

The purpose of this dissertation is to propose a new bidirectional ac-dc converter configuration. Outstanding characteristics of the converter include extremely low harmonic input currents, bidirectional power flow, and an adjustable power factor. The converter is basically developed from modifying a non-inverting buck-boost. Duality theory is applied to obtain the new bidirectional ac-dc converter. The power circuit configuration is simple, since two switches are required for a single phase. The converter under development is verified and examined by the PSPICE program. The results indicate that bidirectional power flow can be easily controlled. A state space averaging method is used for mathematical modeling. The mathematical model is numerically simulated using the MATLAB program.

I wish to express sincere appreciation to Dr. Allison for his encouragement and advice throughout my graduate program. Many thanks also go to Dr. Ramakumar, Dr. Rhoten, and Dr. Mayfield for serving on my graduate committee. Their suggestions and support were very helpful throughout the study.

I am grateful to National Science and Technology Development Agency (NSTDA) of The Royal Thai Government, Thailand, for the scholarship.

TABLE OF CONTENTS

LIST OF TABLES

LIST OF FIGURES

Figure Page

Figure Page

NOMENCLATURE

$\boldsymbol{Ai}$	state coefficient matrix, $\boldsymbol{i} = 1,2$
$\boldsymbol{Bi}$	source coefficient matrix, $\boldsymbol{i} = 1,2$
D	duty cycle
D'	$1 - D$
$iLs(t)$	instantaneous current in the inductor Ls
$iL1(t)$	instantaneous current in the inductor $L1$
$is(t)$	instantaneous input current
Is	maximum value of the input current
$p(t)$	instantaneous power
P	average power
$vc(t)$	instantaneous voltage across the capacitor C1
VC	dc voltage across the capacitor C1
$vo(t)$	instantaneous output voltage
VO	dc output voltage
$vL1(t)$	instantaneous voltage across the inductor $L1$
$VL1$	maximum value of the voltage across the inductor $L1$
$vL1(t)$	instantaneous voltage across the inductor Ls
VLs	maximum value of the voltage across the inductor Ls
$vs(t)$	instantaneous input voltage

Vs	maximum value of the input voltage
$vx(t)$	instantaneous voltage across the capacitor $C1$
Vx	maximum value of the ripple voltage across the capacitor $C1$
$vy(t)$	instantaneous voltage across the capacitor $C2$
Vy	maximum value of the ripple voltage across the capacitor $C2$
$\boldsymbol{x}(t)$	state variable vector
θ, α	phase angle
ω	radian frequency

CHAPTER I

INTRODUCTION

Generation of Harmonic Distortion

The increasing use of power electronic equipment over a wide range of application has resulted in increasing power line harmonic currents and harmonic voltages. Harmonics have been reaching levels that interfere with other power system components. Most harmonics result from static converters such as dc switching power supplies, adjustable speed drives, and uninterruptible power supplies (Domijan, 1992).

In most power electronic applications, the input is in the form of a sinusoidal voltage from the power line. It is first converted to a dc voltage by using a rectifier. The dc output voltage of the rectifier should be as ripple-free as possible. A large capacitor is usually connected as a filter on the dc side to reduce ripple. This capacitor is charged to a value close to the peak of the ac input voltage. As a consequence, the current through the rectifier does not flow continuously. It is zero for some time during each half-cycle of the input sinusoidal wave, as shown in Figure 1.

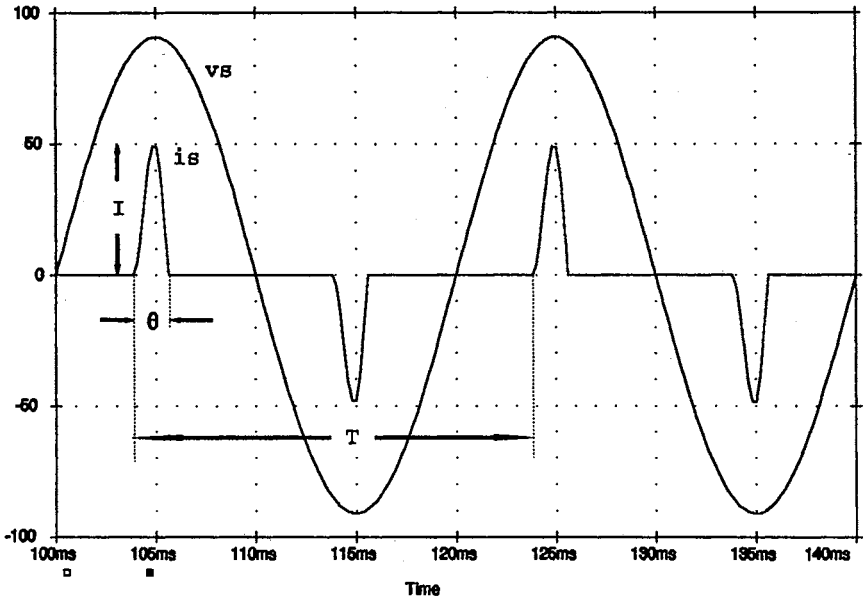

Figure 1 An input current and a supply voltage waveforms from a conventional rectifier with a filter capacitor

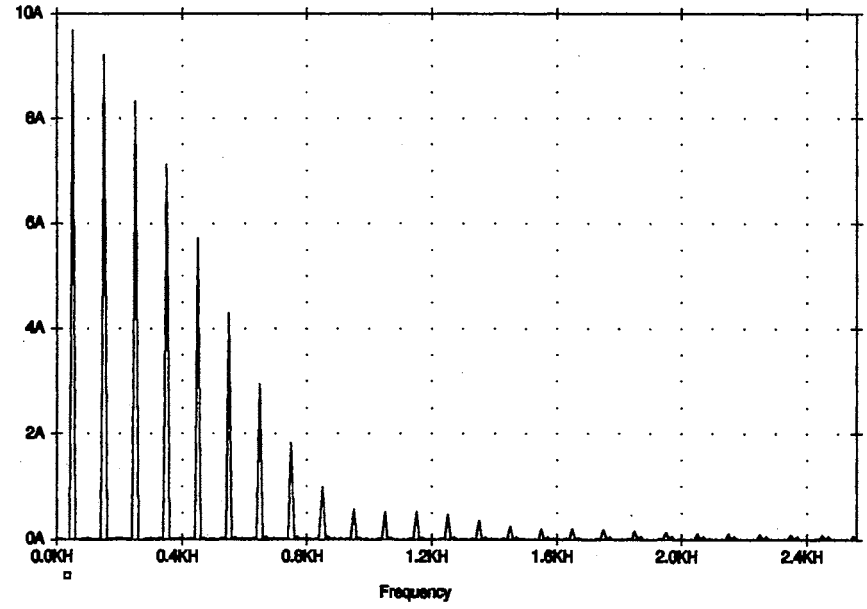

Figure 2 A frequency spectrum of the input current

The distortion in the line current waveform in a full-wave rectifier can be expressed in terms of its fundamental frequency component plus other harmonic currents as follows.

$$I_n = \frac{8\alpha I}{\pi} \sum_{n=1,3,5,..}^{\infty} \frac{\cos n\alpha\pi}{1-n^2\alpha^2\pi^2} \cos n\omega t \qquad (1\text{-}1)$$

where $\alpha = \theta/T$,

θ = the conduction angle,

T = the period of the line frequency,

I = the crest value of the current impulse, and

n = harmonic frequencies.

There are no even harmonics presenting in the equation because the negative half-waves are similar to the positive half-waves. A frequency spectrum of an input current of a conventional rectifier with a filter capacitor is plotted in Figure 2. It obviously shows a large number of odd-integer harmonics.

The nonlinear character of the input current drawn by standard rectifier circuits creates a number of problems for the power distribution network and other electrical systems in the vicinity of the rectifier. Various standards have been established that specify limits on the magnitudes of harmonic currents and harmonic voltage distortion.

Harmonic Effects on Power System Components

The main effects of harmonic currents and harmonic voltage distortion within the power system are (Arrillaga et al., 1985):

I. Amplification of harmonics resulting from series and parallel resonances,

II. Reduction of efficiency in power generation, transmission, and utilization,

III. Aging of power system components,

IV. Plant malfunction.

The use of shunt capacitors to improve power factor and voltage has a significant influence on harmonic levels. Capacitors do not generate harmonics, but provide network loops for possible resonant conditions. Resonance can cause overvoltages and excessive currents in the system. Furthermore, the effect of the harmonic components causes additional heating and higher dielectric stress on the capacitors (IEEE Working Group on Power System Harmonics, 1983).

Harmonic currents in induction and synchronous machines increase losses in the stator windings, rotor circuits, and stator and rotor laminations. The losses in the stator and rotor are increased because of eddy currents and skin effect. In induction motors, harmonic current can produce significant torque pulsations. Pulsating torques are produced by the interaction of air gap flux and rotor mmf waves with different

harmonics. The general torque equation, expressed as a function of air gap flux, rotor current, and the phase angle between the air gap flux and the rotor current, is

$$T_e = K\psi_m I_r \sin\delta \qquad (1\text{-}2)$$

where K is the torque constant,

ψ_m is the air gap flux linkage,

I_r is the rotor current, and

δ is the phase angle between the air gap flux and the rotor current.

Torque pulsations are produced when the angle between the air gap flux and the rotor current varies with time. The pulsating torque frequency may be near the mechanical resonance of the drive system, resulting in severe shaft vibration, causing fatigue, wearing of gear teeth, and unsatisfactory performance in the feedback control system (Bose, 1986).

The flow of harmonic currents in a transmission system produces two main effects. One is the additional transmission loss caused by the increased RMS value of the current waveform. The second is the creation of harmonic voltage drops across the various circuit impedances (Kimbark, 1971).

In addition, in a transformer, the presence of harmonic voltages increases the hysteresis and eddy current losses. Another important consideration for a transformer is a dc component resulting from supplying an asymmetrical load such as a conventional half-wave rectifier. The

transformer could be saturated by such a dc component. Moreover, possible resonance may occur between transformer's inductance and line's capacitance (Domijan and Embriz-Santander, 1992).

Harmonics can distort the operating characteristics of protective relays. Protective functions are usually intended to operate in terms of fundamental voltages and currents. Electromechanical relays are inherently less sensitive to higher harmonics. In practice, measuring instruments used on a distorted electricity supply can be susceptible to error (Arrillaga et al., 1985).

Effect of Harmonic Distortion on Power Factor

In general, the instantaneous values of the voltage and current components can be expressed as (Shepherd and Zakikhani, 1973)

$$v = \sum_{1}^{n} \sqrt{2} V_n \sin(n\omega t + \alpha_n) + \sum_{1}^{m} \sqrt{2} V_m \sin(m\omega t + \alpha_m) \qquad (1\text{-}3)$$

$$i = \sum_{1}^{n} \sqrt{2} I_n \sin(n\omega t + \alpha_n - \phi_n) + \sum_{1}^{p} \sqrt{2} I_p \sin(p\omega t + \alpha_p - \phi_p) \qquad (1\text{-}4)$$

where V_n, V_m= RMS values of n and m groups of supply voltage harmonics,

I_n, I_p = RMS values of n and p groups of load current harmonics,

n = group of harmonics common to supply voltage and load current,

m = group of harmonics of supply voltage having no corresponding load current harmonics,

p = group of harmonics of load current having no corresponding supply voltage harmonics,

α_n ,α_m, α_p = arbitrary angles of the n, m and p groups of supply voltage harmonics,

ϕ_n, ϕ_p = load phase-angles to the n and p groups of load current harmonics,

and the power factor is given by

$$p.f. = \frac{\frac{1}{T}\int_0^T vi\,dt}{V_{rms}I_{rms}} = \frac{\sum_1^n V_n I_n \cos\phi_n}{[(\sum_1^n V_n^2+\sum_1^m V_m^2)(\sum_1^n I_n^2+\sum_1^p I_p^2)]^{1/2}} \qquad (1\text{-}5)$$

If the voltage waveform is sinusoidal, then equation (1-5) reduces to

$$p.f. = \frac{V_1 I_1 \cos\phi_1}{V_1 I_{rms}} = \frac{I_1}{I_{rms}} \cos\phi_1 = \mu \cos\phi_1, \qquad (1\text{-}6)$$

where $\cos\phi_1$ is the displacement factor between the fundamental components of voltage and current and μ is a current distortion factor.

The harmonic currents should be low to yield a high current distortion factor. Unity power factor can only be achieved when $\mu = 1$ since $\cos\phi_1$ cannot be greater than 1. Power factor compensation is not straightforward with distorted waveforms.

Harmonic Standards and Recommended Practices

In view of the rapid increase in power electronic equipment connected to the utility system, various national and international agencies have been considering limits on harmonic current injection to maintain good power quality. As a consequence, various standards and guidelines have been established that specify limits on the magnitudes of harmonic currents and harmonic voltage distortion at various harmonic frequencies. Two criteria are used to evaluate harmonic distortion. The first is a limitation in the harmonic currents that a user can transmit into the utility system. The second criterion is the quality of the voltage that the utility must furnish the user.

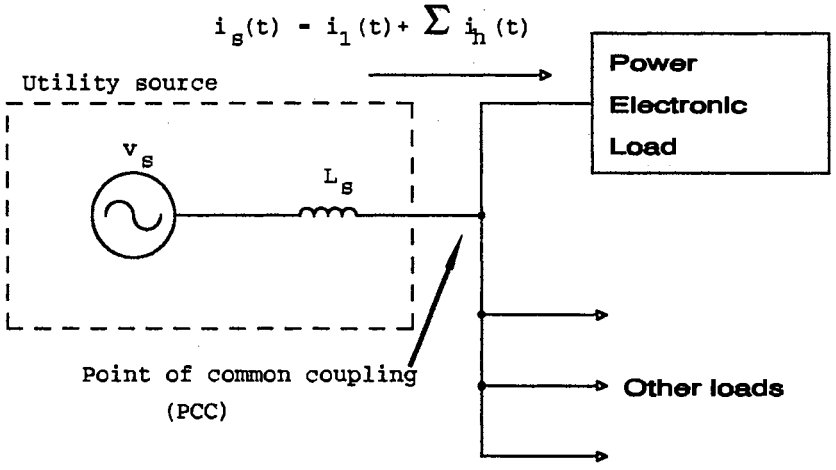

Figure 3 Utility interface

The voltage distortion at the point of common coupling (PCC) in Figure 3 depends on the internal impedance of the ac source and the magnitudes of the injected harmonic currents. In practice, the internal impedance of the source is highly inductive and therefore is represented by L_s. At a harmonic h of the line frequency ω, the RMS harmonic voltage at PCC is

$$V_h = (h\omega L_s)\, I_h \tag{1-7}$$

where I_h is the h harmonic current injected into the ac source, and L_s is the internal inductance of the ac source.

Let I_{sc} is the short-circuit current at the point of common coupling. We obtain

$$I_{sc} = \frac{V_s}{\omega L_s} \tag{1-8}$$

where V_s is the RMS value of the per-phase internal voltage of the ac source, which is assumed to be sinusoidal. A large I_{sc} represents a large capacity of the system at PCC.

The total harmonic distortion (THD) in the input current is defined as

$$THD = \frac{\sqrt{\sum_{h=2}^{\infty} I_h^2}}{I_1} \tag{1-9}$$

where I_1 is the fundamental-frequency current (Mohan, 1989).

By 1981, the IEEE introduced ANSI/IEEE standard 519-1981, IEEE guide for Harmonic Control and Reactive Compensation of Static Converter. The revision was submitted to the IEEE standards Board in 1989 as shown in Table I and Table II respectively (Duffey and Stratford 1989).

TABLE I

HARMONIC CURRENT LIMITS FOR NONLINEAR LOADS AT THE POINT-OF-COMMON COUPLING WITH OTHER LOADS AT VOLTAGES OF 2.4 TO 69 kV

MAXIMUM HARMONIC CURRENT DISTORTION IN % OF FUNDAMENTAL						
	HARMONIC ORDER (ODD HARMONICS)					
I_{sc}/I_L	<11	11≤h<17	17≤h<23	23≤h<35	35≤h	THD
<20*	4.0	2.0	1.5	0.6	0.3	5.0
20-50	7.0	3.5	2.5	1.0	0.5	8.0
50-100	10.0	4.5	4.0	1.5	0.7	12.0
100-1000	12.0	5.5	5.0	2.0	1.0	15.0
>1000	15.0	7.0	6.0	2.5	1.4	20.0

Even harmonics are limited to 25% of the odd harmonic limits above

* All power generation equipment is limited to these values of current distortion, regardless of actual I_{sc}/I_L

Where I_{sc}= Maximum short circuit current at PCC.

And I_L = Maximum load current (fundamental frequency) at PCC

TABLE II

HARMONIC VOLTAGE LIMITS FOR POWER PRODUCERS

(PUBLIC UTILITIES OR CO-GENERATORS)

	HARMONIC VOLTAGE DISTORTION IN % AT PCC		
	2.3-69kV	69-138kV	>138kV
Maximum for Individual Harmonic	3.0	1.5	1.0
Total Harmonic Distortion (THD)	5.0	2.5	1.5

Harmonic standards vary from country to country. The standards set limits on the total harmonic distortion of voltage, with the majority incorporating limits on individual harmonic voltages. The permitted level of harmonic content is generally linked to the system voltage. Limits on harmonic current levels are set by a few of the standards (Arrillaga et al. 1985).

In France, Electricité de France establishes limits due to each consumer acting alone at the point of common coupling. These are 0.6% of fundamental for even harmonic, 1.0% of fundamental for odd harmonics, and 1.6% total harmonic distortion. These limits are chosen to ensure that a level of about 5% total harmonic distortion at the point of common

coupling is not exceeded when all consumers are connected.

In Germany, the standard DIN 57160 (VDE 0160/11.81) sets a rating for harmonic generating equipment of not greater than 1% of the system fault level. Individual harmonic levels are limited to 5% of the fundamental voltage level up to the 15th harmonic: the levels decrease to 1% at the 100th harmonic according to a defining curve. The total harmonic voltage is not to exceed 10%.

In the United Kingdom, Engineering Recommendation G5/3 presents a three-stage approach to the assessment of converter sizes. In addition, total harmonic voltage distortion for 415 volts at a point of common coupling is 5% with 4% for odd individual harmonic voltage distortion and 2% for even individual harmonic voltage distortion.

In Sweden, the total harmonic distortion permitted for 430/250 volts is restricted to 4%, and is reduced to 3% for 3.3 kV to 24 kV.

Scope of the Dissertation

This dissertation proposes a new ac-dc converter configuration with extremely low harmonic currents. In contrast to a conventional ac-dc converter, the new converter allows bidirectional power flow. Furthermore, the power factor can be controlled from 90 degrees leading to 90 degrees lagging in both directions of power flow.

The original idea of the new converter was developed from a non-

inverting buck-boost. Duality theory is applied to create a new ac-dc converter topology. A state space averaging method is used as a tool for modeling the converter. The analysis of the mathematical model is investigated by a MATLAB program, a scientific software for numeric computation. A PSPICE program, an industry-standard program for electronic circuit simulations, is used to examine and verify the behavior of the converter in various aspects.

CHAPTER II

LITERATURE REVIEW

Review of an AC-DC Converter Topology

Ac-dc converters with low harmonic currents are still in the initial stages of development. Some techniques described in the literature are discussed in this chapter.

Passive Filter

A primitive approach to harmonic reduction uses a passive filter on the ac side of the rectifier bridge. Undesired harmonic currents can be prevented from flowing into the power system by a high series impedance or a low impedance shunt path. Series filters must carry full load current. In contrast, shunt filters carry only a fraction of the current that a series filter must carry. The practical approach usually is to use shunt filters. The most common shunt filter is a single tuned filter. A single tuned filter is a series RLC circuit. A single tuned filter presents a low impedance at or near one frequency only. Ideally an infinite number of arms, shunt filter circuits, are required because harmonics range from audible frequencies into

the radio spectrum. A suitable compromise is to use resonant arms for harmonic orders 5, 7, 11, 13 plus a lowpass filter arm for harmonic orders 17 and upwards (Cory, 1965).

Double tuned filters can be designed to resonate for two resonant frequencies, and can act as two single tuned filters in parallel. Triple and quadruple tuned filters can also be designed, but these are rarely justified because of the difficulty of adjustment (Arrillaga et al. 1985).

Passive filters represent a substantial part of the total cost, weight, and size of an ac-dc converter.

Pulse-Width Controlled AC-DC Converter

Thyristor ac-dc converters of the phase control type are widely used because such converters are easy to commutate and are inherently stable. However, such converters operate at a poor power factor and relatively high harmonic currents. A method for improving these deficiencies is pulse-width control.

Pulse-width controlled ac-dc converters operate by turning off the main thyristors of the converter several times in each half cycle of the ac line voltage so that a pulse-shaped dc output may be obtained. The mean output voltage can be continuously controlled by varying the pulse widths. Thus, the power factor of the fundamental wave is kept unity regardless of the output voltage, and also lower harmonics of the line current can be

reduced by selecting the appropriate number and width of the pulses (Thorborg, 1988).

However, pulse-width controlled converters have rather complex commutation circuits that usually contain auxiliary thyristors. The adjustable range of the output voltage is limited when some of these converters operate under light load. A pulse-width controlled converter that overcomes this disadvantage is shown in Figure 4 (Kataoka 1977).

In Figure 4, thyristors *TH1*, *TH2*, *TH3*, and *TH4* form a standard bridge rectifier circuit. Capacitor *C* and inductors *L1* and *L2* form a commutation circuit for *TH1* and *TH2*. Diodes *D1*, *D2*, *DL1*, and *DL2* are the components to prevent the capacitor *C* from losing its charge that is necessary for commutation. The thyristor *TH3* and *TH4* are commutated by the ac line. The inductor *Ls* provides the commutation voltage across the capacitor *C* when the instantaneous line voltage is low. The commutation circuit does not contain auxiliary thyristors and in this sense the converter shown in Figure 3 is simpler than conventional converters. The switching frequency is limited by the time constant of the commutation circuit. Although the low frequency harmonic currents of the line current may decrease, high frequency harmonic currents near the switching frequency increase. Moreover, the circuit requires special commutation capacitors.

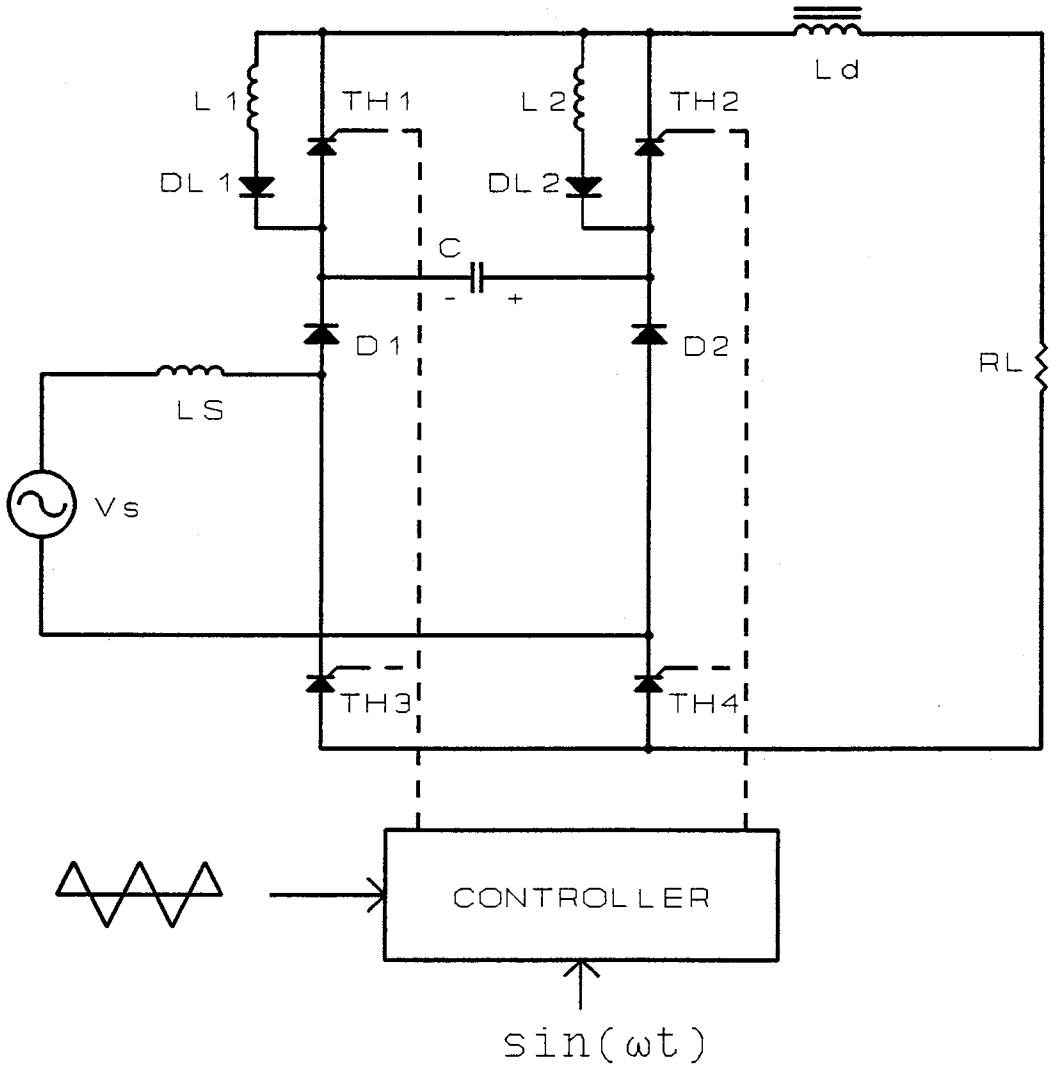

Figure 4 Circuit configuration of the pulse-width controlled ac-dc converter

In 1991, the configuration of Figure 4 was further developed as a three phase pulse width modulated half-controlled rectifier, as shown in Figure 5 (Biswas 1991). The half-controlled rectifier yields almost the same performance as a fully controlled rectifier at a lower cost, but it does not allow regeneration.

Flyback AC-DC Converter

The recent availability of high-power devices with high frequency switching capability has made the possible use of pulse width modulation techniques to improve the quality of supply current waveforms and power factor in ac-dc converters. A flyback ac-dc converter with sinusoidal supply currents is shown in Figure 6 (Itoh, 1991; Mechi, 1993). See more details about a flyback converter in Chapter III. Gate Turn-Off thyristors (GTOs) are employed as switches. The control signal is produced by comparing the triangular carrier wave and the sinusoidal modulating wave. The converter is capable of producing near sinusoidal supply currents at close to unity power factor. However, the inductor *L1* must be large enough to keep the dc current continuous, since sinusoidal supply current cannot be achieved if the dc current is discontinuous. A sufficiently large capacitor is required to obtain a smooth output voltage. The converter does not allow bidirectional power flows or provide a controllable power factor.

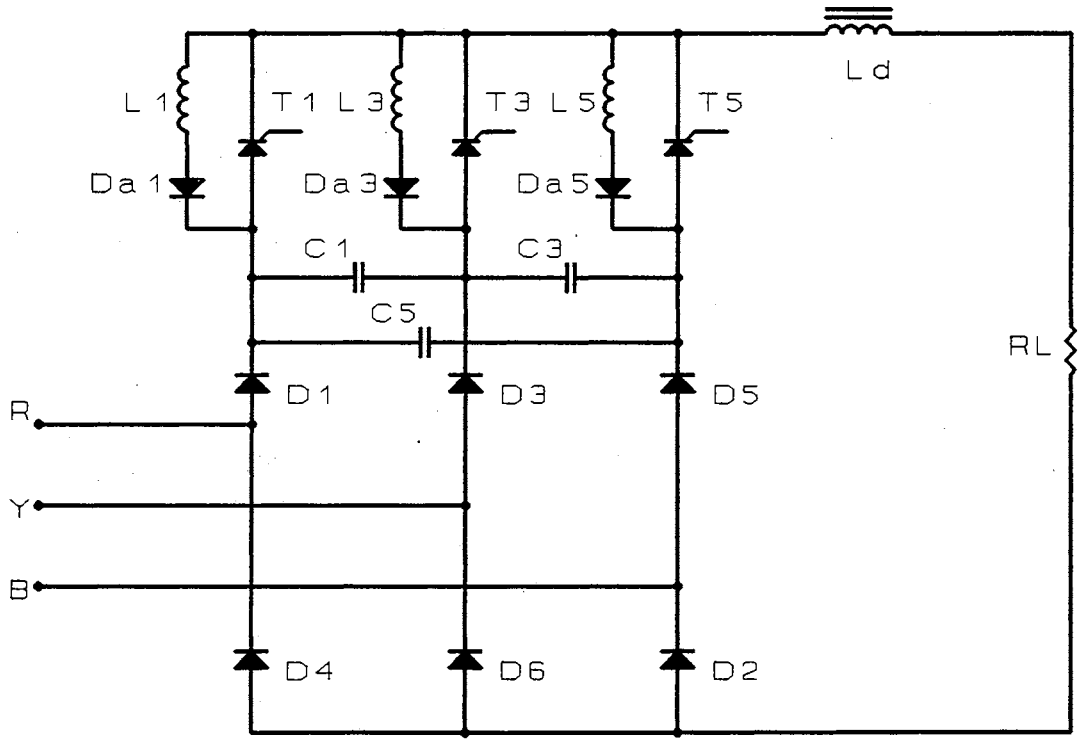

Figure 5 Three phase half-wave controlled ac-dc converter

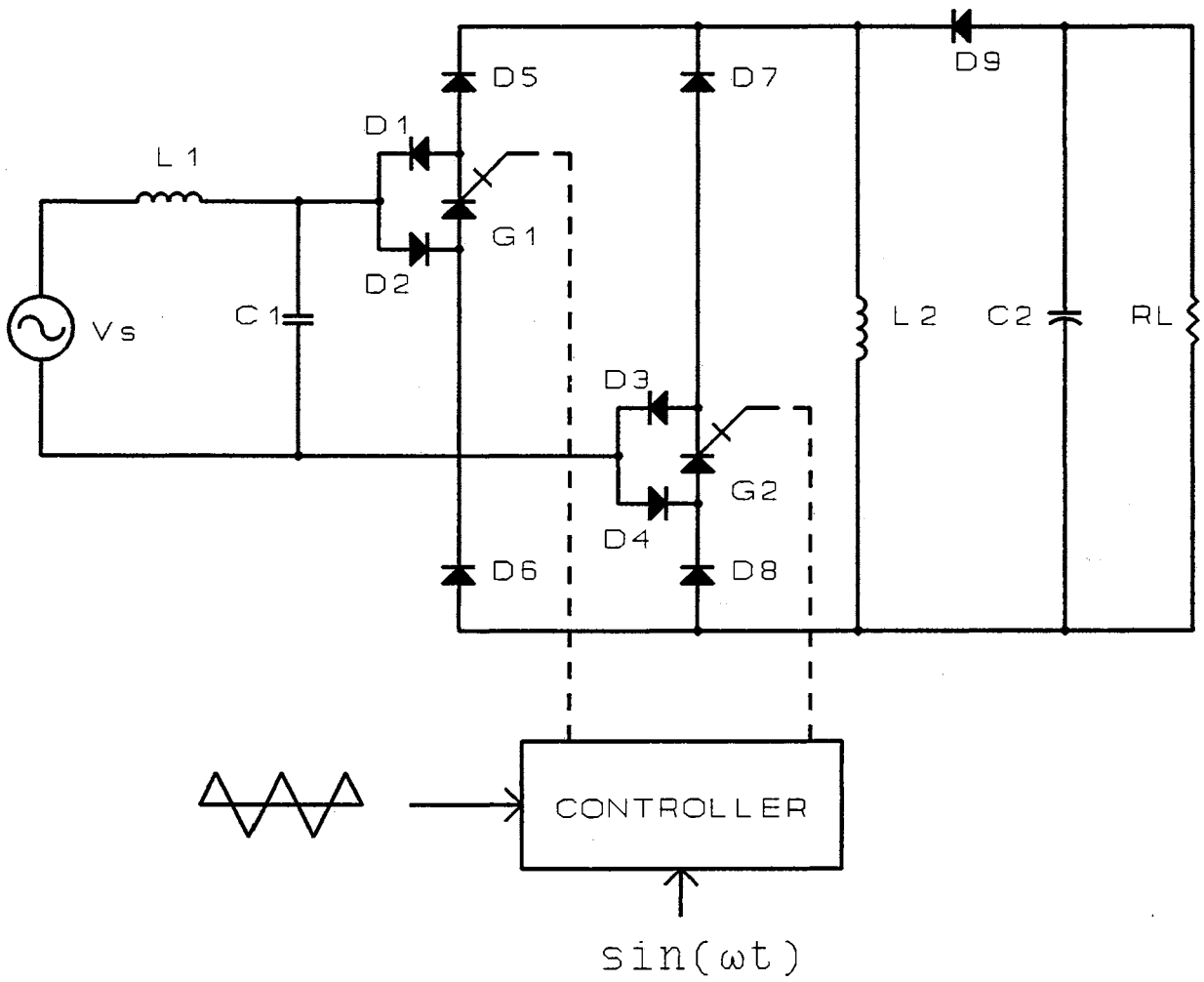

Figure 6 Single phase flyback converter with dc inductor for energy transfer

Boost Configuration AC-DC Converter

A boost type converter without a current sensor is shown in Figure 7 (Chen, 1992; Prasad, 1991). This converter consists of a front end diode rectifier in series with a boost type inductor. (See more details about a boost converter in Chapter III.) The converter uses only one switch to achieve a unity power factor and output voltage control. The converter is operated at a fixed switching frequency. The input inductor current is in a discontinuous mode. It is seen that application of the front end diode rectifier, together with keeping the operation mode of a boost stage in a discontinuous conduction mode, makes the converter draw nearly sinusoidal ac current from the ac source with a unity power factor. The converter has a small output dc ripple voltage and low switching losses. A simple control logic is one of its merits.

However, since the converter is operated in a discontinuous mode, a large input filter is required. In addition, it cannot operate regeneratively.

High-Frequency AC-DC Converter

A high-frequency off-line switch mode rectified converter with improved performance characteristics is shown in Figure 8 (Prasad, 1991). The converter consists of two main power conversion stages. The first stage is an ac-dc rectifier fed from a single phase or a three phase ac source. The second stage is a dc-dc converter with a high frequency transformer. An

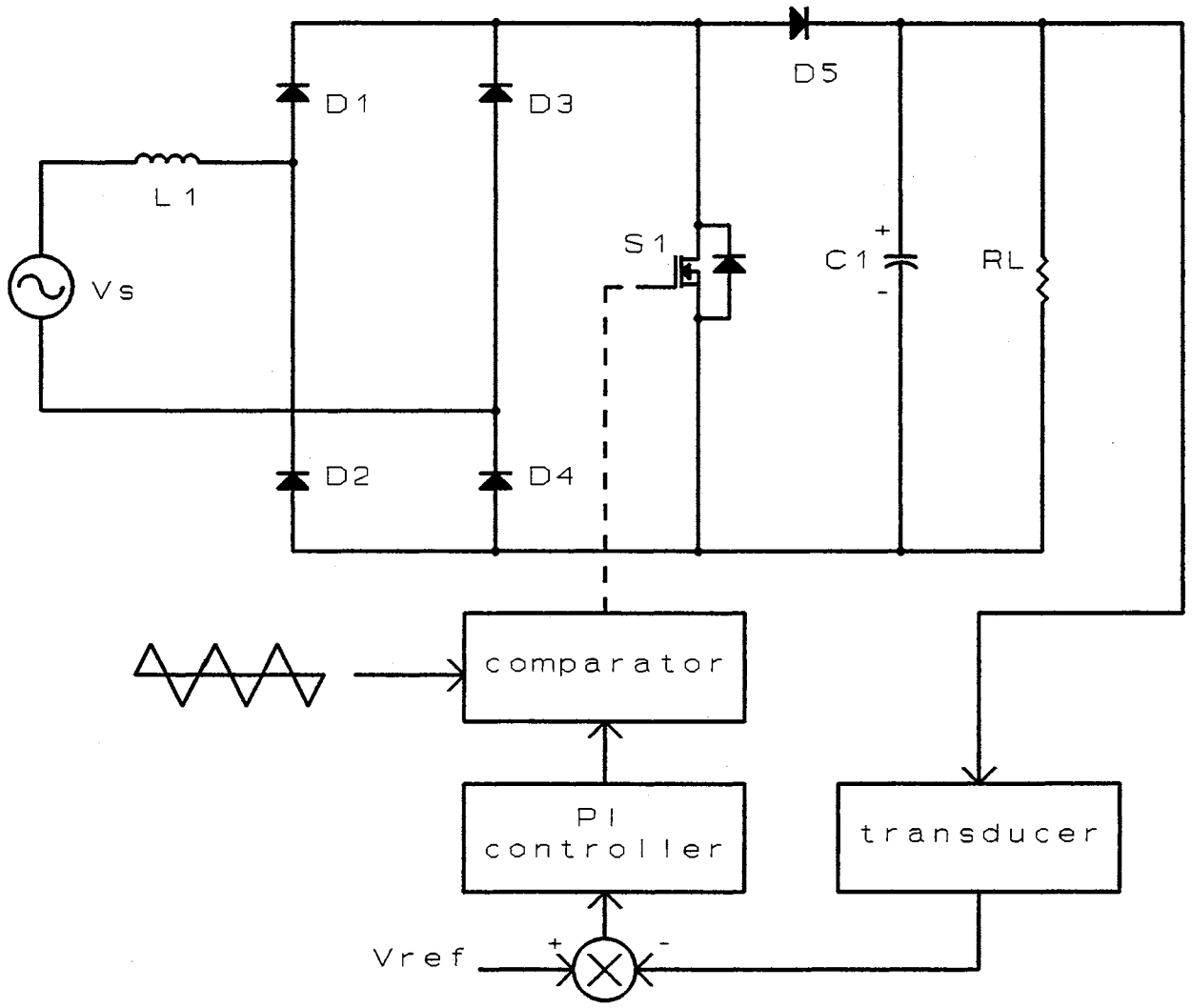

Figure 7 Single phase boost configuration ac-dc converter

increase in the switching frequency is used for size reduction because the volume of the converter depends mainly on the size of the magnetic components and associated filter capacitors. The dc-dc converter generally operates at fixed frequency and controls the output voltage by controlling pulse-width modulation. Consequently, the converter input harmonic currents are pushed to higher frequencies. Those harmonic currents are filtered by the input network. However, the circuit shown in Figure 8 requires a large filter network to improve the input current waveform and the circuit is fairly complex. Moreover, the converter has no regenerative capability.

Controlled-Current AC-DC Converter

A single-phase controlled-current pulse width modulation rectifier is shown in Figure 9 (Stihi, 1988). The power circuit consists of four bipolar transistors with anti-parallel diodes. Normal operation consists of initially building up magnetic energy in the inductance *Lr* by shorting the phase voltage through an ON-transistor and allowing the *Ldi/dt* voltage to force the stored magnetic energy through the freewheeling diode to the dc side. The filter capacitor initially requires a charge above the magnitude of the ac input voltage. Otherwise, the freewheeling diodes across the transistors will act as a conventional rectifier.

Although the converter is reversible, the dc voltage must be greater

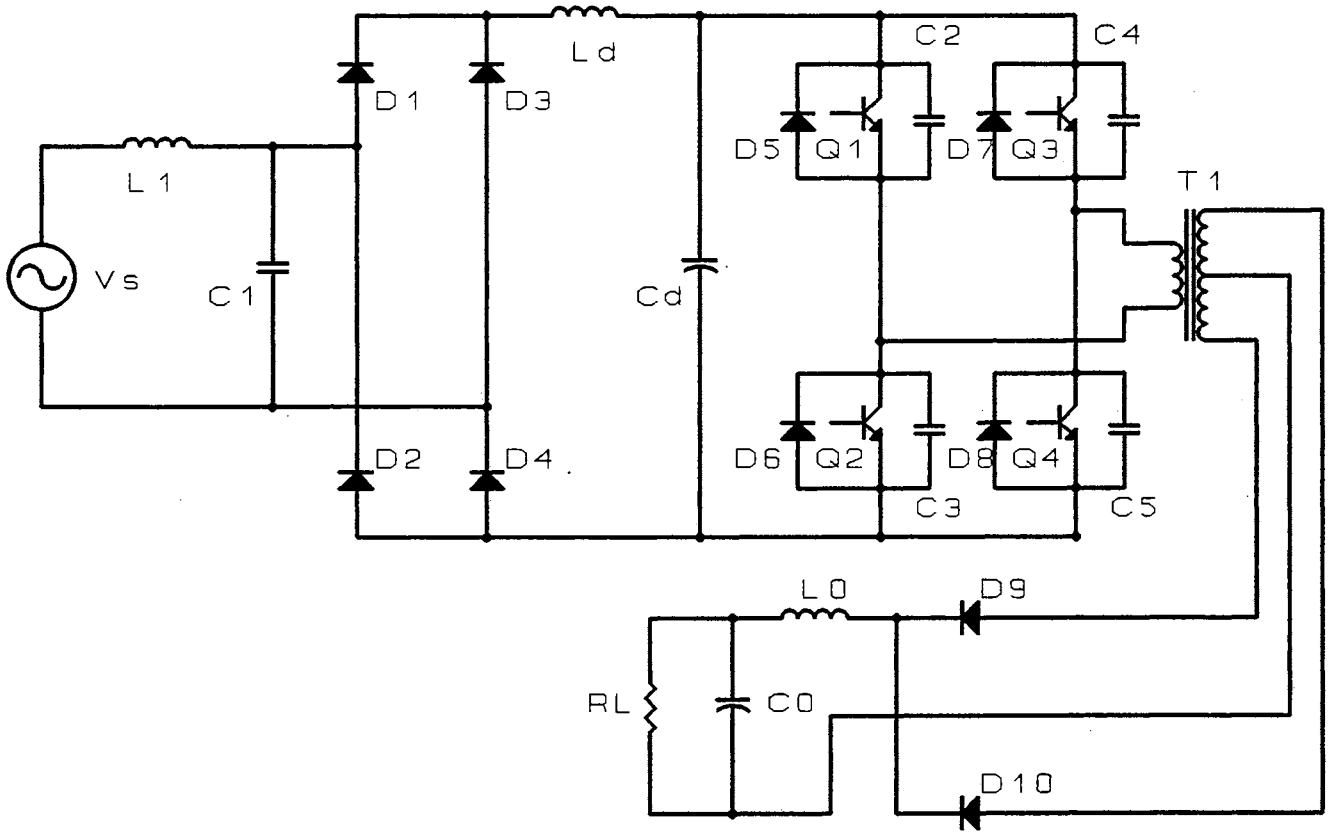

Figure 8 High-frequency off-line switch mode rectified converter

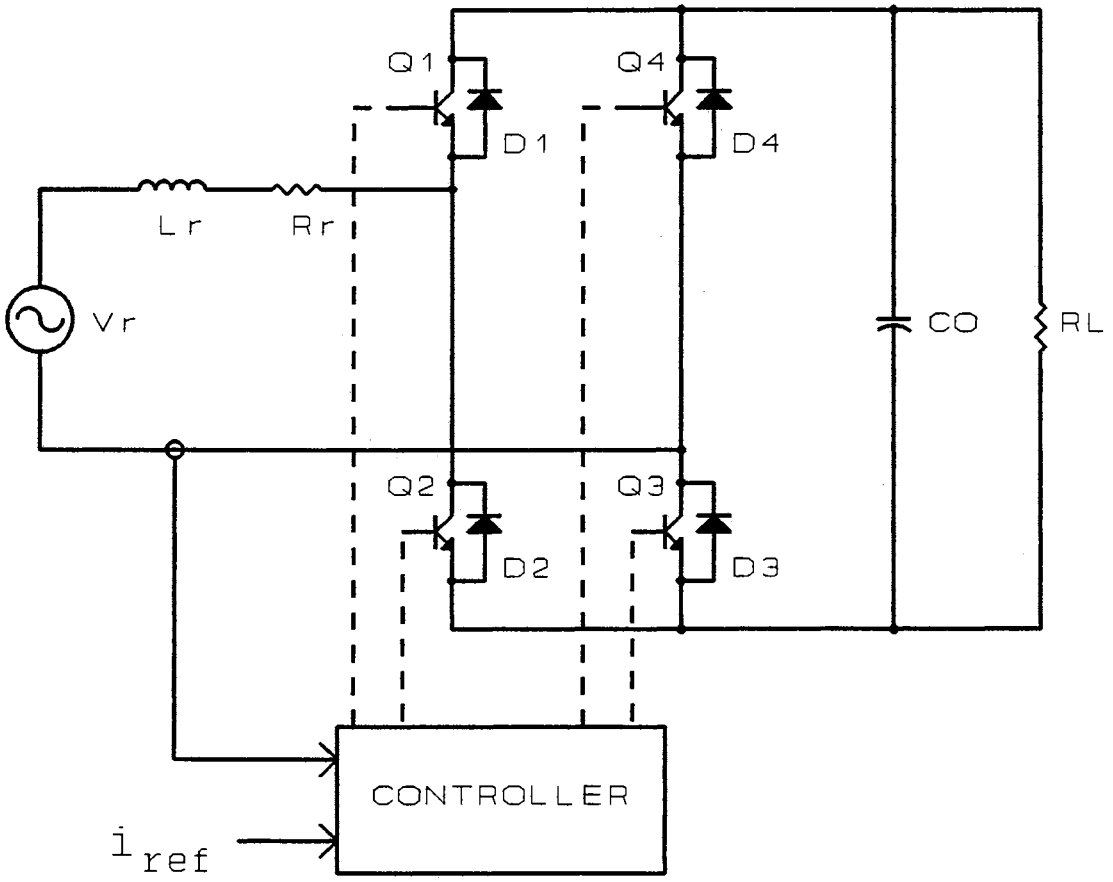

Figure 9 Controlled-current pulse-width modulation rectifier

than twice times of the peak input voltage. Moreover, a very large output capacitor is required and some special initiation is needed before activation.

Summary

At present, there are still some problems associated with the development of ac-dc converters with low harmonic currents, including excessive control switches and complicated control logic. In a boost type converter, the output dc voltage can only be twice the peak input voltage. A large dc capacitor is required. A flyback converter cannot operate in a regenerative mode, and it requires a large input network.

CHAPTER III

A NEW PROPOSED CONFIGURATION

Basic Concepts of a DC-DC Converter

Generally, a converter can be defined as a device converting one form of energy into another on a continuous basis. High efficiency is usually an overriding requirement in most applications for switchmode power converter circuits, so resistive circuit elements must be avoided. In switchmode power converters, the semiconductor switch controlling the dynamic transfer of power from input to output is either fully ON or fully OFF, with very short transition times. Semiconductor components normally employed as switching elements in switchmode power converters include fast recovery diodes, bipolar junction transistors (BJTs), metal oxide semiconductor field effect transistors (MOSFETs), gate turn-off thyristors (GTOs), and insulated gate bipolar transistors (IGBTs).

Three basic configurations for a dc-dc converter are shown in Figure 10. The circuit in Figure 10 (a) is called a buck converter because the output voltage is always less than the input voltage. The circuit of Figure 10 (b) is referred to as a boost converter, since its output voltage is always

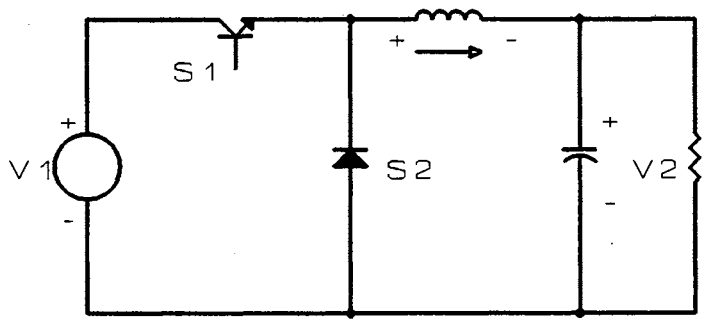

V2 = DV1

(a) Buck converter

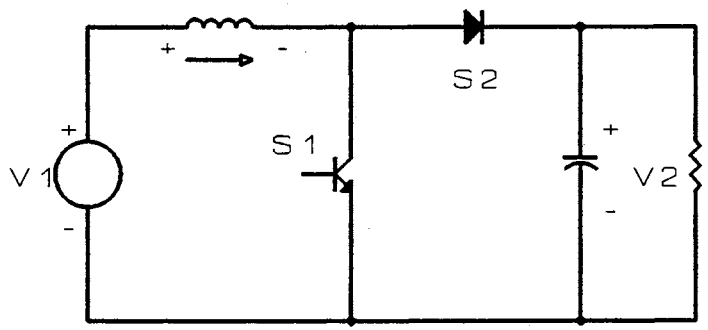

V2 = V1/(1-D)

(b) Boost converter

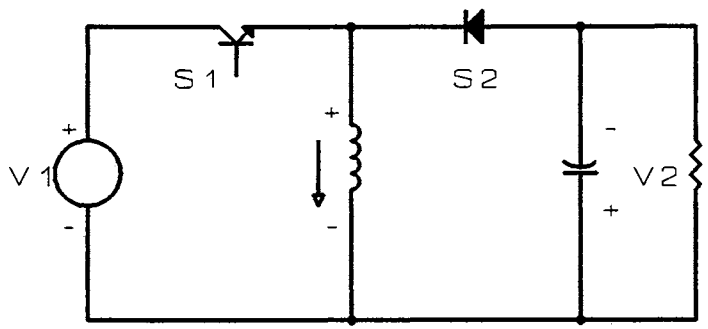

V2 = -DV1/(1-D)

(c) Buck-boost converter

Figure 10 Three basic configurations for dc-dc converters

greater than the input voltage. Finally, the circuit as shown in Figure 10 (c), which has the output voltage greater or less than the input voltage, is called a buck-boost converter. All dc-dc converters can be derived from combinations of buck, boost, and buck-boost converters.

In a dc-dc converter with a given input voltage, the average output voltage is regulated by controlling the switch on and off durations. The duty cycle D is defined as the ratio of ON duration to the switching time period. As shown in Figure 11, we define

$$D = \frac{t1}{TS} \tag{3-1}$$

where $t1$ is an interval of ON state of the S1, TS is a switching period.

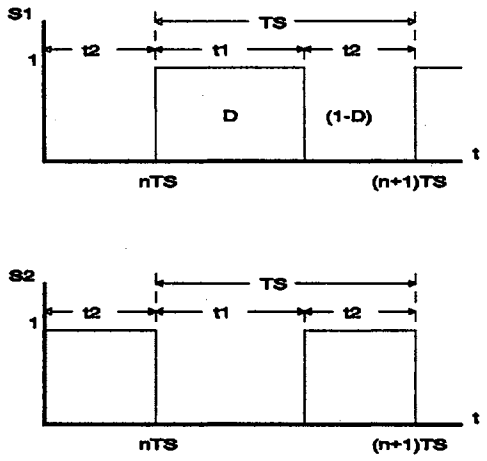

Figure 11 The duty cycle

Since $t1 = TS - t2$, we have

$$(1-D) = \frac{t2}{TS} \tag{3-2}$$

where $t2$ is an interval of ON state of the S2. S2 is normally ON when S1 is OFF, and vice versa.

To determine the output voltage, we use the inductor current constraint that a voltage across an inductor per cycle must be zero for steady-state operation. For two switch conditions, we generally have

$$VL1\ (D) + VL2\ (1-D) = 0 \tag{3-3}$$

where $VL1$ is the inductor voltage during S1 on and S2 off,

$VL2$ is the inductor voltage during S1 off and S2 on.

From Figure 10, for a buck converter we have

$$\begin{aligned} (V1 - V2)D - V2(1-D) &= 0 \\ V2 &= DV1 \end{aligned} \tag{3-4}$$

For a boost converter, we have

$$\begin{aligned} V1D + (V1 - V2)(1-D) &= 0 \\ V2 &= \frac{V1}{1-D} \end{aligned} \tag{3-5}$$

For a buck-boost converter, we have

$$\begin{aligned} V1D + V2(1-D) &= 0 \\ V2 &= \frac{-DV1}{1-D} \end{aligned} \tag{3-6}$$

The conversion ratios also depend on the behavior of the inductor currents. As shown in Figure 12 (a), the inductor current is in the continuous conduction mode. In the discontinuous conduction mode, the inductor current goes to zero during each switching cycle as shown in Figure 12 (b).

The value of L for which $iL = 0$ at one and only one point per cycle is defined as critical inductance Lc, which is calculated from the following equations.

For buck converters,

$$Lc = \frac{R(1-D)}{2fs} \tag{3-7}$$

For boost converters,

$$Lc = \frac{R(1-D)^2D}{2fs} \tag{3-8}$$

For buck-boost converters,

$$Lc = \frac{R(1-D)}{2fs} \tag{3-9}$$

where fs = switching frequency

R = resistance for a resistive load

In the discontinuous conduction mode of a Buck converter, by assuming that the switching period TS and the input voltage $V1$ are constant, we get

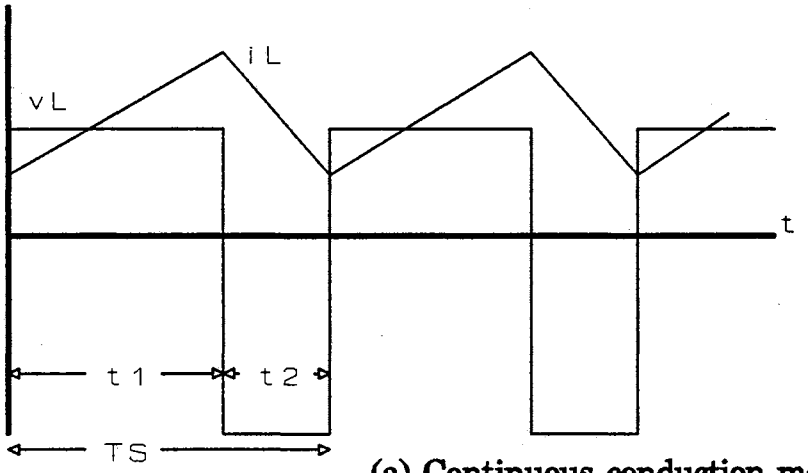

(a) Continuous conduction mode

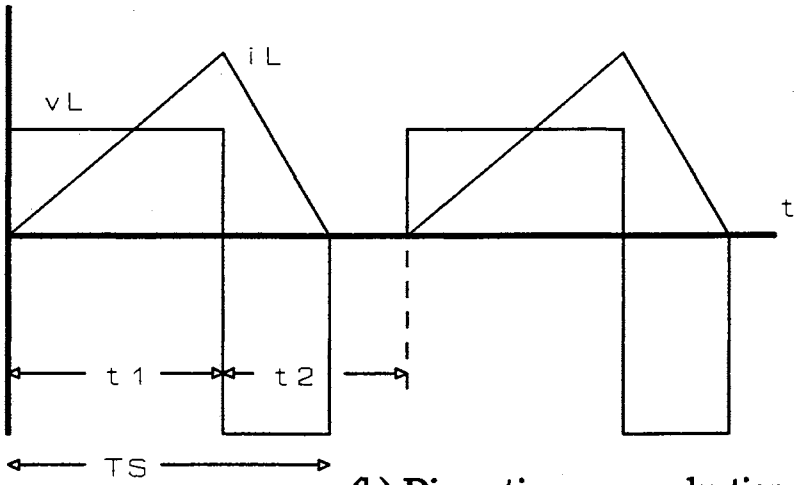

(b) Discontinuous conduction mode

Figure 12 Inductor current modes

$$V2 = \frac{D^2\, V1}{D^2 + \frac{1}{4}\left(\frac{8\, L\, Io}{Ts\, V1}\right)} \tag{3-10}$$

where *Io* is the load current.

However, the equations for a boost and a buck-boost converter are not available in simple terms of the conversion ratio. Nevertheless, we can express them in the functions of the duty cycle.

For a boost converter, we assume that V1 and V2 are constant. We obtain

$$D = \frac{V2}{V1}\sqrt{\frac{2LIo}{Ts(V1-V2)}} \tag{3-11}$$

As above, in the discontinuous conduction mode of a buck-boost converter, we have

$$D = \frac{V2}{V1}\sqrt{\frac{2LIo}{V2\,Ts}} \tag{3-12}$$

From these basic concepts, we can extend to the fourth-order voltage converter, corresponding to the four independent energy storage elements, as shown in Figure 13 (a), (b), and (c). The first of these circuits is the basic buck converter with an additional input filter stage. The second is the basic boost converter with an additional output filter stage. The conversion ratios of these two circuits are the same as the corresponding basic circuits. The third extended converter is the Ćuk converter, named for Dr. Slobodan Ćuk

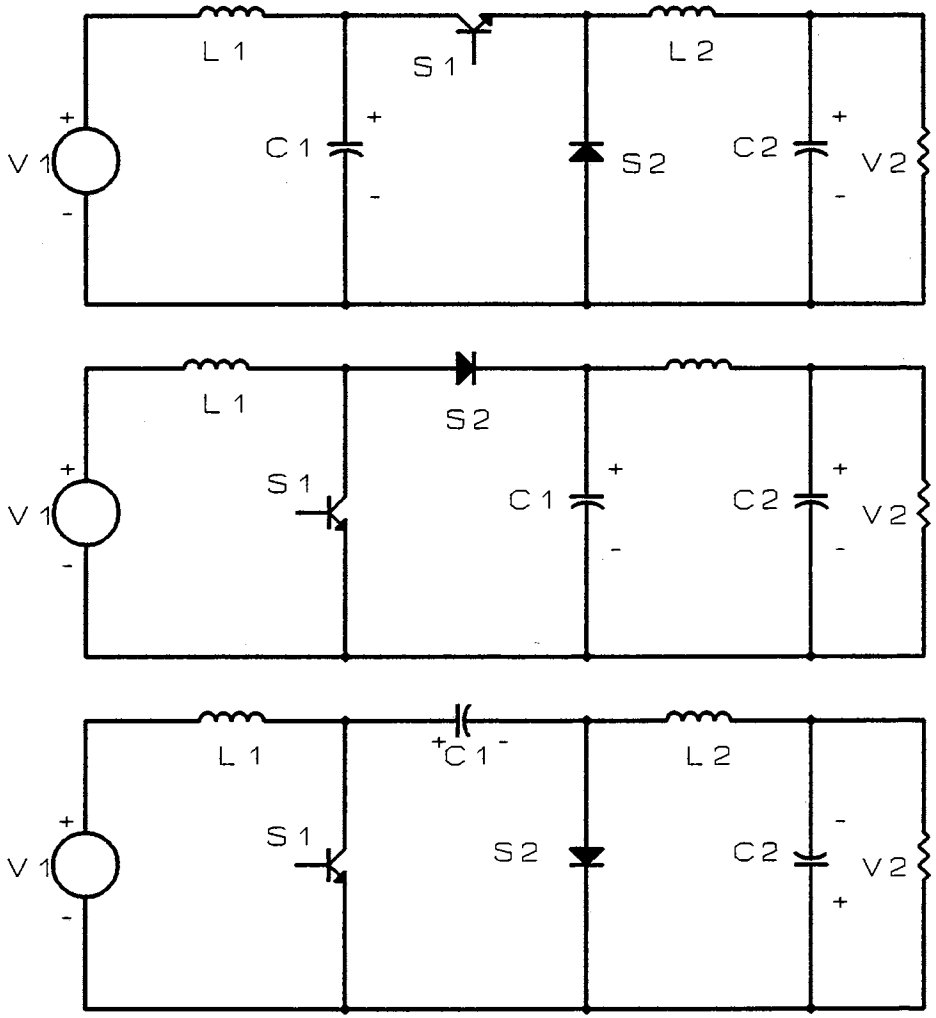

(a) Buck with additional input filter

(b) Boost with additional output filter

(c) Ćuk

Figure 13 Three extended voltage converters

of the California Institute of Technology (Mitchell, 1988).

The Ćuk configuration provides continuous input and output currents. In addition, the input and output inductors can be coupled in such a way that the switching component of either the input current or the output current can be nulled to zero. The Ćuk converter provides a negative polarity output voltage with respect to the common terminal of the input voltage.

Additional fourth-order converter topologies are shown in figure 14 (a), (b), and (c). The first two circuits are buck-boost and boost converters with additional input filters. The third converter circuit is a Single-Ended Primary Inductor Converter (SEPIC) (Mitchell, 1988). It was introduced by Bell Labs. Its advantage compared to using the buck-boost converter with a similarly placed transformer is that the possibility of transformer saturation due to dc offset is precluded by the series capacitor.

Transformer-isolated versions of the buck converter are shown in Figure 15 (a), (b) and Figure 16 (a), (b). These converters with appropriate transformations can be modeled as a basic buck converter.

The forward converter of Figure 15 (a) is a single-ended topology using only one controlled switch. The transformer is employed only in the first quadrant of its B-H curve. The forward converters are generally used in low voltage and low power applications.

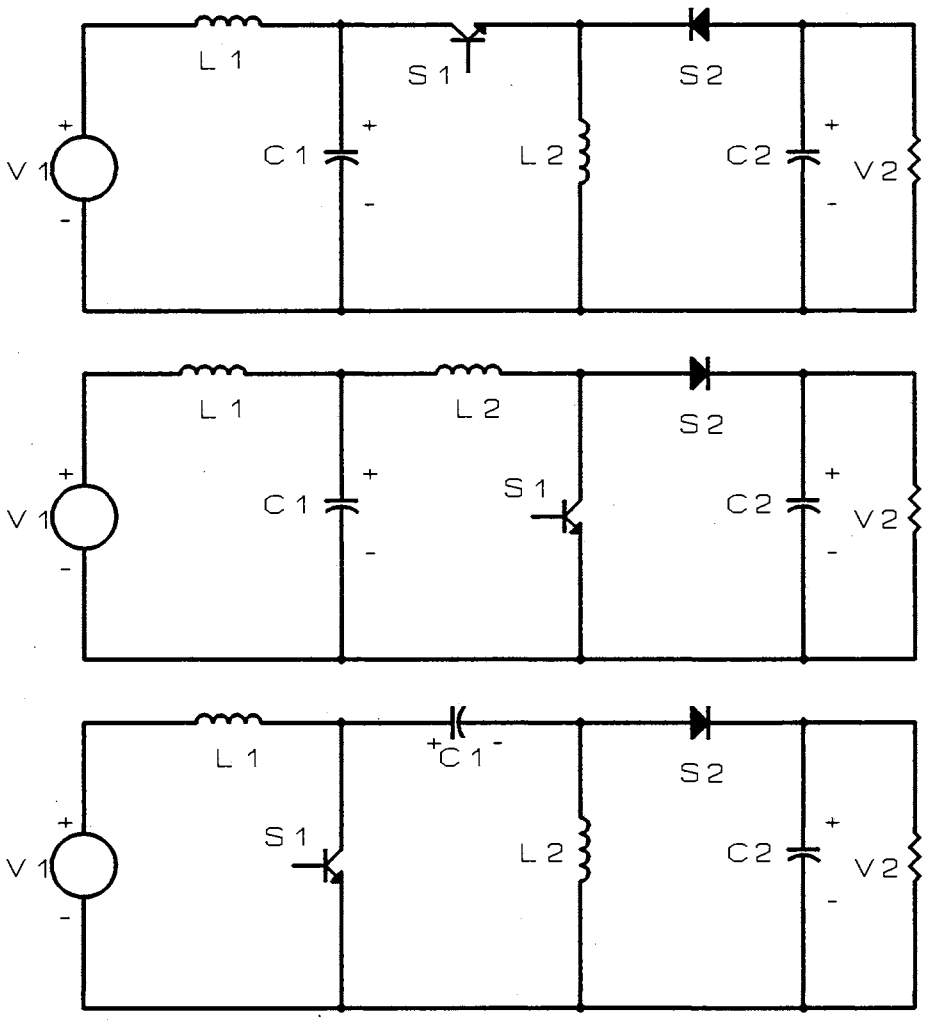

(a) Buck-boost with additional input filter

(b) Boost with additional input filter

(c) SEPIC

Figure 14 Three additional extended converters

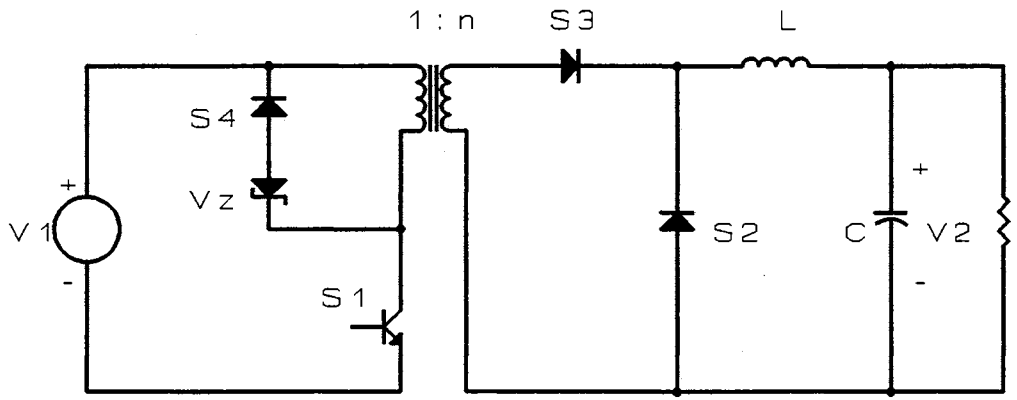

(a) Forward converter

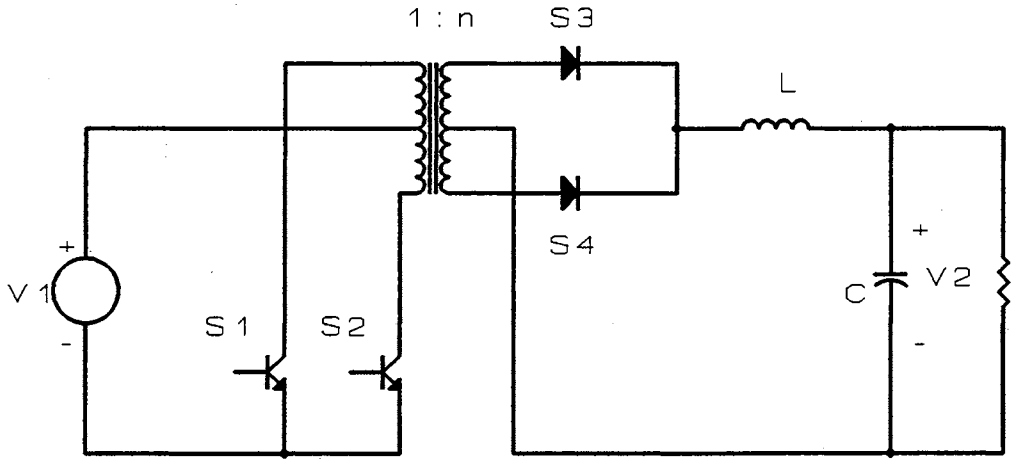

(b) Push-pull converter

Figure 15 Buck-derive converter

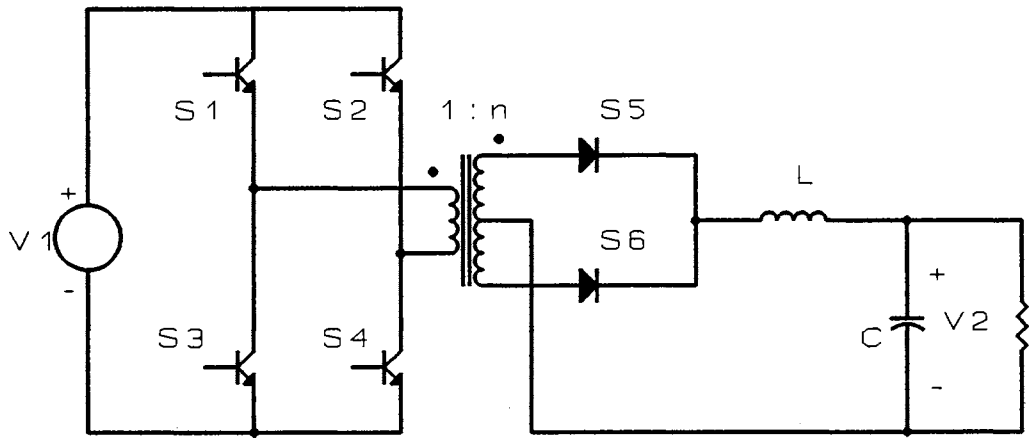

(a) Full-bridge converter

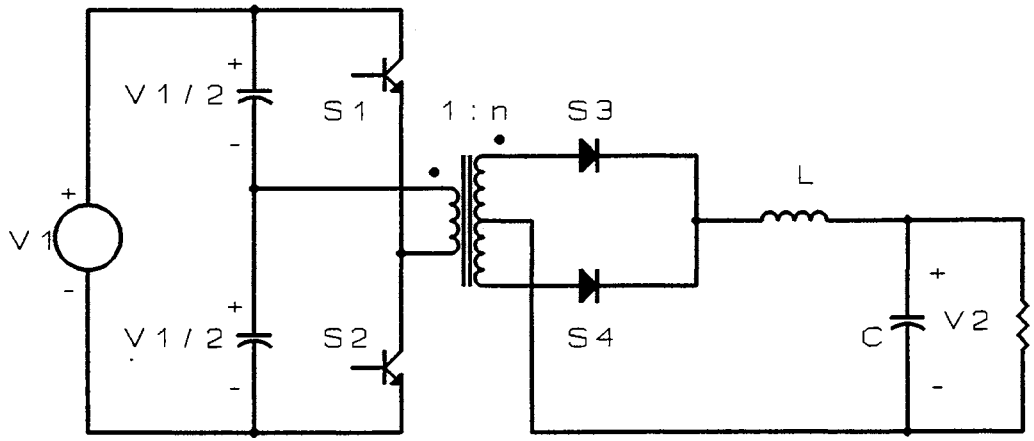

(b) Half-bridge converter

Figure 16 Transformer-isolated version of the buck converter

The push-pull converter shown in Figure 15 (b) operates in the first and the third quadrant of the transformer. Therefore, its size is relatively small. Moreover, the switching frequency of this converter can be operated at twice the cut off frequency of the switches.

Figure 16 (a) and (b) show full-bridge and a half bridge converters. The bridge converter is often used for higher input voltage and high power applications. However, because of the complexity of controlled switches and their associated drive circuit, its cost is high.

A boost-derived push-pull converter, which is developed from the boost converter, is shown in Figure 17 (a). It is commonly called a current-fed converter. This converter is particularly useful in high output voltage applications.

The most common of all converters is the transformer-isolated buck-boost converter or flyback converter, shown in Figure 17 (b). The flyback transformer requires an appropriate air gap to serve as the inductor and the transformer. Isolation and polarity reversal can be achieved in a practical flyback converter with no more power components than are in a basic buck-boost converter.

A process of cascading can develop another level of converters. Such cascaded converters can be reduced to a topology consisting of one transistor and one diode. A cascaded boost and buck-boost converter and a cascaded buck-boost and buck converter are shown in Figure 18 (a) and (b)

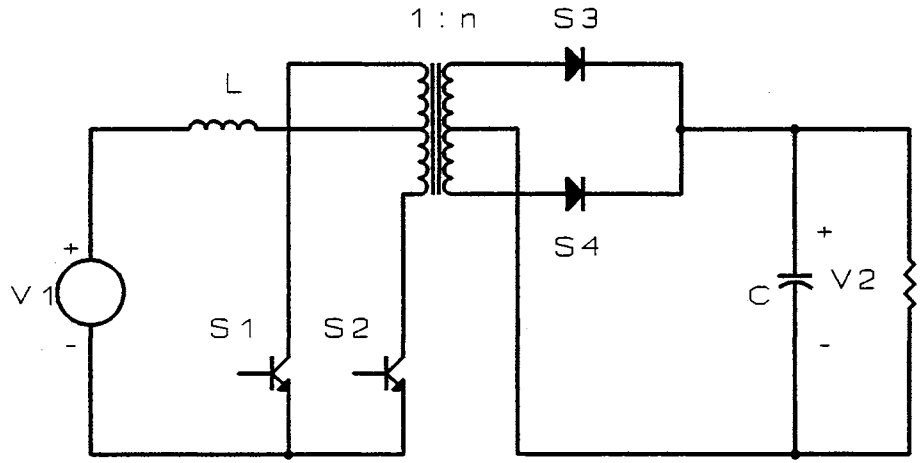

(a) Current-fed converter

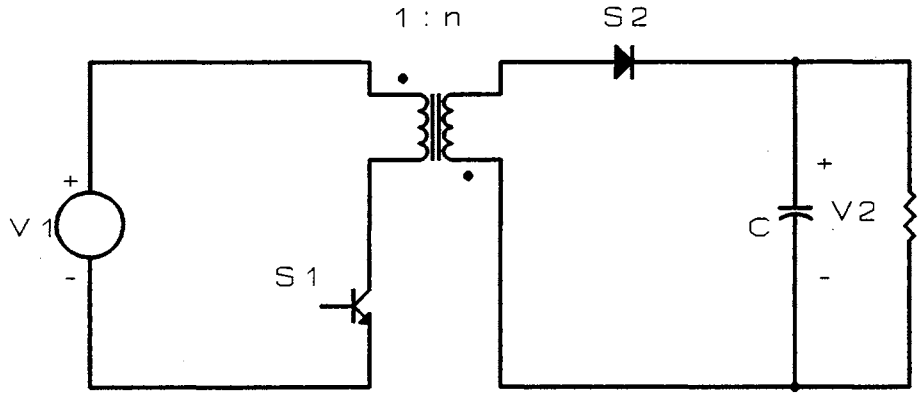

(b) Flyback converter

Figure 17 Boost-derive push-pull converter and transformer-isolated buck-boost converter

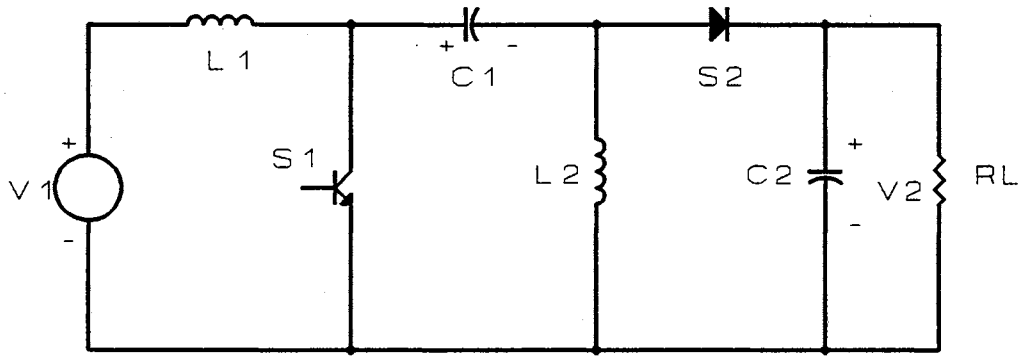

(a) A cascaded boost and buck-boost converter

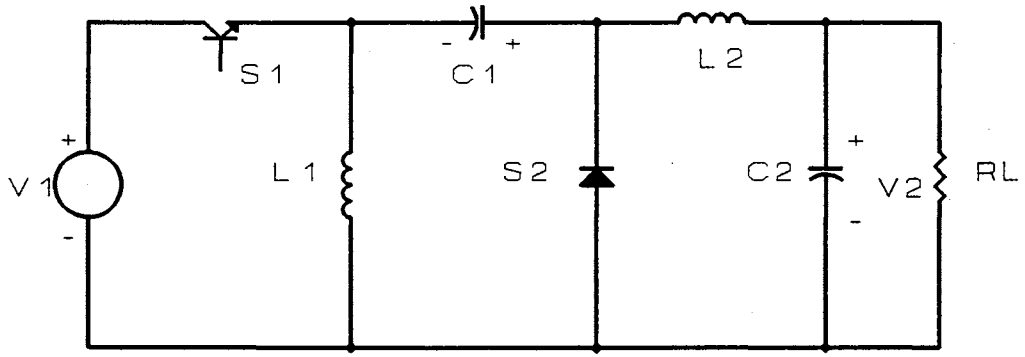

(b) A cascaded buck-boost and buck converter

Figure 18 Cascaded Converters

respectively. A cascaded buck-boost and buck converter may be called a non-inverting buck-boost since it has the same conversion ratio as the basic buck-boost converter and an inverted output polarity.

A New AC-DC Converter Topology

An ac-dc converter may be developed from a dc-dc converter with appropriate transformations. An ideal ac-dc converter is a converter which has a conversion ratio of

$$\frac{Vo}{Vs} = \frac{-1}{(1-2D)} \tag{3-13}$$

From the conversion ratio, if we modulate the duty cycle with a constant plus a sine wave function, the input voltage Vs can be an ac voltage source, and the output voltage Vo can be a dc voltage.

To demonstrate the ac-dc conversion, we substitute D with a variation in terms of sinusoidal wave around 0.5 that is

$$D = 0.5 + m(\sin(\omega t)) \tag{3-14}$$

where m is a modulated duty cycle variation. Substituting $Vs = VS(\sin(\omega t))$ and equation (3-14) into equation (3- 13). We have

$$Vo = \frac{-VS(\sin(\omega t))}{1-1-2m(\sin(\omega t))} = \frac{VS}{2m} \quad (3\text{-}14)$$

This means we obtain a dc output voltage that can be controlled by the modulated duty cycle variation.

Developments of a New AC-DC Converter

The main objective of this dissertation is to present a new ac-dc converter configuration with low harmonic input currents, bidirectional power flow capability, and an adjustable power factor.

We begin by modifying a non-inverting buck-boost converter. A non-inverting buck-boost shown in Figure 19. has a conversion ratio as

$$\frac{Vs}{Vo} = \frac{D}{(1-D)} \quad (3\text{-}15)$$

where Vs is the input voltage and Vo is the output voltage.

The conversion ratio is the same as the basic buck-boost converter except for inverted output polarity. From the conversion ratio, the output voltage Vo equals to the input voltage Vs when the duty cycle is 0.5 of a switching period. By controlling the duty cycle more or less than 0.5, the output voltage can be equal to the input voltage plus some desired voltage. The desired output voltage can be any value depending on the duty cycle. For example, if the duty cycle is 0.65, the output voltage will be $1.85Vs$ or

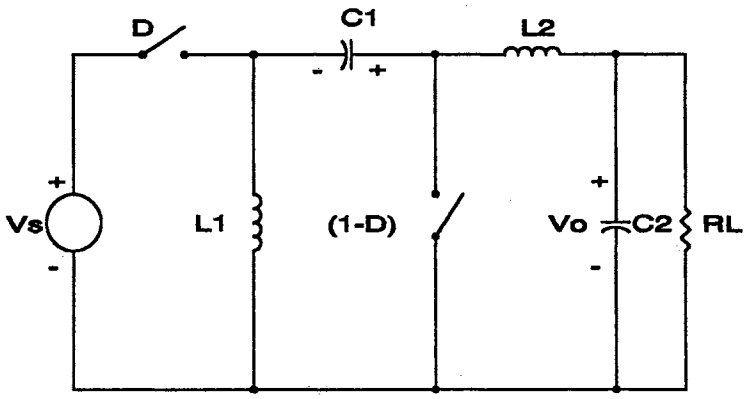

Figure 19 A non-inverting buck-boost converter

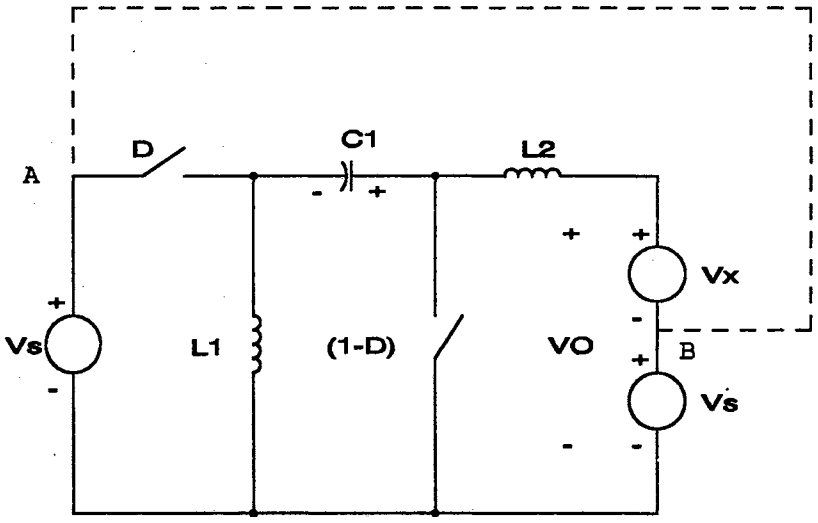

Figure 20 The non-inverting buck-boost converter with a separated output

$1.0Vs + 0.85Vs$. In contrast, the output voltage will be $0.82Vs$ or $1.0Vs + (-0.18)Vs$ if the duty cycle is 0.45. It is significant to note that the output voltage will be a sinusoid when the duty cycle is modulated with a sine wave.

Theoretically, we can assume a charged capacitor is a voltage source. At this point, the RC output circuit in Figure 19 can be represented by two voltage sources in any case of the duty cycle as shown in Figure 20. The output voltage is equal the input voltage VS plus some voltage VX. Since the voltage at the point A and B are the same potential, both points can virtually be connected. Consequently, one of the duplicated voltage sources may be eliminated.

The duality transformation is now used to generate a new converter topology. Two circuits are dual if the mesh equations that characterize one of them have the same mathematical forms as the nodal equations that characterize the other. The principle of duality applied to dual networks is summarized in TABLE III (Freeland 1992).

TABLE III

Quantity	Dual quantity
Resistance	Conductance
Inductance	Capacitance
Impedance	Admittance
Voltage source	Current source
Series connection	Parallel connection
Mesh current	Node voltage
Open-circuit voltage	Short-circuit current

In electrical networks, duality is usually limited to linear circuits whose graphs are planar. A graph G is said to be planar if it can be drawn on a plane in such a way that no two branches cross at a point which is not a node (Carter 1972). For example, the graph in Figure 21 (a) is planar while that of Figure 21 (b) is not.

A graph G* is said to be the dual of another graph G if the following three conditions are satisfied:

CONDITION 1. There is a one-to-one correspondence between all meshes of G and the nodes of G*.

CONDITION 2. There is a one-to-one correspondence between all nodes of G and the meshes of G*.

CONDITION 3. There is a one-to-one correspondence between the branches of each graph such that, whenever two meshes of one graph have a branch in common, the corresponding nodes of the other graph have the corresponding branch which connects these nodes.

In analyzing electrical networks, the direction of the assumed current flow in each branch is usually indicated. The graph of such a network is called an oriented graph, with a current direction indicated on each of its branches. For an oriented graph G, where each branch current has a reference direction, the orientation of the dual graph G* can be obtained by rotating the current reference direction of each branch by 90 degrees clockwise to obtain the current direction of the corresponding branch in G*.

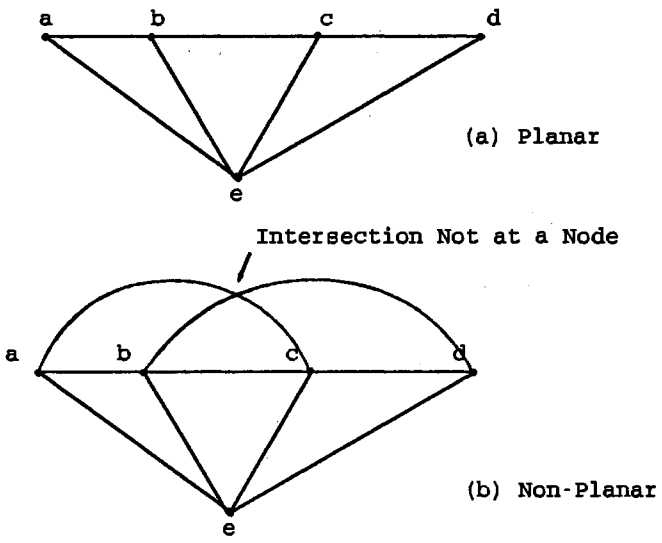

Figure 21 Example of planar and nonplanar graphs

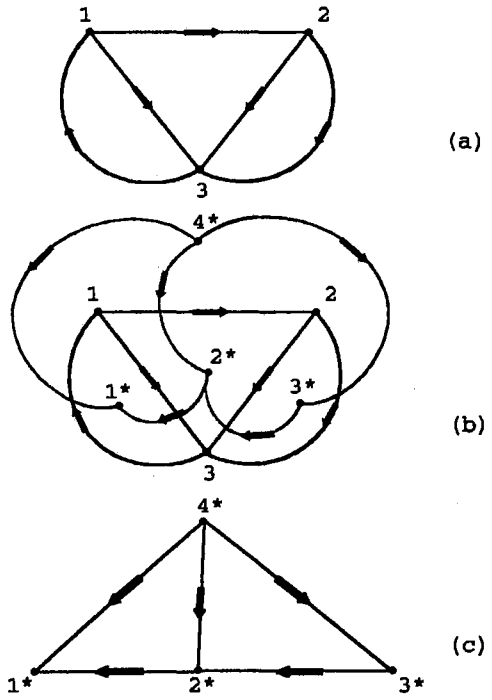

Figure 22 Derivation of the dual of an oriented graph

For instance, an oriented graph is shown in Figure 22 (a). In Figure 22 (b), we place a node inside each mesh including the outer mesh. Then, branches are connected between the new nodes so that one branch of the new graph intersects each of the branches of the original one. As shown in Figure 22 (c), we now have the dual graph. Next, each corresponding branch in the dual graph is determined.

By applying duality theory to the configuration in Figure 23 (a), the modified topology in Figure 23 (b) is obtained. The configuration of both topologies is almost the same except for an exchange of the input voltage and the output voltage with inverted polarities. Therefore, the modified converter has a bidirectional power transfer capability. In practice, power flow direction is controlled by swapping the command of the switches.

The new configuration is shown in Figure 24. Note that if the duty cycle is a sine wave, one of the source voltages can be an ac voltage source, and another can be a dc voltage source. As a result, the converter can operate in either the rectifier mode or the inverter mode.

The conversion ratio of the converter is derived as follows:

For *VL1*,

$$\begin{aligned} (Vs-Vo)\,D + (Vs+Vc)(1-D) &= 0 \\ Vs\,D + Vo\,D + Vs + Vc - Vs\,D - Vc\,D &= 0 \\ Vc &= \frac{Vo\,D - Vs}{(1-D)} \end{aligned} \qquad (3\text{-}16)$$

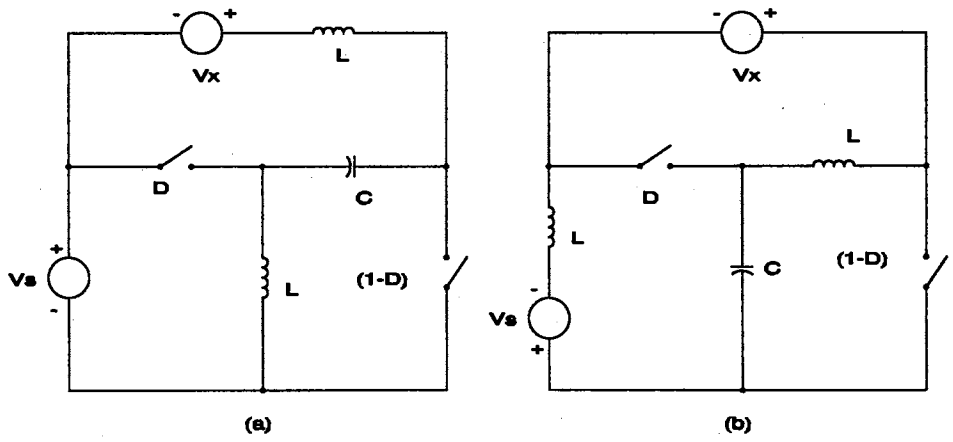

Figure 23 The dual converter configurations

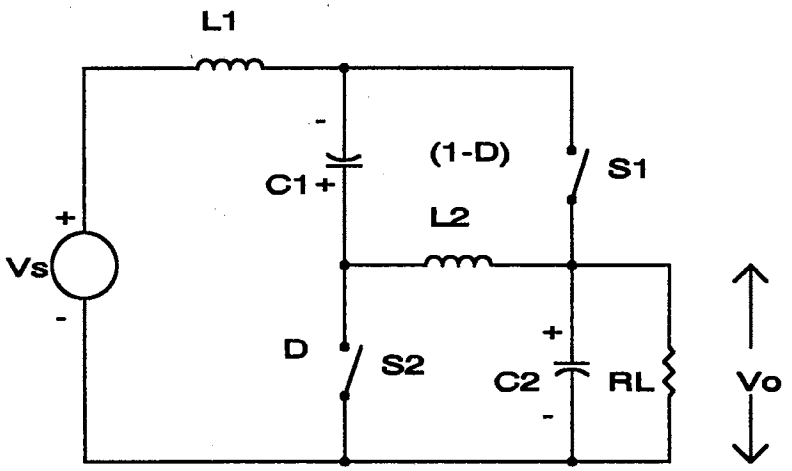

Figure 24 The new proposed converter topology

For *VL2*,

$$-Vc\ D + Vo(1-D) = 0$$
$$Vo = \frac{D\ Vc}{(1-D)} \tag{3-17}$$

Combining equations (3-16) and (3-17), we arrive at

$$\frac{Vo}{Vs} = \frac{-D}{(1-2D)} \tag{3-18}$$

The conversion ratio of the new topology is nonlinear, as shown in Figure 25. When the duty cycle is above 0.5 the conversion ratio is positive. In contrast, the conversion ratio is negative when the duty cycle is below 0.5. This confirms the capability to operate as a rectifier or inverter.

For operation as an ac-dc converter, the input voltage source, *Vs*, is represented by $VS(\sin(\omega t))$ and the duty cycle is represented by $0.5 + m(\sin(\omega t))$, where m is a magnitude of the duty cycle variation. It follows that

$$Vo = \frac{-(0.5+m\ \sin(\omega t))}{1-2(0.5+m\ \sin(\omega t)} \times VS\ \sin(\omega t)$$
$$Vo = \frac{VS}{4m} + \frac{VS\ \sin(\omega t)}{2} \tag{3-19}$$

From equation (3-19), the output voltage is described as dc voltage plus a ripple voltage. Ripple voltage will be reduced by choosing an appropriate duty cycle. The appropriate duty cycle can be generated by a

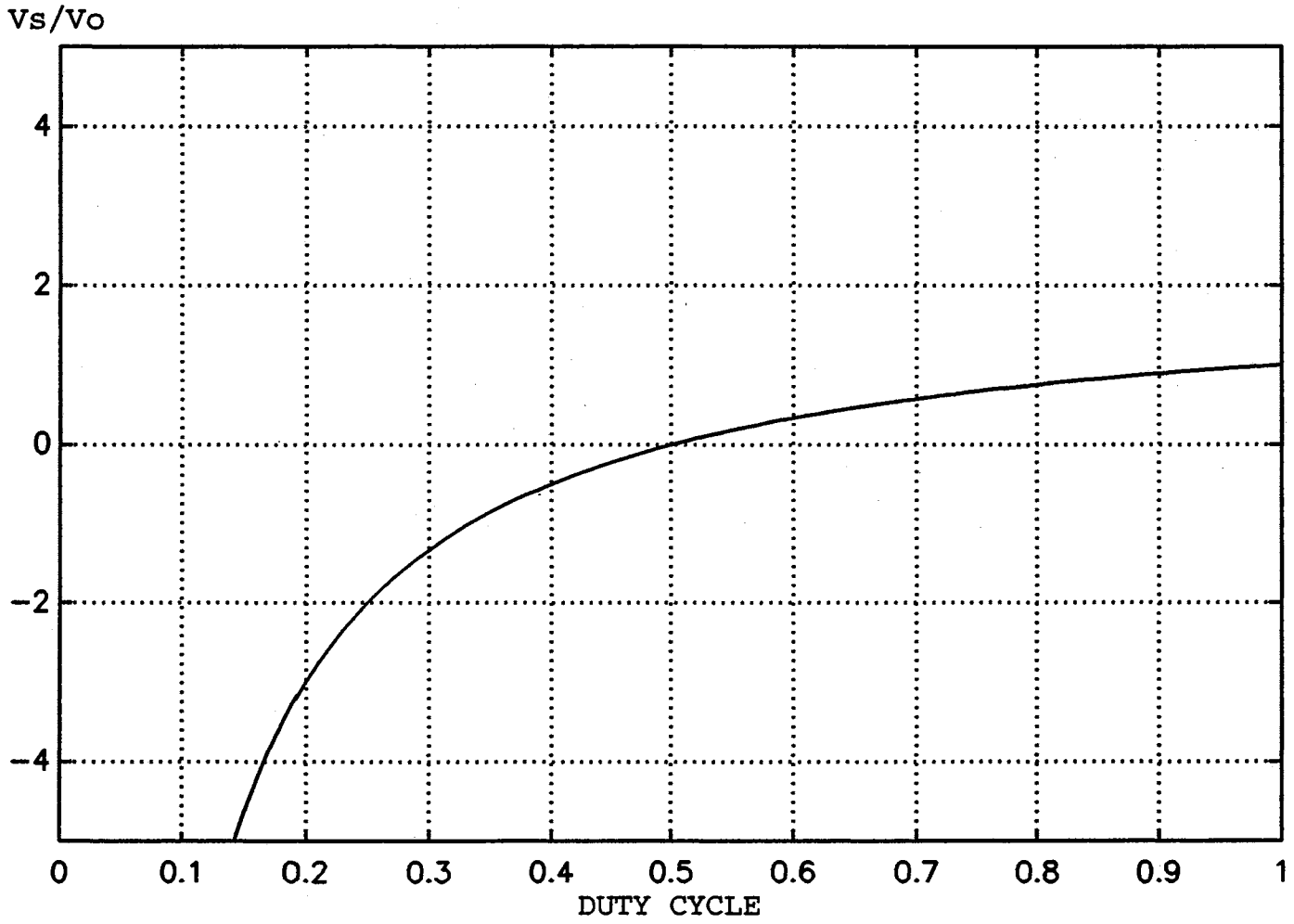

Figure 25 Conversion ratio versus duty cycles

close loop control. The duty cycle for zero ripple voltage, which can be obtained by holding the output voltage in equation (3-18) constant, is

$$D = \frac{VO}{2VO - Vs \sin(\omega t)} \tag{3-20}$$

where VO is the dc output voltage.

Unfortunately, the harmonic currents will increase if the variation of the duty cycle is not sinusoidal. The duty cycle is plotted in terms of the constant output voltage in Figure 26. From the plot, we find that the higher the conversion ratio, the smaller the variation of the duty cycle. In addition, at a high conversion ratio, the variation of the duty cycle approaches a sinusoidal waveform.

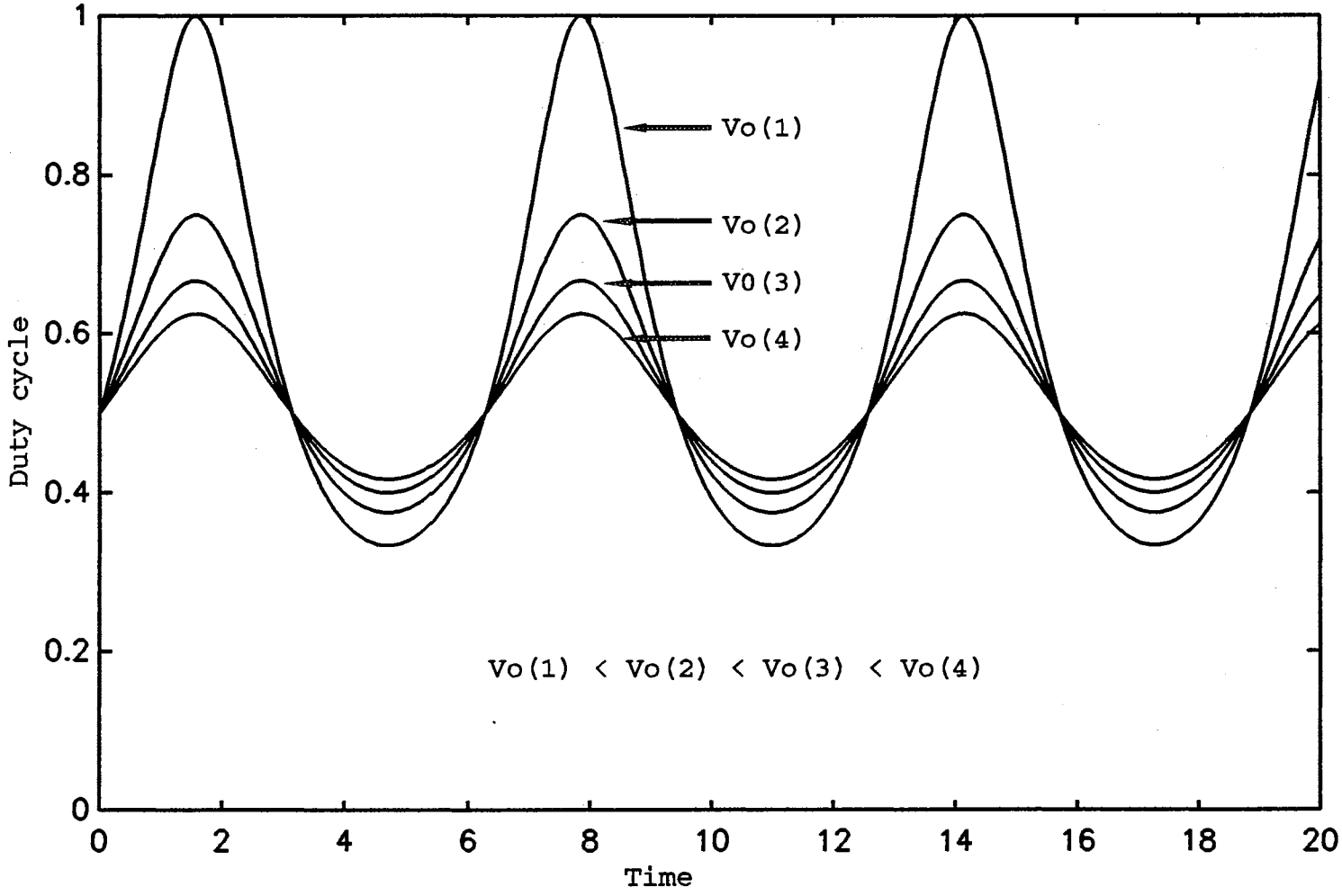

Figure 26 The family plot of the duty cycle function

CHAPTER IV

ANALYTICAL MODELING

Mathematical Modeling

A hysteresis band current control technique is employed to cause the input current to track a reference waveform. A control configuration for the proposed converter is illustrated in Figure 27. The control circuit generates a reference current signal with a desired magnitude and phase angle, which synchronizes with the input voltage source. Switch commands are produced by comparing the reference current and the actual current. The actual current is measured by a dc current transformer. As the current exceeds a prescribed hysteresis band, the switch S2 is turned off and the switch S1 is turned on. As a result, the current starts to decay. As the current crosses the lower band limit, the switch S2 is turned on and the switch S1 is turn off. The actual current wave is thus forced to track the sine reference wave within the desired hysteresis band by back and forth switching of the upper and the lower switch. A profile of a controlled current corresponding a switch command is shown in Figure 28.

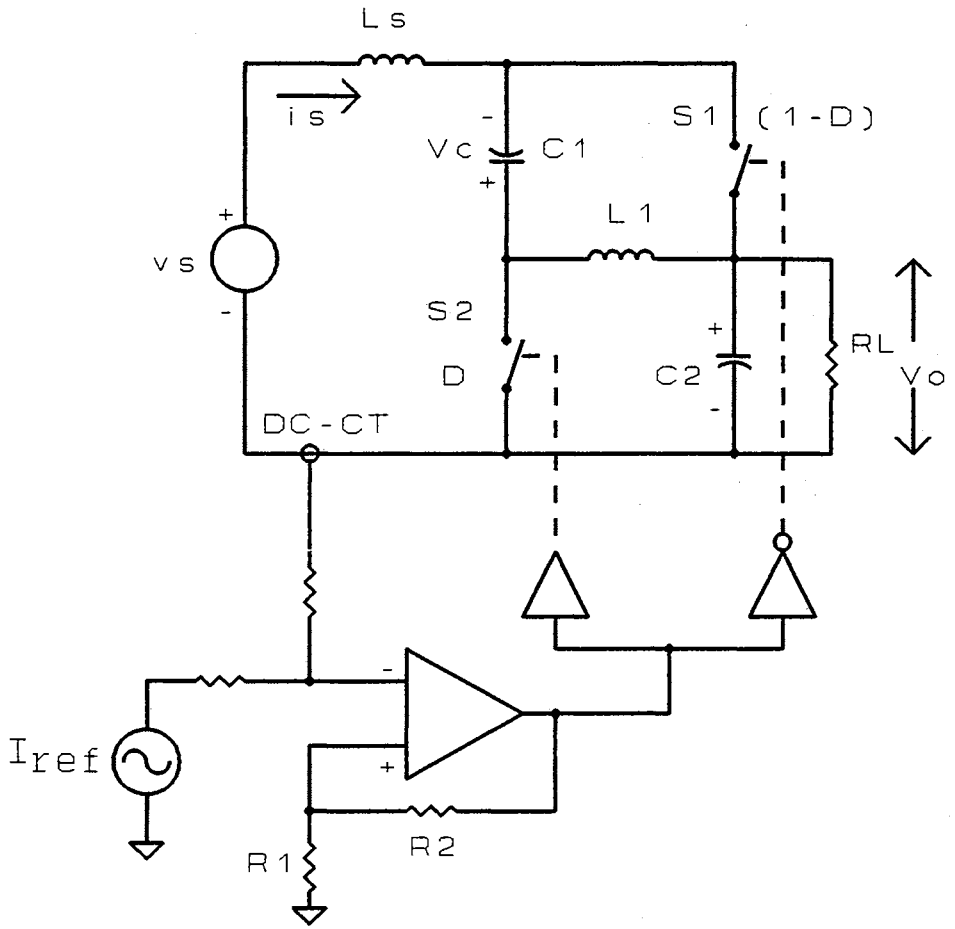

Figure 27 A new ac-dc converter configuration

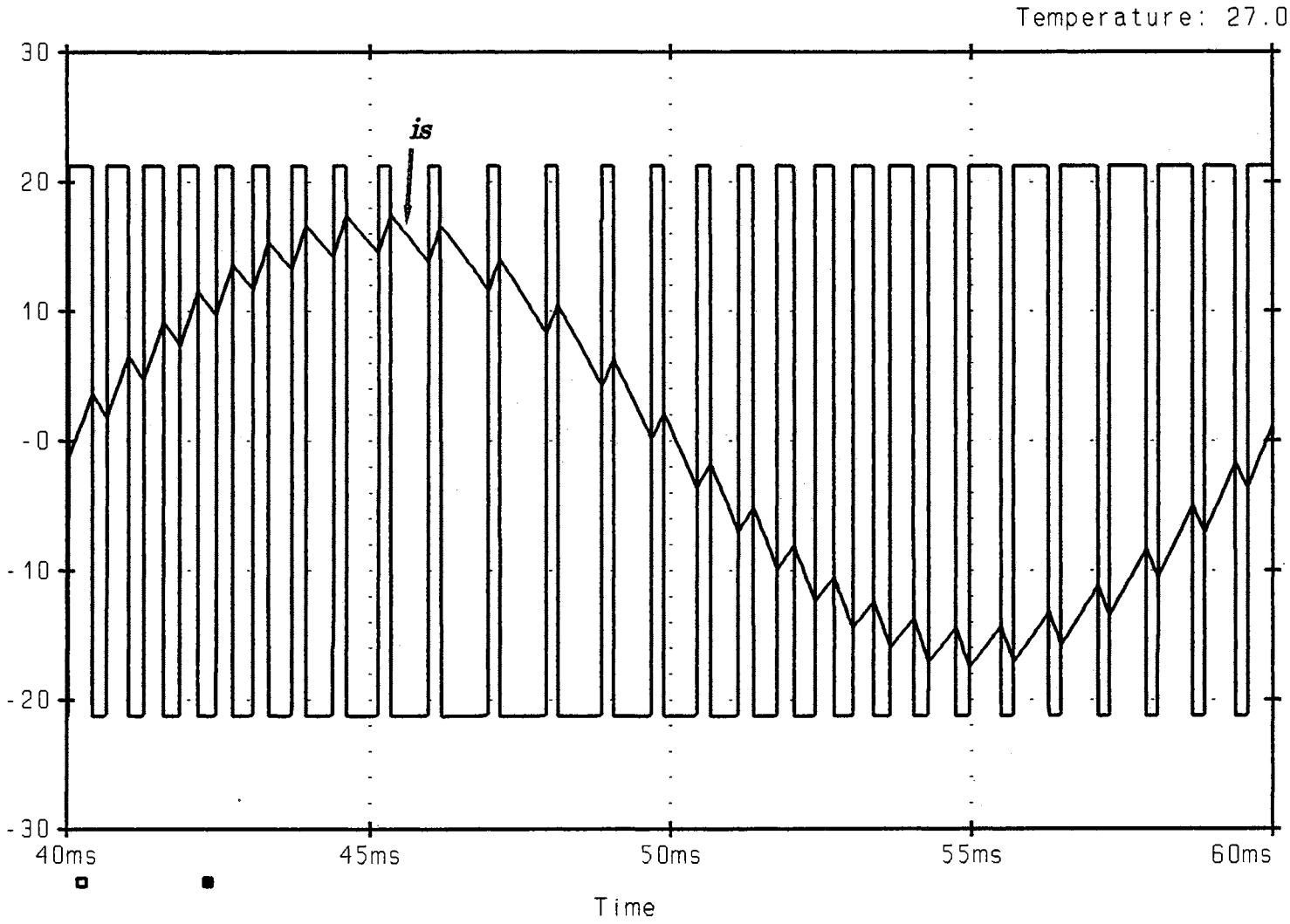

Figure 28 The input current and the switch command

In practice, the switches can be implemented with power MOSFETs or power BJTs with anti-parallel diodes. These switches allow bidirectional flows of currents while withstanding one voltage polarity in their blocking state.

The actual current measured by a dc current transformer is converted into a voltage that is proportional to the measured current. Let N be a controlled voltage to the input current ratio. As shown in Figure 29, the ripple current is found from

$$\begin{aligned} \Delta i &= 2[(\frac{V_{hys}}{2} + V_{ref})N - V_{ref}N] \\ &= V_{hys}\, N \end{aligned} \tag{4-1}$$

where

$$V_{hys} = \frac{R_1}{R_1+R_2}[+V_{sat}-(-V_{sat})] \tag{4-2}$$

where $+V_{sat}$ and $-V_{sat}$ are the saturation output voltage of the operational amplifier.

The switching frequency is controlled by the hysteresis band and the inductor *Ls*. Reducing the hysteresis band increases switching frequency. Inductor *Ls* is used to determine the instantaneous slope of the controlled current.

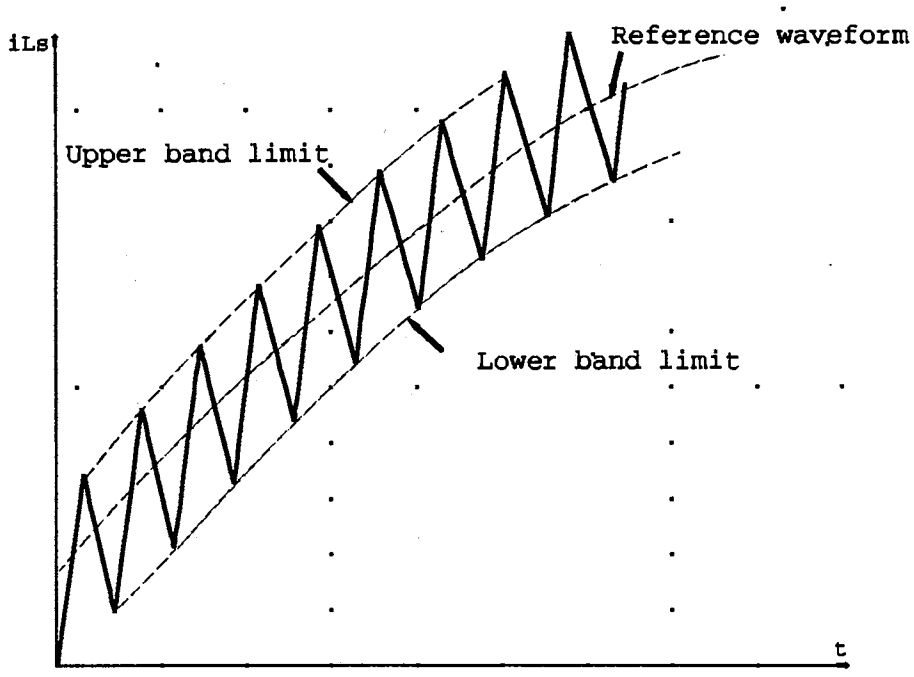

Figure 29 Bang-bang current control

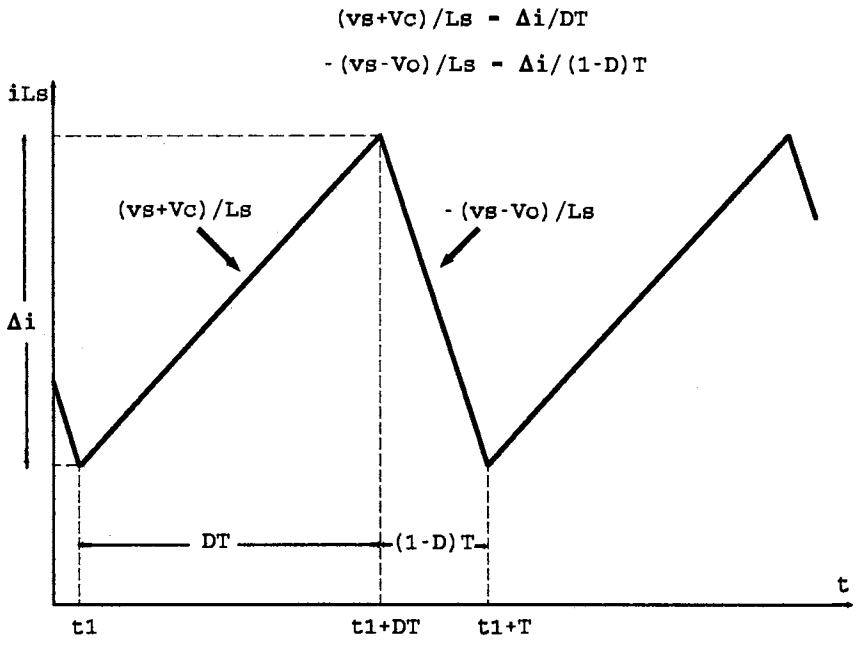

Figure 30 A small interval of the bang-bang current control

Note that the switching frequency is not constant. If the switching frequency is assumed much higher than the line frequency, the ripple current may appear as shown in Figure 29. When S1 is off, and S2 is on, we set

$$\begin{aligned} vs + Vc &= Ls\frac{\Delta i}{DT} \\ DT &= \frac{Ls\,\Delta i}{vs + Vc} \end{aligned} \tag{4-3}$$

When S1 is on, and S2 is off, we obtain

$$\begin{aligned} -(vs - Vo) &= L\frac{\Delta i}{(1-D)T} \\ (1-D)T &= \frac{-L\,\Delta i}{vs - Vo} \end{aligned} \tag{4-4}$$

Combining equation (3) and (4), we have

$$\begin{aligned} DT+(1-D)T &= \left(\frac{Ls\,\Delta i}{vs + Vc}\right) + \left(\frac{-Ls\,\Delta i}{vs - Vo}\right) \\ T &= Ls\,\Delta i\left(\frac{1}{vs + Vc} - \frac{1}{vs - Vo}\right) \end{aligned} \tag{4-5}$$

We know that in steady state $Vo = Vc$ because the average voltage at the input terminal must be zero, and vs is a sine wave. Therefore, from the equation (5), we find that the switching period is minimum when $vs = 0$. Maximum switching frequency is found from

$$f_{max} = \frac{0.5Vo}{Ls\ \Delta i} \tag{4-6}$$

Moreover, the minimum switching frequency occurs when *vs* is at either a positive or a negative peak. Rearranging equation (5), we obtain

$$f_{min} = \frac{Vo^2 - Vs^2}{2\ Ls\ Vo\ \Delta i} \tag{4-7}$$

The Fundamentals of State Space Averaging Method

A state space averaging technique can be used to develop a mathematical model for the system described in this dissertation. State space averaging methods were first applied to dc-dc switching converters, by Middlebrook and Ćuk (1976).

If a converter circuit is assumed to operate in a continuously conducting mode, there are only two different states of the circuit. Each state can be represented by a linear circuit model or by a corresponding set of state space equations.

Let the two linear systems be described by

(I) interval DT; $0<t<t_0$:

$$\dot{x} = A1\ x \tag{4-8}$$

(II) interval $(1\text{-}D)T$; $t_0<t<T$:

$$\dot{x} = A2\ x \tag{4-9}$$

where x = state vector; Ai = state coefficient matrix, i = 1,2

The exact solutions of these state space equation are:

$$\begin{aligned} x(t) &= e^{A1t}x(0) && t\in[0,t_0] \\ x(t) &= e^{A2t}x(t_0) && t\in[t_0,T] \end{aligned} \tag{4-10}$$

The state variable vector $x(t)$ is continuous across the switching instance t_0. Thus,

$$x(T) = e^{A2(T-DT)}x(t_0) = e^{(1-D)A2T}e^{DA1T}x(0) \tag{4-11}$$

The following approximation by Baker-Campbell-Hausdorff series is now introduced into the equation (Middlebrook 1976):

$$e^{(1-D)A2T}e^{DA1T} \approx e^{(DA1+(1-D)A2)T} \tag{4-12}$$

resulting in an approximate solution

$$x(T) \approx e^{(DA1+(1-D)A2)T}x(0) \tag{4-13}$$

However, this is the same as the solution of the following linear system equation for $x(T)$. Therefore, the averaged model obtaining from the two switched models is

$$\dot{x} = (DA1+(1-D)A2)x \tag{4-14}$$

The nonhomogeneous set of state equations is further developed as shown in the reference (Mitchell 1988). The basic state space averaged model can be written as follows.

$$\dot{x} = Ax + Bu \tag{4-15}$$

where

$$\begin{aligned} A &\triangleq DA1+(1-D)A2 \\ B &\triangleq DB1+(1-D)B2 \end{aligned} \tag{4-16}$$

where u = source vector

Bi = source coefficient matrix, i = 1,2

From the circuit shown in Figure 27, we can write state space equation by assuming that the ripple current in *Ls* is very small. In addition, the inductor current *iLs* is controlled to be sin wave and inphase with the voltage. As a consequence, The state space equation can be written as follows.

With S1 on and S2 off, we obtain

$$\begin{aligned} Ls\frac{diLs}{dt} &= -vo+vs \\ L1\frac{diL1}{dt} &= vc \\ C1\frac{dvc}{dt} &= -iL1 \\ C2\frac{dvo}{dt} &= -\frac{vo}{R}+is \end{aligned} \tag{4-17}$$

In a matrix form, we have

$$\begin{bmatrix} \frac{diLs}{dt} \\ \frac{diL1}{dt} \\ \frac{dvc}{dt} \\ \frac{dvo}{dt} \end{bmatrix} = \begin{bmatrix} 0 & 0 & 0 & -\frac{1}{Ls} \\ 0 & 0 & \frac{1}{L1} & 0 \\ 0 & -\frac{1}{C1} & 0 & 0 \\ \frac{1}{C2} & 0 & 0 & -\frac{1}{RC2} \end{bmatrix} \begin{bmatrix} iLs \\ iL1 \\ vc \\ vo \end{bmatrix} + \begin{bmatrix} \frac{1}{Ls} \\ 0 \\ 0 \\ 0 \end{bmatrix} vs \tag{4-18}$$

With S1 off and S2 on, we obtain

$$\begin{aligned} Ls\frac{diLs}{dt} &= vc + vs \\ L1\frac{diL1}{dt} &= -vo \\ C1\frac{dvc}{dt} &= -is \\ C2\frac{dvo}{dt} &= iL1 - \frac{vo}{R} \end{aligned} \tag{4-19}$$

In a matrix form, we have

$$\begin{bmatrix} \frac{diLs}{dt} \\ \frac{diL1}{dt} \\ \frac{dvc}{dt} \\ \frac{dvo}{dt} \end{bmatrix} = \begin{bmatrix} 0 & 0 & \frac{1}{Ls} & 0 \\ 0 & 0 & 0 & -\frac{1}{L1} \\ -\frac{1}{C1} & 0 & 0 & 0 \\ 0 & \frac{1}{C2} & 0 & -\frac{1}{RC2} \end{bmatrix} \begin{bmatrix} iLs \\ iL1 \\ vc \\ vo \end{bmatrix} + \begin{bmatrix} \frac{1}{Ls} \\ 0 \\ 0 \\ 0 \end{bmatrix} vs \tag{4-20}$$

By using a state space averaging method, we arrive at

$$\begin{bmatrix} \frac{diLs}{dt} \\ \frac{diL1}{dt} \\ \frac{dvc}{dt} \\ \frac{dvo}{dt} \end{bmatrix} = \begin{bmatrix} 0 & 0 & \frac{(1-D)}{Ls} & -\frac{D}{Ls} \\ 0 & 0 & \frac{D}{L1} & -\frac{(1-D)}{L1} \\ -\frac{(1-D)}{C1} & -\frac{D}{C1} & 0 & 0 \\ \frac{D}{C2} & \frac{(1-D)}{C2} & 0 & -\frac{1}{RC2} \end{bmatrix} \begin{bmatrix} iLs \\ iL1 \\ vc \\ vo \end{bmatrix} + \begin{bmatrix} \frac{1}{Ls} \\ 0 \\ 0 \\ 0 \end{bmatrix} vs \qquad (4\text{-}21)$$

where

$$A1 = \begin{bmatrix} 0 & 0 & 0 & -\frac{1}{Ls} \\ 0 & 0 & \frac{1}{L1} & 0 \\ 0 & -\frac{1}{C1} & 0 & 0 \\ \frac{1}{C2} & 0 & 0 & -\frac{1}{RC2} \end{bmatrix} \qquad B1 = \begin{bmatrix} \frac{1}{Ls} \\ 0 \\ 0 \\ 0 \end{bmatrix}$$

and

$$A2 = \begin{bmatrix} 0 & 0 & \frac{1}{Ls} & 0 \\ 0 & 0 & 0 & -\frac{1}{L1} \\ -\frac{1}{C1} & 0 & 0 & 0 \\ 0 & \frac{1}{C2} & 0 & -\frac{1}{RC2} \end{bmatrix} \qquad B2 = \begin{bmatrix} \frac{1}{Ls} \\ 0 \\ 0 \\ 0 \end{bmatrix}$$

with

$$A = A1D + A2(1-D)$$

$$B = B1D + B2(1-D)$$

resulting in approximate state coefficients

$$A = \begin{bmatrix} 0 & 0 & \frac{(1-D)}{Ls} & -\frac{D}{Ls} \\ 0 & 0 & \frac{D}{L1} & -\frac{(1-D)}{L1} \\ -\frac{(1-D)}{C1} & -\frac{D}{C1} & 0 & 0 \\ \frac{D}{C2} & \frac{(1-D)}{C2} & 0 & -\frac{1}{RC2} \end{bmatrix} \qquad B = \begin{bmatrix} \frac{1}{Ls} \\ 0 \\ 0 \\ 0 \end{bmatrix}$$

Pre-multiplying the equation (4-21) by the row matrix [*iLs iL1 vc vo*] and substituting *(1-D)* by D' for convenience, we get

$$LsiLs\frac{diLs}{dt} + L1iL1\frac{diL1}{dt} + C1vc\frac{dvc}{dt} + C2vo\frac{dvo}{dt} =$$

$$= -D'vc\ iLs + DvoiLs - DvciL1 + D'voiL1 + D'vciLs + DVciL1$$
$$-DvoiLs - D'voiL1 - \frac{vo^2}{R} + vsis$$

$$= -\frac{vo^2}{R} + vsis \qquad (4\text{-}22)$$

By substituting $vs = Vs\sin(\omega t)$ and $is = Is\sin(\omega t)$ into the equation (4-22), we arrive at

$$Ls\,iLs\frac{diLs}{dt}+L1\,iL1\frac{diL1}{dt}+C1\,vc\frac{dvc}{dt}+C2\,vo\frac{dvo}{dt}=$$
$$=-\frac{vo^2}{R}+(Vs\,Is)\sin(\omega t)\sin(\omega t) \qquad (4\text{-}23)$$
$$=-\frac{vo^2}{R}+\frac{Vs\,Is}{2}-\frac{Vs\,Is}{2}\cos(2\omega t)$$

The input power must equal to the output power in a steady state condition. Thus,

$$Ls\,iLs\frac{diLs}{dt}+L1\,iL1\frac{diL1}{dt}+C1\,vc\frac{dvc}{dt}+C2\,vo\frac{dvo}{dt}= \qquad (4\text{-}24)$$
$$=-\frac{Vs\,Is}{2}\cos(2\omega t)$$

This equation states that at any instant the difference between the input and output powers of the converter is equal to the power in its reactive elements

We can assume that *vo(t)* and *vc(t)* are composed of a dc component and an ac component, which are

$$vc(t) = VC+Vx\cos(\omega t+\alpha_1) \qquad (4\text{-}25)$$

and

$$vo(t) = VO-Vy\cos(\omega t+\alpha_2) \qquad (4\text{-}26)$$

where *Vx* and *Vy* are the magnitude of the ripple voltages of *vc(t)* and *vo(t)* respectively.

We find that in the steady state the sum of dc component at the source input terminal must be zero, so VO must equal VC. Moreover, the phase shift angles α_1 and α_2 are small, so they may be ignored initially to simplify the analysis. Thus,

$$\begin{aligned} vc(t) &= VO + Vx\cos(\omega t) \\ vo(t) &= VO - Vy\cos(\omega t) \end{aligned} \tag{4-27}$$

From the state space averaged equation (4-21), we have the inductor voltage equations that are

$$Ls\frac{dis(t)}{dt} = D'vc(t) - Dvo(t) + vs(t) \tag{4-28}$$

and

$$L1\frac{diL1(t)}{dt} = Dvc(t) - D'vo(t) \tag{4-29}$$

Combining both equations, with $D + D' = 1$, we arrive at

$$Ls\frac{dis(t)}{dt} + L1\frac{diL1(t)}{dt} = vc(t) - vo(t) + vs(t) \tag{4-30}$$

By substituting equation (4-27) into the equation (4-30), we obtain

$$vLs(t)+vL1(t) = (VO+Vx\cos(\omega t))-(VO-Vy\cos(\omega t))+Vs\sin(\omega t) \tag{4-31}$$

where $Ls(dis(t)/dt) = vLs(t)$ is the instantaneous voltage across the inductor Ls, and $L1(diL1(t)/dt) = vL1(t)$ is the instantaneous voltage across the inductor $L1$.

The input current is controlled by a sine wave and it is in phase with the voltage source. Thus, the voltage across the inductor *Ls* is *VLs* cos(ω*t*). Substituting *vLs(t)* = *VLs* cos(ω*t*) = ω*LsIs* cos(ω*t*) into equation (4-31), we obtain

$$\begin{aligned} vL1(t) &= Vx\cos(\omega t)+Vy\cos(\omega t)+Vs\sin(\omega t)-\omega L1\,Is\cos(\omega t) \\ &= (Vx+Vy-\omega L1\,Is)\cos(\omega t)+Vs\sin(\omega t) \end{aligned} \tag{4-32}$$

also,

$$vL1(t) = VL1\sin(\omega t+\theta) \tag{4-33}$$

where

$$VL1 = \sqrt{(Vx+Vy-\omega LsIs)^2 + Vs^2}$$

$$\theta = \tan^{-1}\frac{(Vx+Vy-\omega LsIs)}{Vs}$$

However, the ripple voltages *Vx* and *Vy* are to be as small as possible, and the inductor *Ls* is normally small. Accordingly, as the term *(vx+vy-*ω*LsIs)* becomes small, the phase shift angle θ approaches zero.

The inductor current is found from an integrating equation (4-33) and dividing by ωL1. The result is

$$iL1(t) = \frac{VL1}{\omega L1}\cos(\omega t+\theta) + dc\ term \tag{4-34}$$

The dc term, a constant from the integration, is the dc current flowing in the inductor $L1$. The average duty cycle that the inductor $L1$ is connected to the load is 0.5. The average current in the output capacitor $C2$ must be zero; otherwise, the output voltage will not stabilize. Hence, we may conclude that the dc current in the inductor $L1$ is equal to the load current. Therefore,

$$iL1(t) = \frac{VL1}{\omega L1}\cos(\omega t+\theta) + \frac{VO}{R} \tag{4-35}$$

With the capacitor current equations from the state space averaging equation, we have

$$C1\frac{dvc(t)}{dt} = -D'is(t) - DiL1(t) \tag{4-36}$$

and

$$C2\frac{dvo(t)}{dt} = Dis(t) + D'iL1(t) - \frac{vo(t)}{R} \tag{4-37}$$

From the steady state analysis, we know that the duty cycle is varied only slightly with a sinusoidal function. The average of the duty cycle is 0.5. Therefore, in the steady state consideration, we can substitute D and D' with 0.5.

Substituting equations (4-35) and $is = Is\ \sin(\omega t)$ into equations (4-36) and (4-37), we obtain

$$C1\frac{dvc(t)}{dt} = -0.5Is\sin(\omega t)-0.5(\frac{VL1}{\omega L1}\cos(\omega t+\theta)+\frac{VO}{R})$$
$$vc(t) = \frac{Is}{2\omega C1}\cos(\omega t)-\frac{VL1}{2\omega^2 C1L1}\sin(\omega t+\theta)-\frac{VO}{2C1R}t \quad (4\text{-}38)$$

and

$$C2\frac{dvo(t)}{dt} = 0.5Is\sin(\omega t)+0.5(\frac{VL1}{\omega L1}\cos(\omega t+\theta)+\frac{VO}{R})-\frac{VO}{R}$$
$$vo(t) = -\frac{Is}{2\omega C2}\cos(\omega t)+\frac{VL1}{2\omega^2 C2L1}\sin(\omega t+\theta)-\frac{VO}{2C2R}t \quad (4\text{-}39)$$

We know that equations (4-38) and (4-39) equal the equation (4-25) and (4-26) respectively. The ripple voltages *vx(t)* and *vy(t)* can be found by eliminating the dc terms, so we arrive at

$$vx(t) = \frac{Is}{2\omega C1}\cos(\omega t)-\frac{VL1}{2\omega^2 C1L1}\sin(\omega t+\theta) \quad (4\text{-}40)$$

and

$$vy(t) = -\frac{Is}{2\omega C2}\cos(\omega t)+\frac{VL1}{2\omega^2 C2L1}\sin(\omega t+\theta) \quad (4\text{-}41)$$

In practice, the inductor current *IL1*, which is *VL1/ωL1*, will be small when compared to the input current *Is*. Thus, from the equations (4-40) and (4-41) can be simplified to

$$vx(t) = Vx\cos(\omega t) = \frac{Is}{2\omega C1}\cos(\omega t) \quad (4\text{-}42)$$

and

$$vy(t) = Vy\cos(\omega t) = -\frac{Is}{2\omega C2}\cos(\omega t) \qquad (4\text{-}43)$$

Therefore, the voltage across the capacitor $C2$ in terms of the input voltage and input current is

$$vo(t) = \frac{VsIs}{2R} - \frac{Is}{2\omega C2}\cos(\omega t) \qquad (4\text{-}44)$$

and the voltage across the capacitor $C1$ is

$$vc(t) = \frac{VsIs}{2R} + \frac{Is}{2\omega C1}\cos(\omega t) \qquad (4\text{-}45)$$

The technique described above can be used to design an ac-dc converter with low harmonic input currents. The most important step in the design of the converter is to choose the values of the energy storage elements.

CHAPTER V

COMPUTER SIMULATIONS

Simulation Study

Computer simulation was employed to examine and verify the new proposed converter. Two different software packages were used to perform the simulations. First, a PSPICE program was used to analyze the circuit. Then, a MATLAB program is used to solve the state space equations of the mathematical modeling of the converter. Results from PSPICE simulations and MATLAB simulations are compared in many aspects.

PSPICE is a well-known circuit simulation program. It is an extremely versatile industry-standard program that simulates analog and digital circuits. PSPICE contains built-in models for passive elements such as resistors, capacitors, and inductors; semiconductor devices such as diode, bipolar junction transistor (BJT), junction field-effect transistor (JFET), and metal oxide semiconductor field-effect transistor (MOSFET); independent voltage and current sources, and dependent voltage and current sources. An input file for PSPICE simulations can be directly created from a circuit description. An input file is described in terms of element models and the

way in which they are interconnected. The simulation allows the prediction of behavior performance of complicated circuits and systems without solving loop and node equation. By including control lines in an input file, PSPICE can be made to perform many kinds of circuit analysis.

MATLAB is a sophisticated mathematics and simulation environment that can be used to model and analyze dynamic system. It handles continuous, discrete, linear, or nonlinear system. MATLAB has extensive features for matrix manipulations. Because MATLAB is an interactive environment, many specialized toolboxes are provided. These toolboxes add specific functionality for applications such as digital signal processing, automatic control system design, nonlinear simulation, and optimization. MATLAB is different from PSPICE because it requires mathematical models that represent system configurations. These models are combinations of algebraic and differential equations.

Converter Configuration

As discussed earlier, a hysteresis band current control technique is used to produce a sinusoidal input current. The input current is measured and compared to a reference signal obtained from multiplying a unit reference signal and the feedback control signal. The unit reference signal is a reference signal with a unity amplitude. The phase angle of the unit reference signal is controllable. In practice, a phase lock loop can be used to

generate the unit reference signal. The feedback control signal is produced from an error voltage between a set value and an actual output voltage. A proportional controller is used in the simulated circuit. More details of the controller will be presented in Chapter VI.

The power circuit consists of two switches, two inductors, and two capacitors. The switches are power MOSFETs. They allow bidirectional flows of currents while withstanding one voltage polarity in their blocking state. Power BJTs with anti-parallel diodes also can be used. Nevertheless, power MOSFETs can operate at higher frequency than power BJTs with lower switching losses.

The converter control circuit and a power circuit used in PSPICE simulations are shown in Figure 31.

PSPICE Simulations

First, we consider the ripple input current and switching frequencies. The reference current is a sinusoidal wave with a unity power factor. The parameters in simulations are: Ls = 20 mH, $L1$ = 150 mH, $C1$ = 3000 uF, $C2$ = 3000 uF, RL = 50 Ω, Vs = 100 V. VO = 160 Vdc. With losses in the reactive components in the system, we add series resistances in the inductors and leakage currents in the capacitors. The Q factor for the inductors selected for lowest cost is usually between 50 and 150 (Arrillaga 1985). The leakage currents are included by adding parallel resistances to

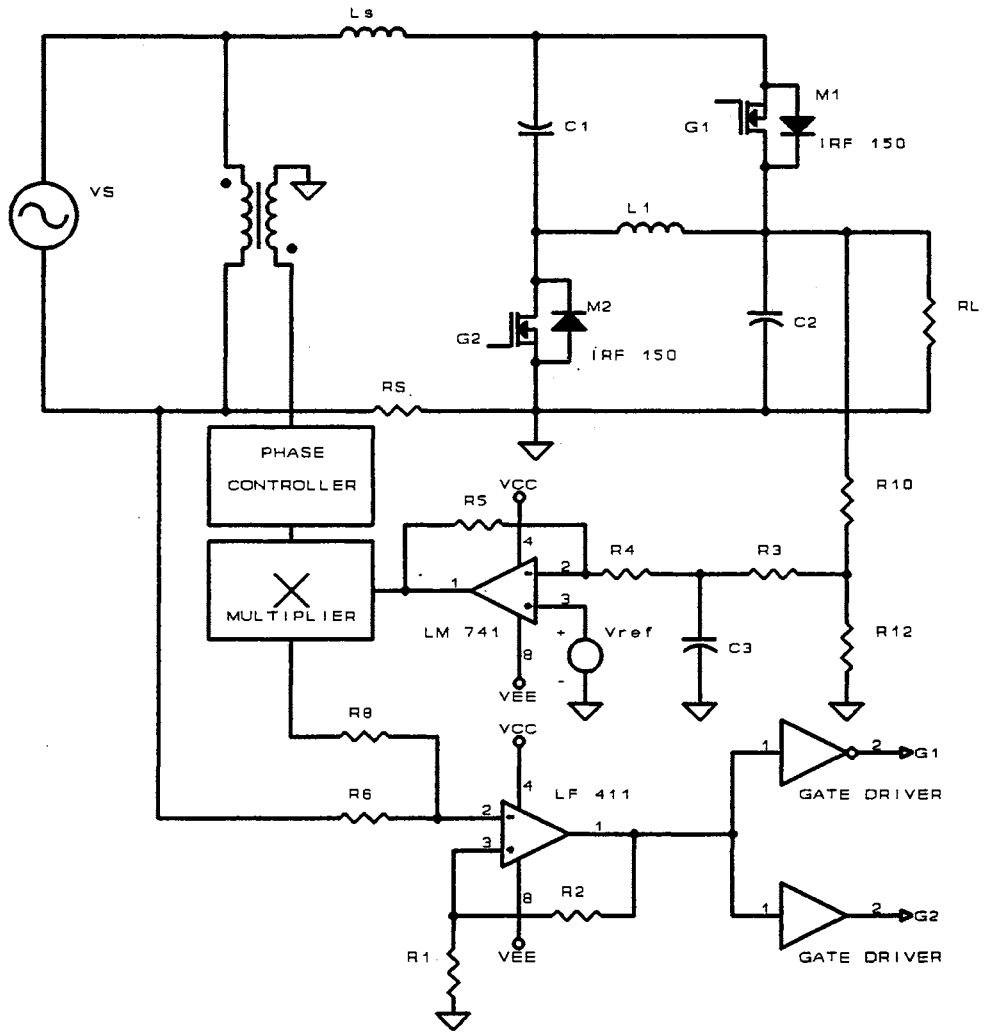

Figure 31 The system under study

the capacitors. The specified maximum leakage current for an electrolytic capacitor is approximately six times of the multiplication of its capacitance and rated voltage (Thorborg). For a 3000 uF capacitor with a rated voltage of 350 V., it will be about 6 mA. Typical values that we used for losses are: $RLs = 0.125\ \Omega$, $RL1 = 0.942\ \Omega$, $RC1 = 50\ k\Omega$, and $RC2 = 50\ k\Omega$. The switches are IRF150, medium speed power MOSFETs. An operational amplifier LM741 is used for the feedback loop control, and the hysteresis band control is performed by a high speed comparator LF 411. The input PSPICE file represented the converter circuit is presented in Appendix.

The simulation result illustrated in Figure 32 shows the input current waveform, which is the current in the inductor *Ls*. The input current is obviously a sinusoidal wave with some ripples. The minimum switching frequency occurs at either a positive or a negative peak of the input current waveform as we predicted by equation (4-7). A frequency spectrum of the input current is shown in Figure 33. The main component is the power line frequency with insignificant switching frequency components. The total harmonic distortion (THD) is 1.83%. Other harmonic components are shown in quantities as follows.

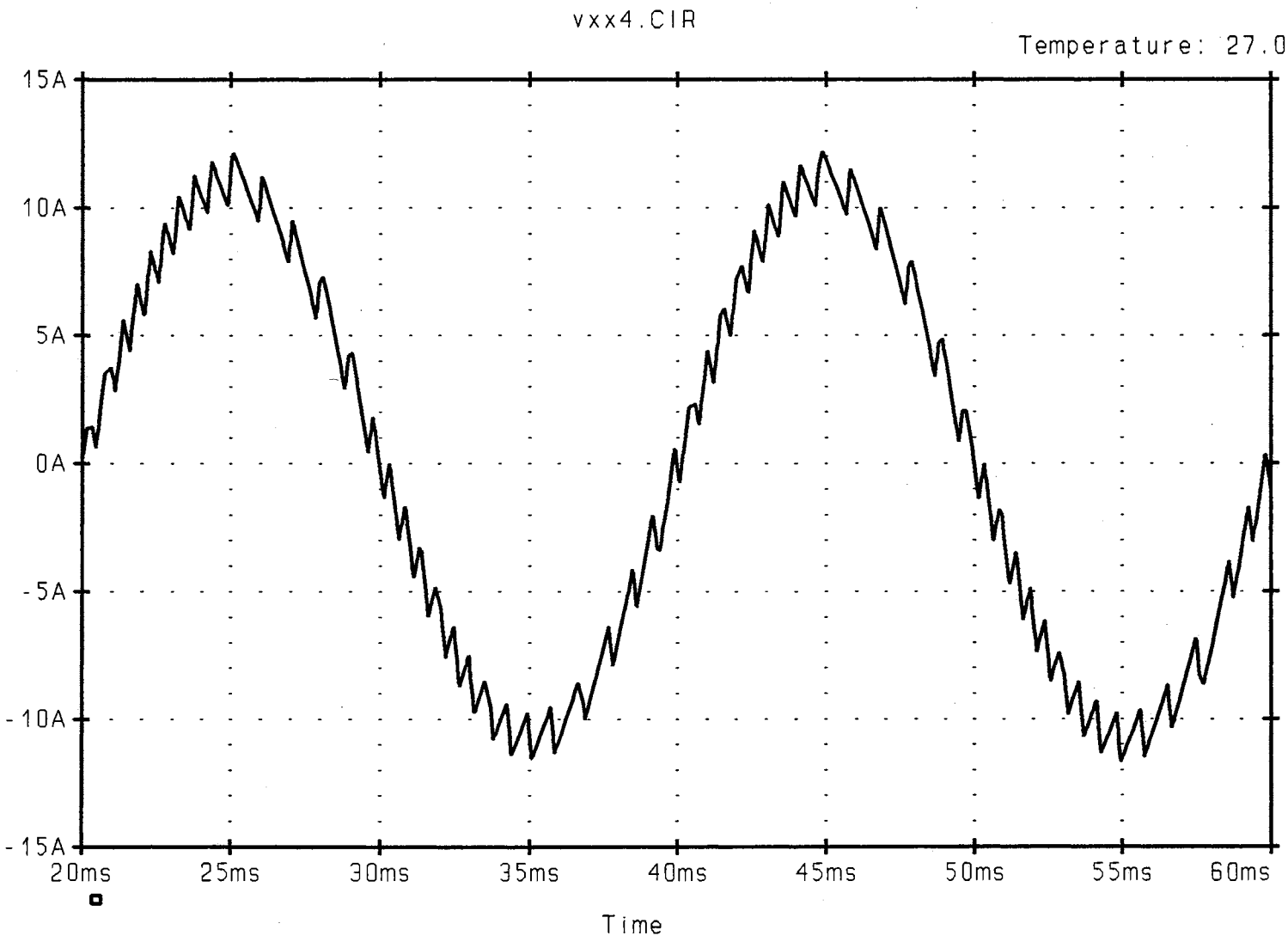

Figure 32 The input current of the converter

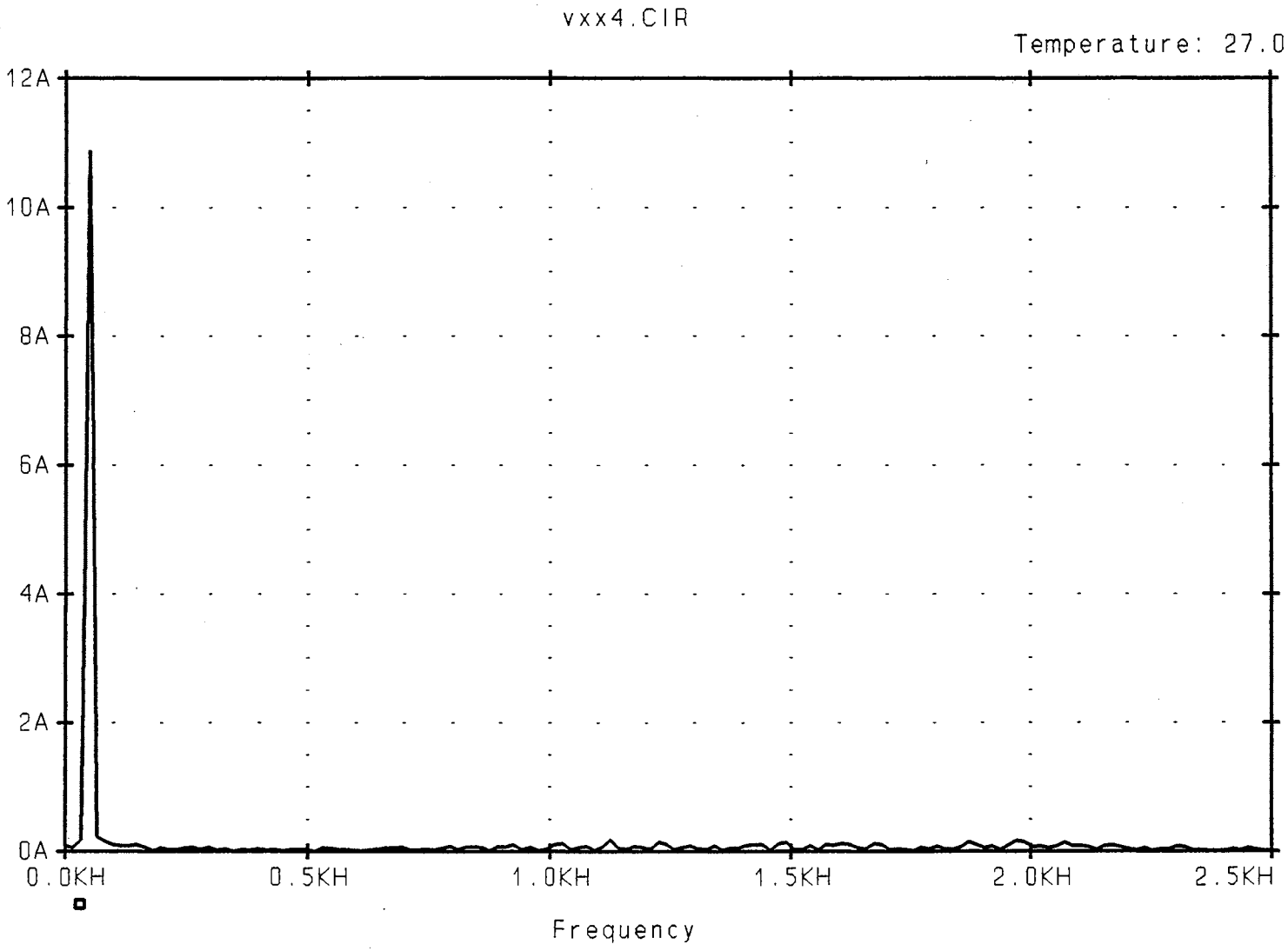

Figure 33 A frequency spectrum of the input current

FOURIER COMPONENTS OF TRANSIENT RESPONSE iLs

HARMONIC NO	FREQUENCY (HZ)	FOURIER COMPONENT	NORMALIZED COMPONENT	PHASE (DEG)	NORMALIZED (DEG)
1	5.000E+01	1.112E+01	1.000E+00	-2.320E-01	0.000E+00
2	1.000E+02	1.765E-01	1.588E-02	-3.178E+01	-3.155E+01
3	1.500E+02	2.903E-02	2.610E-03	-1.319E+02	-1.317E+02
4	2.000E+02	6.581E-02	5.919E-03	-8.362E+01	-8.339E+01
5	2.500E+02	2.279E-02	2.050E-03	-1.713E+02	-1.710E+02
6	3.000E+02	1.515E-02	1.362E-03	1.455E+02	1.457E+02
7	3.500E+02	5.355E-02	4.816E-03	-3.162E+01	-3.139E+01
8	4.000E+02	3.103E-02	2.791E-03	-1.497E+02	-1.494E+02
9	4.500E+02	3.026E-02	2.721E-03	-6.409E+01	-6.385E+01

TOTAL HARMONIC DISTORTION = 1.839499E+00 PERCENT

The hysteresis band can be reduced by adjusting the resistors in the hysteresis control circuit. Consequently, the input current waveform is much closer to the reference current, which is a sinusoidal wave, as shown in Figure 34. In this case, the harmonic distortion is almost negligible. However, the switching frequency is increased.

Simultaneous waveforms of the inductor currents *iLs(t)* and *iL1(t)* are shown in Figure 35. The current in the inductor *L1* consists of an ac component and a dc component. The dc current is equal to the load current. The current waveform in the inductors *L1* has approximately the waveforms and magnitudes as predicted in equation (4-35). The capacitor voltages *vc(t)* and *vo(t)* are shown in Figure 36. The capacitor voltages *vc(t)* and *vo(t)* are composed with dc values and ripple voltages. The dc components are almost

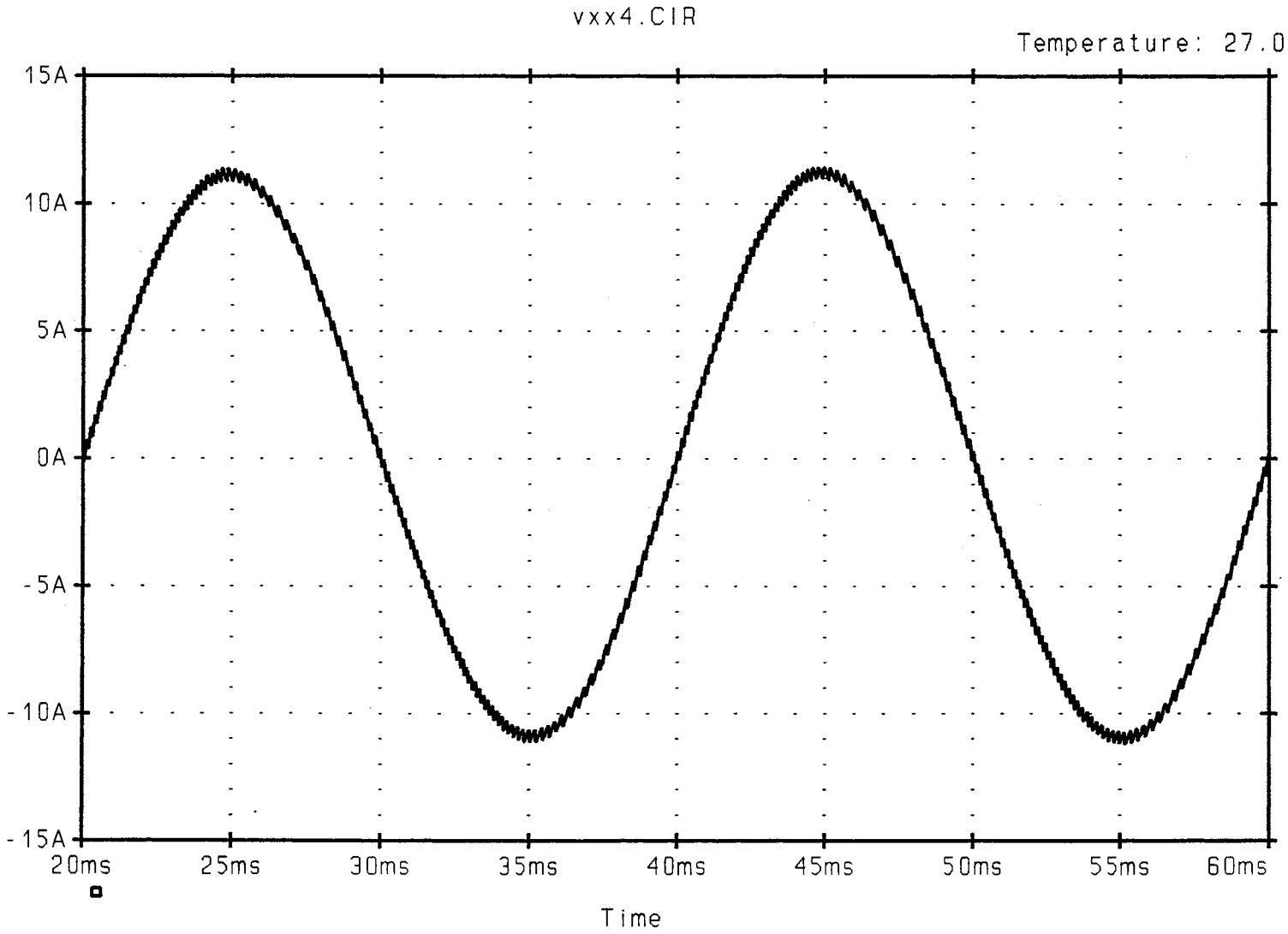

Figure 34 The input current with a small hysteresis band

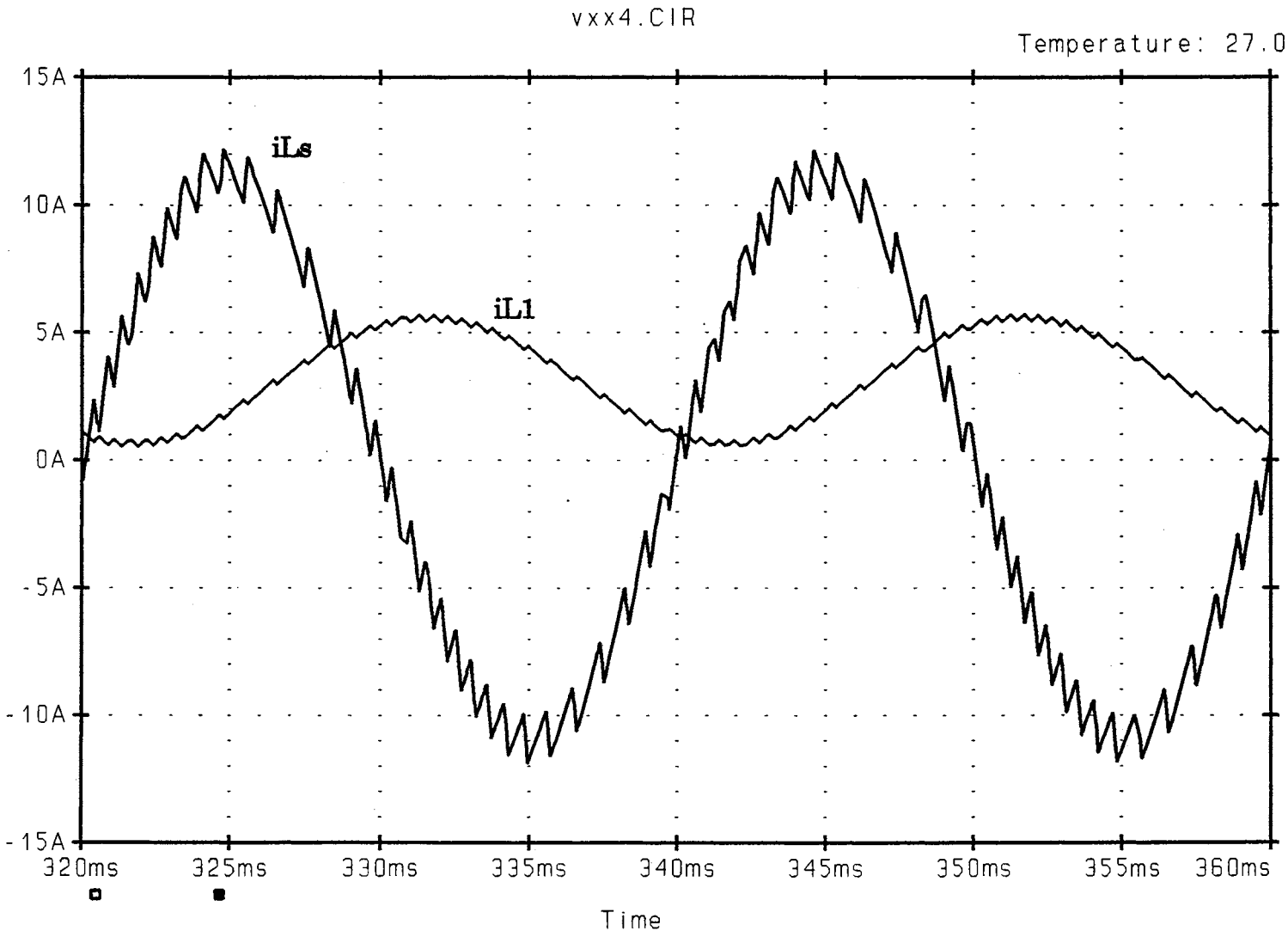

Figure 35 Current waveforms in the inductors Ls and L1

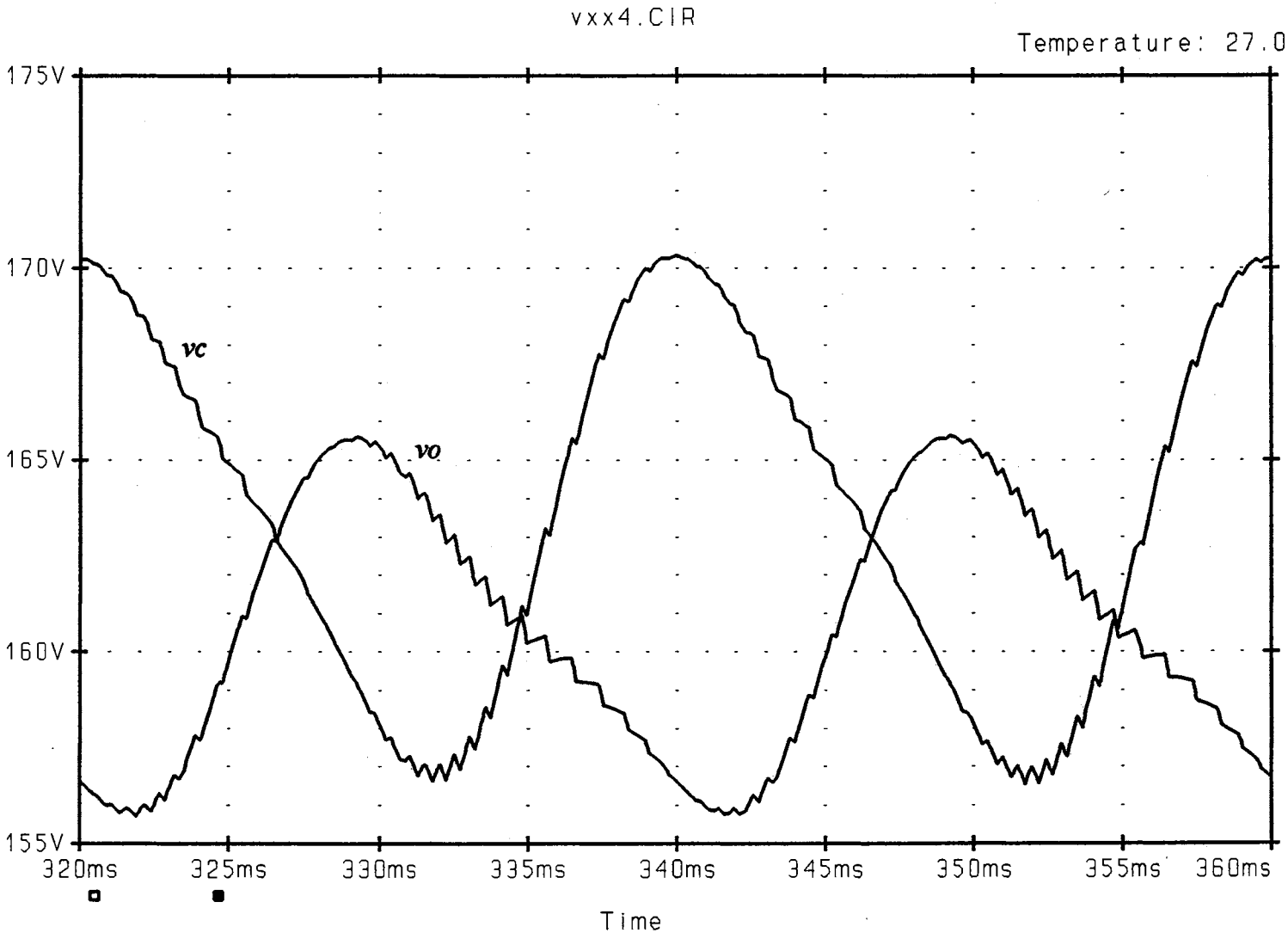

Figure 36 Voltage waveforms across the capacitors C1 and C2

symmetrical as we expect that the sum of dc components across the capacitors should be zero. The dc values and the ripple voltage are close to our calculations.

Converter Efficiency

The efficiency of a converter is defined as the ratio of the total output power to the total input power. The output power can be calculated from VO^2/ RL, and the input power is VS IS, where VS and IS are RMS input voltage and current. From PSPICE simulations in Figure 35 and 36, the converter efficiency is 94%.

We know that the major sources of inefficiency are losses in switches. The switches have saturation losses during its ON time, leakage losses during its OFF time (usually negligible), and switching losses. In almost all cases, the peak instantaneous power dissipation in switches occurs either at turn-on or turn-off period. Switching losses or saturation losses predominate, depending upon the frequency of operation.

To verify that the significant losses come from switches, we omit losses in the passive components. The results from simulations are shown in Figure 37 and 38. The converter efficiency increases to 96.3%. On the other hand, losses in the switches are 3.7%.

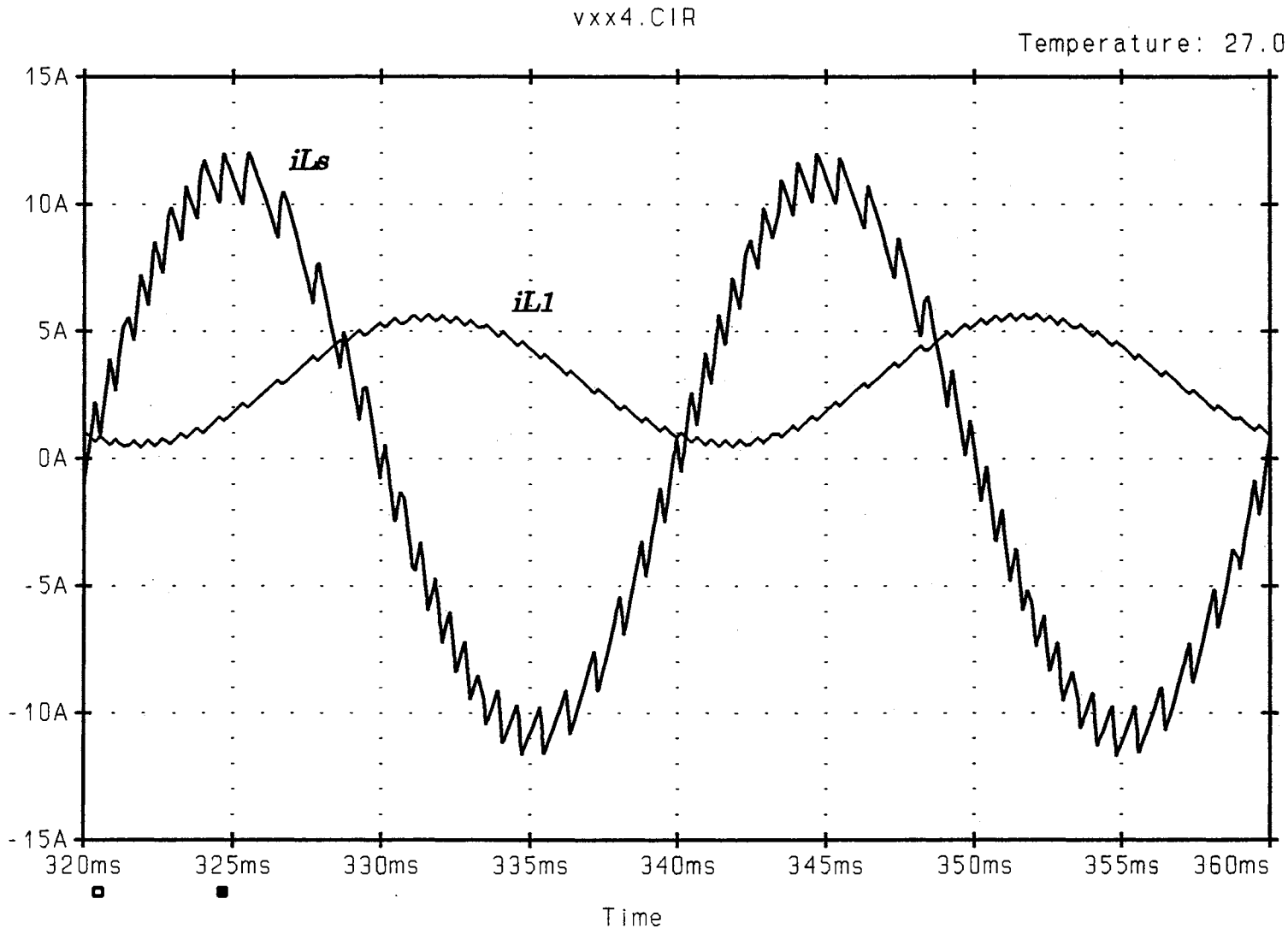

Figure 37 Current waveforms in the inductors Ls and L1 without losses in the reactive components

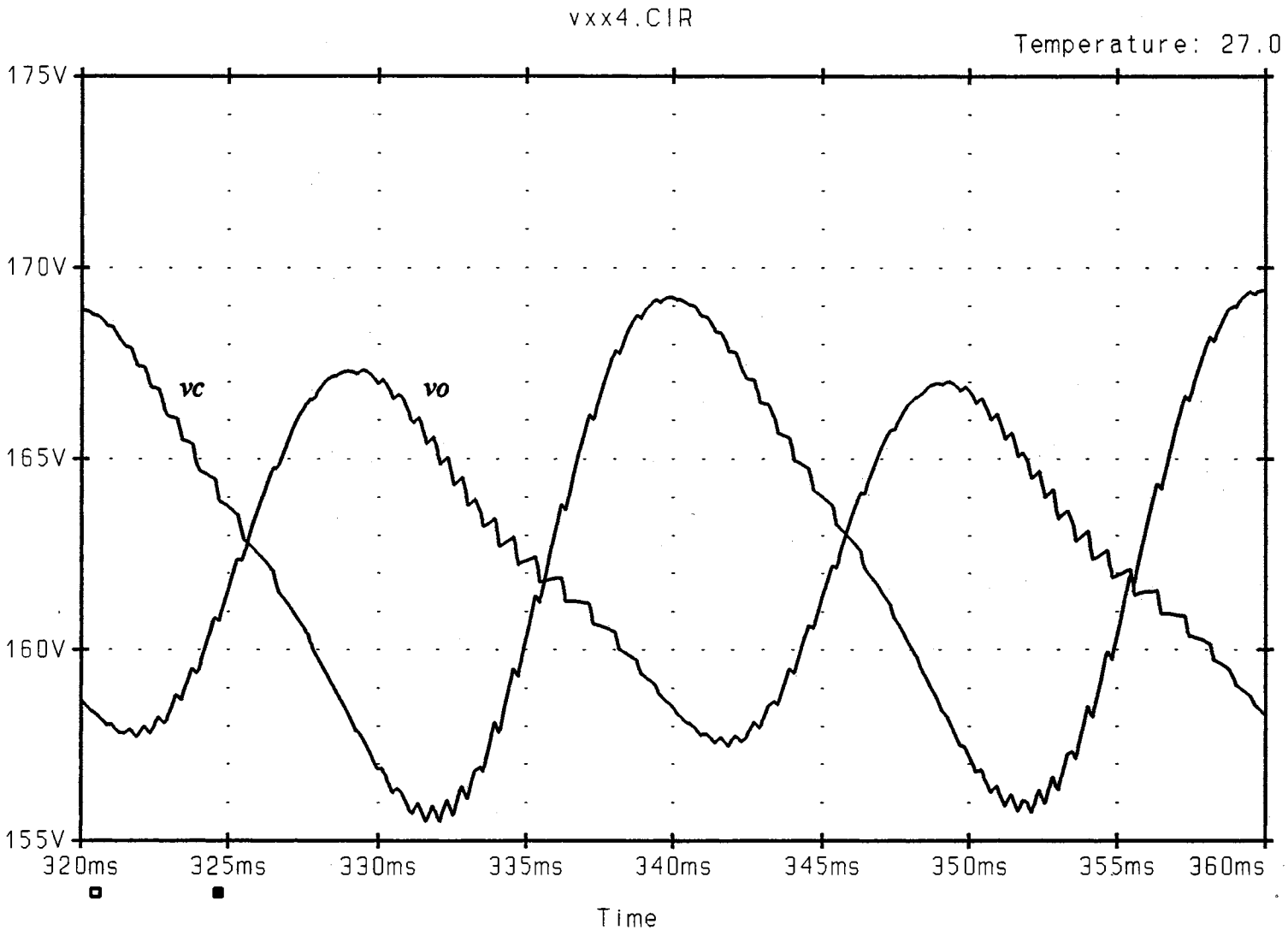

Figure 38 Voltage waveforms across the capacitors C1 and C2 without losses in the reactive components

Bidirectional Power Flow Capability

Two significant features required for an ac-dc converter are a sinusoidal input current and bidirectionality.

The new converter meets these feature requirements. Not only does the new converter have a bidirectional power flow capability, but it also allows a controllable power factor. Real power and reactive power are controllable. These features can be achieved by controlling appropriate switch commands. In practice, the direction of power flow is controlled by inverting switch commands.

To demonstrate bidirectional power flow capability, we first describe the meaning of the direction of power flow. We usually define power flow by considering the sign of the power equation. For example, in a two port network, if $is(t) = Is\ sin(\omega t)$ is an input current, and $vs(t) = Vs\ sin(\omega t)$ is an input voltage, we can calculate an instantaneous input power as follows.

$$p(t) = VsIs\ \sin^2(\omega t) \tag{5-1}$$

An average input power can be found from

$$\begin{aligned} P &= \frac{1}{2\pi}\int_0^{2\pi} VsIs\sin^2(\omega t)dt \\ &= \frac{VsIs}{2} \end{aligned} \tag{5-2}$$

The positive sign indicates that power flows from an input source to the network. However, if an input current leads or lags an input voltage by greater than 90 degrees, we find that the average input power is

$$P = \frac{1}{2\pi}\int_0^{2\pi} Vs\sin(\omega t)Is\sin(\omega t+180\pm\theta) = -\frac{VsIs}{2}\cos(\theta) \quad (5\text{-}3)$$

Hence, since the sign of the power equation is negative, power flows from the network back to the input source.

To examine the bidirectional power flow capability and an adjustable power factor, we use the converter circuit with switching between a resistive load and a dc voltage source at the output terminal of the converter. The dc voltage source replaces the resistive load during the inverse power transfer mode. The input current is forced to track the desired reference signal, which is adjustable in the controller. The desired reference signal can be any angle of the phase shift. The results from PSPICE simulations are shown in Figure 39-44.

In Figure 39 with a reference input voltage waveform, the input current is controlled be a unity power factor while the converter is supplying a dc voltage to a resistive load.

In Figure 40, the input current is reversed at t = 35 ms with a unity power factor for both directions of the power flow. However, the simulation

does not include the feedback loop, so the reversing time depends on the inductor Ls only.

The input current waveforms shown in Figures 41 and 42 illustrate as the input currents are controlled with leading and lagging power factor. In fact, the proposed topology allows the input current can be in any angle in the four quadrants of the current vector space.

To demonstrate the capability to control the input current vector, the input current shown in Figure 43 is forced to reverse from a unity power factor to a leading power factor in an opposite power flow.

In contrast, in Figure 44 the input current is controlled to shift from a unity power factor to a lagging power factor with an opposite power flow.

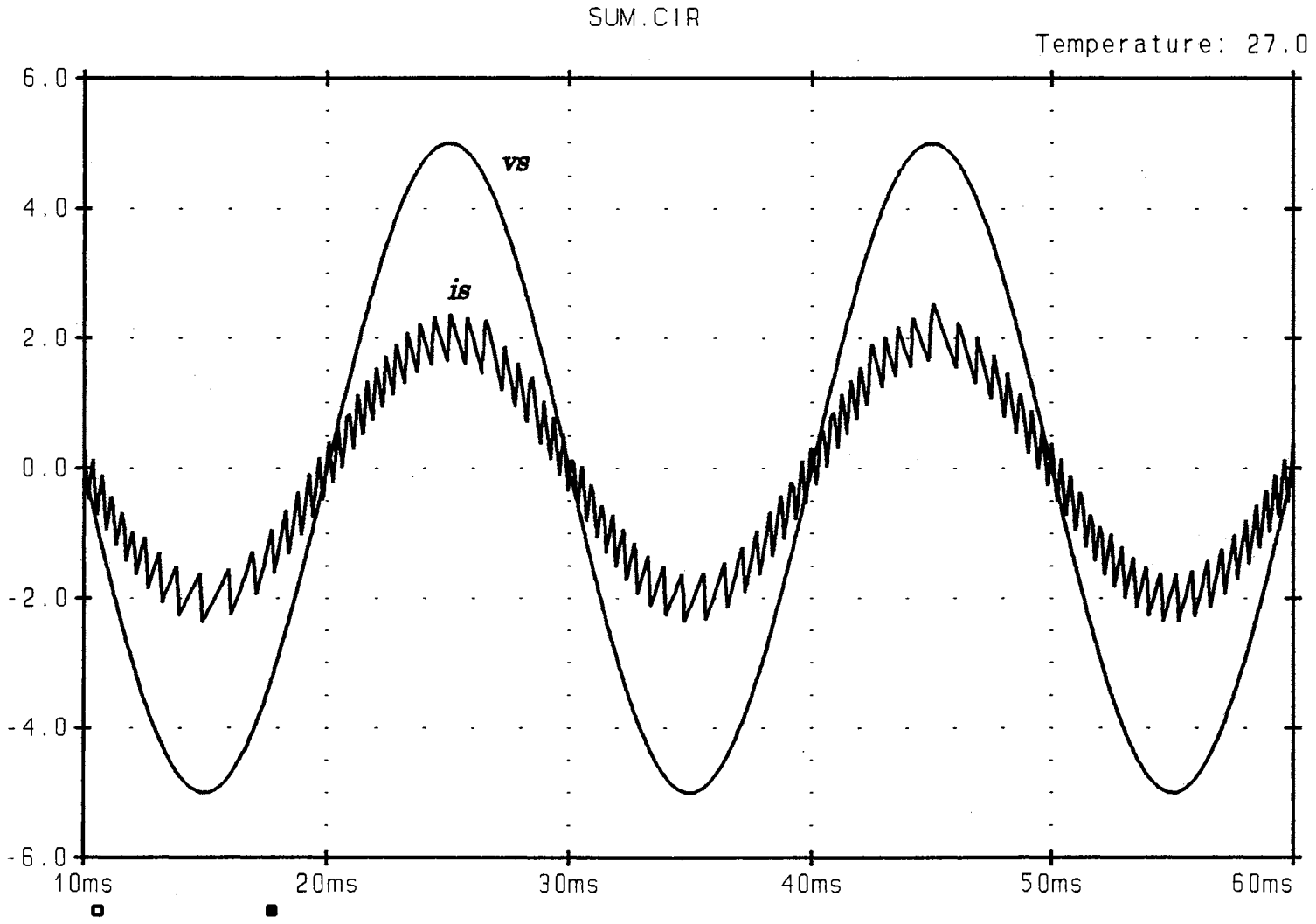

Figure 39 Input current waveform with unity power factor

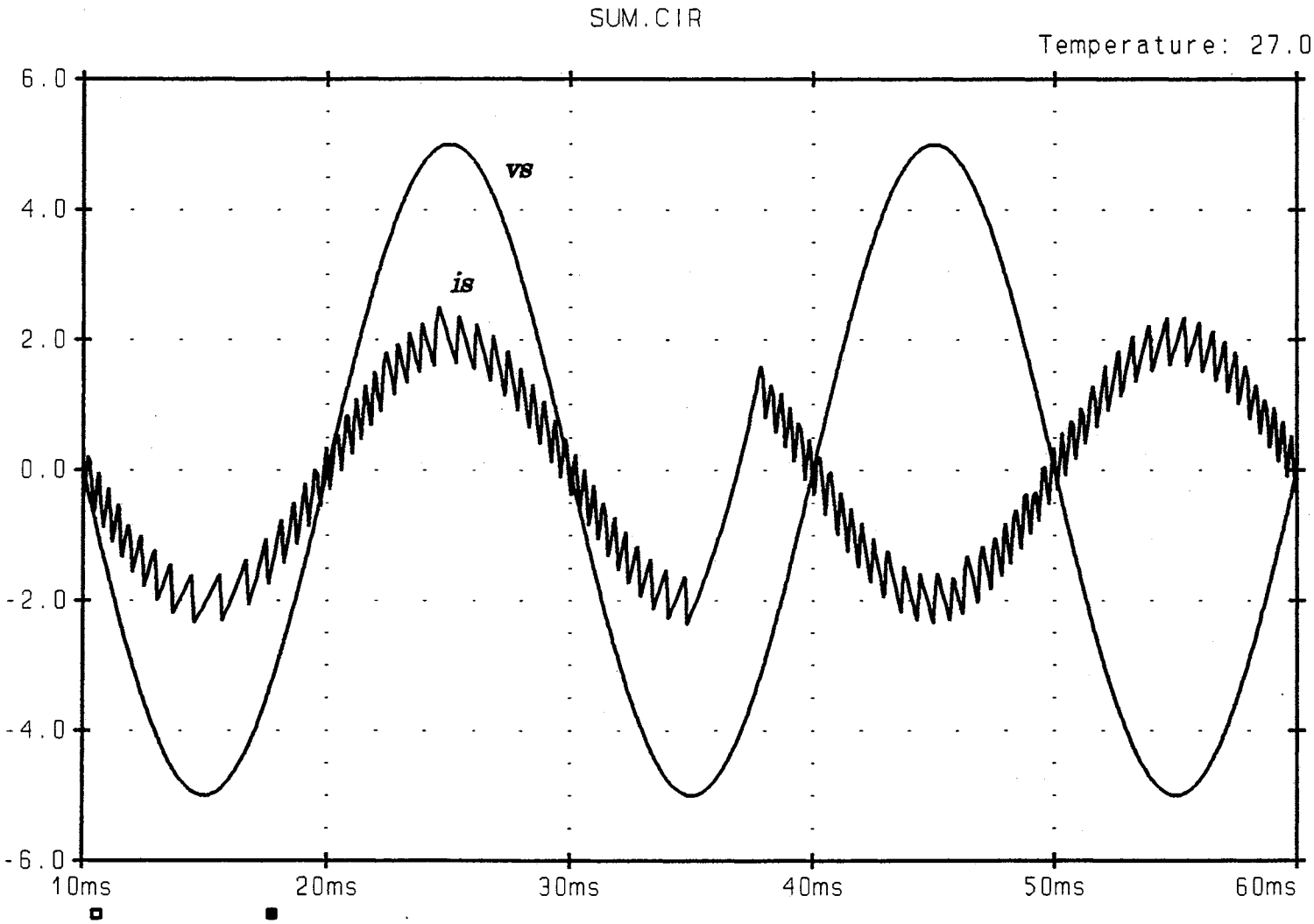

Figure 40 Input current waveform during the power transfer mode from the load side to the source side with a unity power factor

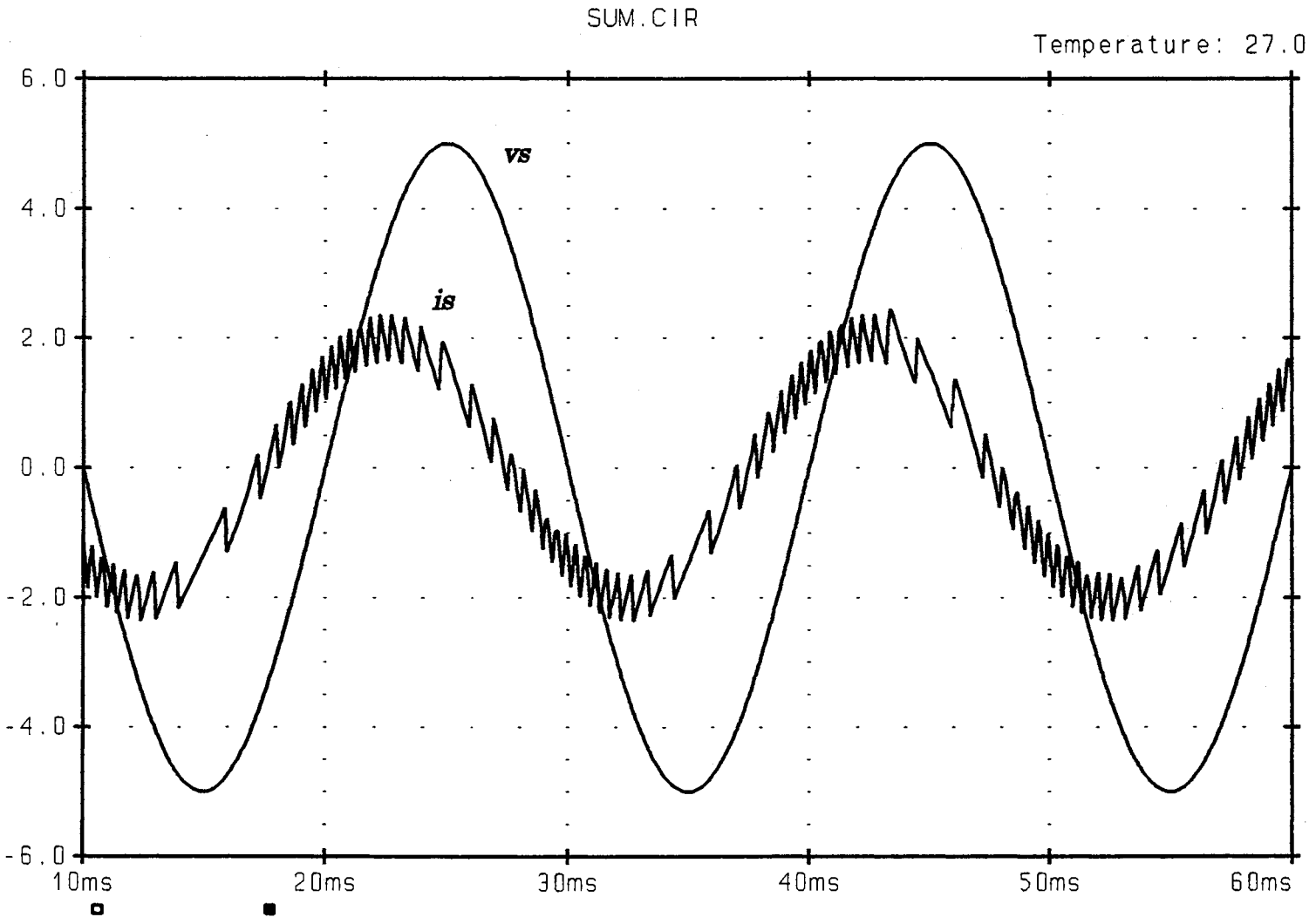

Figure 41 Input current waveform with 0.7 leading power factor

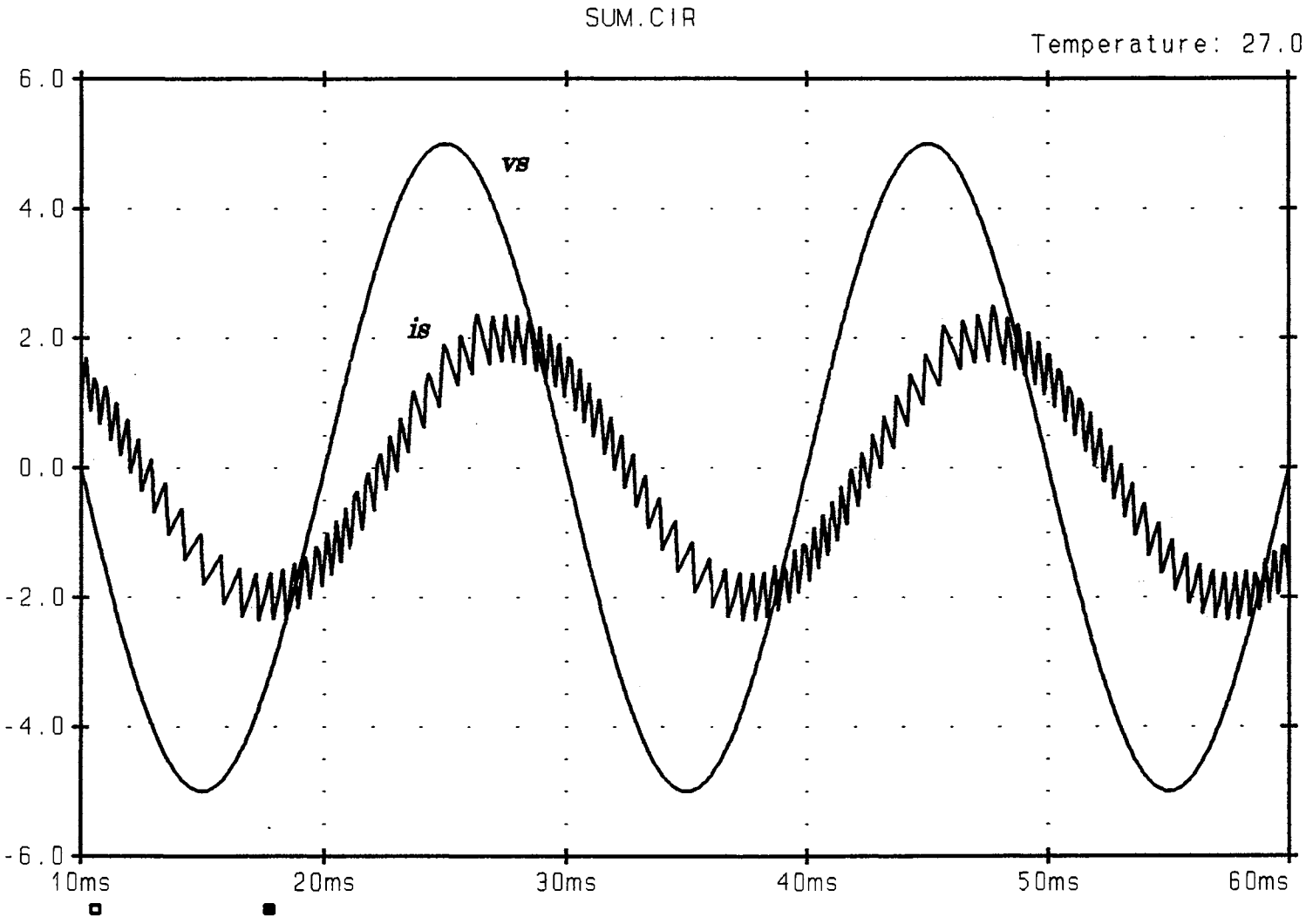

Figure 42 Input current waveform with 0.7 lagging power factor

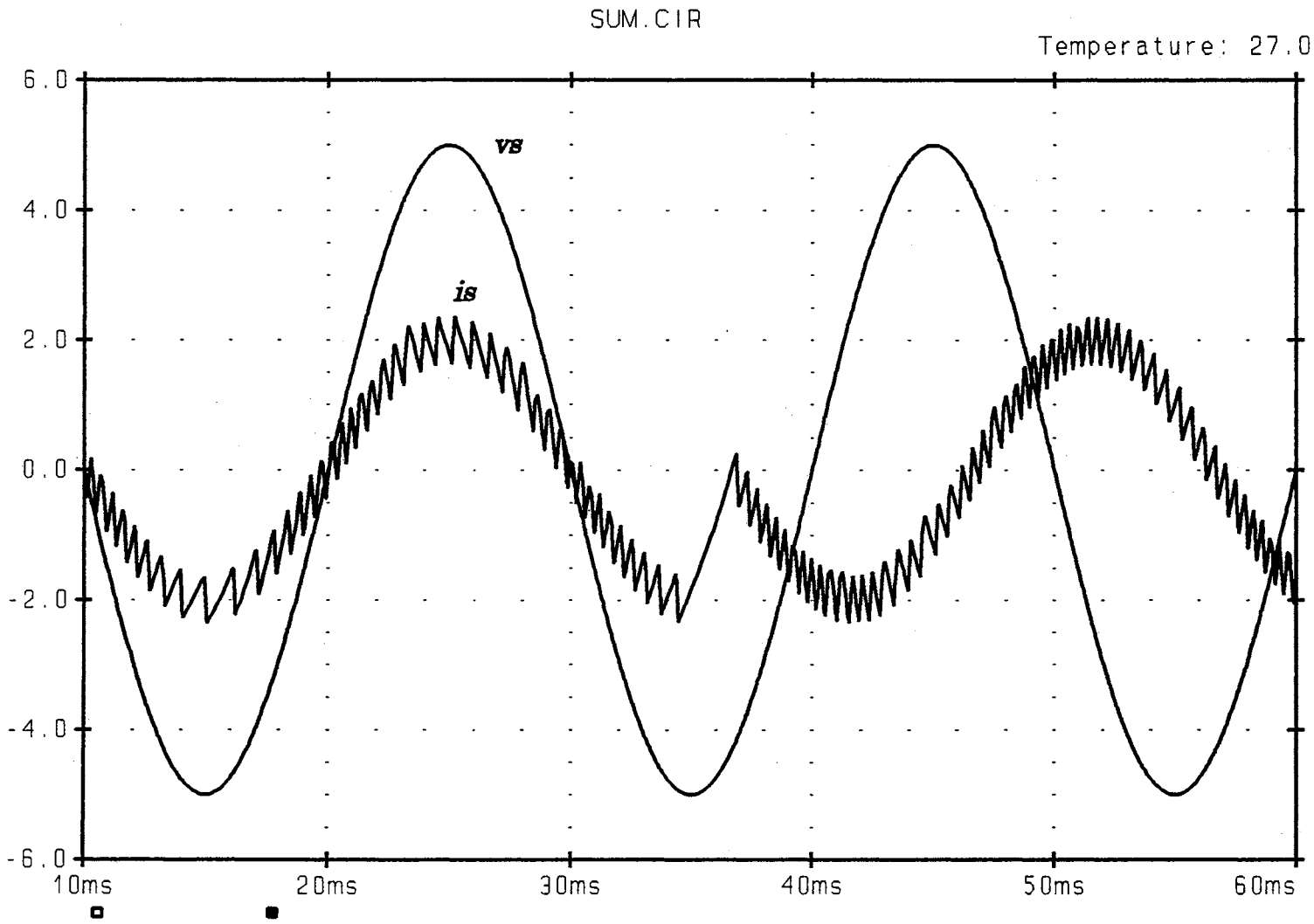

Figure 43 Input current waveform during the power transfer mode from the load side to the source with a 0.5 leading power factor

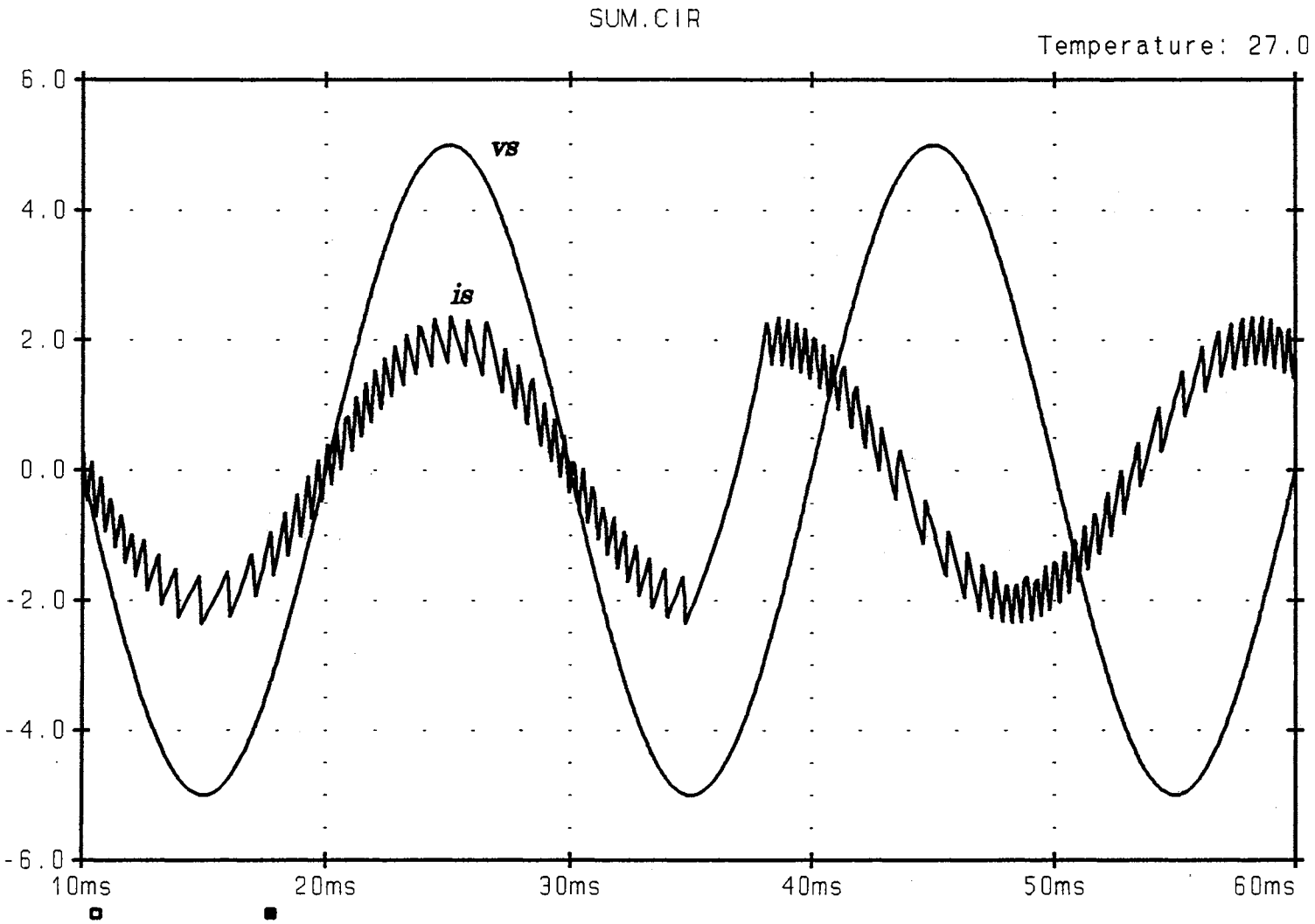

Figure 44 Input current waveform during the power transfer mode from the load side to the source side with a 0.5 lagging power factor

Mathematical Model Computation

As discussed in Chapter IV, the mathematical model representing the converter is:

$$\begin{bmatrix} \frac{diLs}{dt} \\ \frac{diL1}{dt} \\ \frac{dvc}{dt} \\ \frac{dvo}{dt} \end{bmatrix} = \begin{bmatrix} 0 & 0 & \frac{(1-D)}{Ls} & -\frac{D}{Ls} \\ 0 & 0 & \frac{D}{L1} & -\frac{(1-D)}{L1} \\ -\frac{(1-D)}{C1} & -\frac{D}{C1} & 0 & 0 \\ \frac{D}{C2} & \frac{(1-D)}{C2} & 0 & -\frac{1}{RC2} \end{bmatrix} \begin{bmatrix} iLs \\ iL1 \\ vc \\ vo \end{bmatrix} + \begin{bmatrix} 1 \\ 0 \\ 0 \\ 0 \end{bmatrix} vs$$

Since the current in the inductor *Ls* is forced to be a sine wave with both a magnitude and a phase angle, the state variables *iLs* can be eliminated. The reduced configuration is shown in Figure 45.

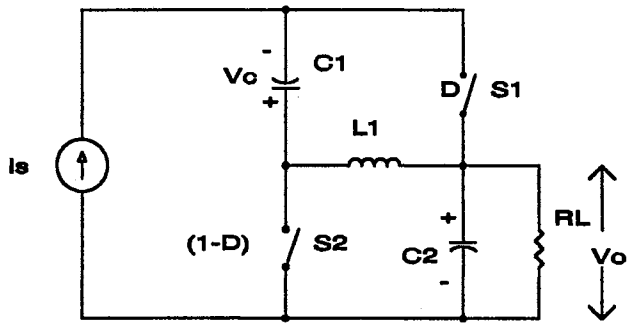

Figure 45 The reduced configuration

Therefore, during S1 on and S2 off, we obtain

$$\begin{aligned} L1\frac{diL1}{dt} &= vc \\ C1\frac{dvc}{dt} &= -iL1 \\ C2\frac{dvo}{dt} &= -\frac{vo}{R}+is \end{aligned} \tag{5-4}$$

In a matrix form, we have

$$\begin{bmatrix} \frac{diL1}{dt} \\ \frac{dvc}{dt} \\ \frac{dvo}{dt} \end{bmatrix} = \begin{bmatrix} 0 & \frac{1}{L1} & 0 \\ -\frac{1}{C1} & 0 & 0 \\ 0 & 0 & -\frac{1}{RC2} \end{bmatrix} \begin{bmatrix} iL1 \\ vc \\ vo \end{bmatrix} + \begin{bmatrix} 0 \\ 0 \\ \frac{1}{C2} \end{bmatrix} is \tag{5-5}$$

In contrast, during S1 off and S2 on, we obtain

$$\begin{aligned} L1\frac{diL1}{dt} &= -vo \\ C1\frac{dvc}{dt} &= -is \\ C2\frac{dvo}{dt} &= iL1 -\frac{vo}{R} \end{aligned} \tag{5-6}$$

In a matrix form, we have

$$\begin{bmatrix} \frac{diL1}{dt} \\ \frac{dvc}{dt} \\ \frac{dvo}{dt} \end{bmatrix} = \begin{bmatrix} 0 & 0 & -\frac{1}{L1} \\ 0 & 0 & 0 \\ \frac{1}{C2} & 0 & -\frac{1}{RC2} \end{bmatrix} \begin{bmatrix} iL1 \\ vc \\ vo \end{bmatrix} + \begin{bmatrix} 0 \\ -\frac{1}{C1} \\ 0 \end{bmatrix} is \tag{5-7}$$

Using state space averaging method, the mathematical model representing the converter with three state variables is:

$$\begin{bmatrix} \frac{diL1}{dt} \\ \frac{dvc}{dt} \\ \frac{dvo}{dt} \end{bmatrix} = \begin{bmatrix} 0 & \frac{D}{L1} & -\frac{(1-D)}{L1} \\ -\frac{D}{C1} & 0 & 0 \\ \frac{(1-D)}{C2} & 0 & -\frac{1}{RC2} \end{bmatrix} \begin{bmatrix} iL1 \\ vc \\ vo \end{bmatrix} + \begin{bmatrix} 0 \\ -\frac{(1-D)}{C2} \\ \frac{D}{C2} \end{bmatrix} is \qquad (5\text{-}8)$$

Unfortunately, the state coefficients are time-varying because the duty cycle D is varied with time. Although the state coefficients are periodic functions, the transition matrix in an algebraic form is not obvious.

However, with a computer numerical method, we can examine the dynamic behavior of the system. MATLAB was used to solve for the dynamic solution. By using 2nd/3rd order Runge-Kutta method, we write a MATLAB input file program. The program is shown in the Appendix. The component parameters are used the same as we used in simulations described earlier by a PSPICE. The input current is represented by an ac current source with no ripple. The results are shown in Figures 46 and 47. Because the mathematical model assumes that the converter is a linear system, the solution from MATLAB simulations cannot express details in terms of ripple currents and switching frequencies. Comparing the results between the MATLAB simulation and the PSPICE simulation, we find that both of the simulations give the same outcome. Hence, the results from both simulation method confirm our model.

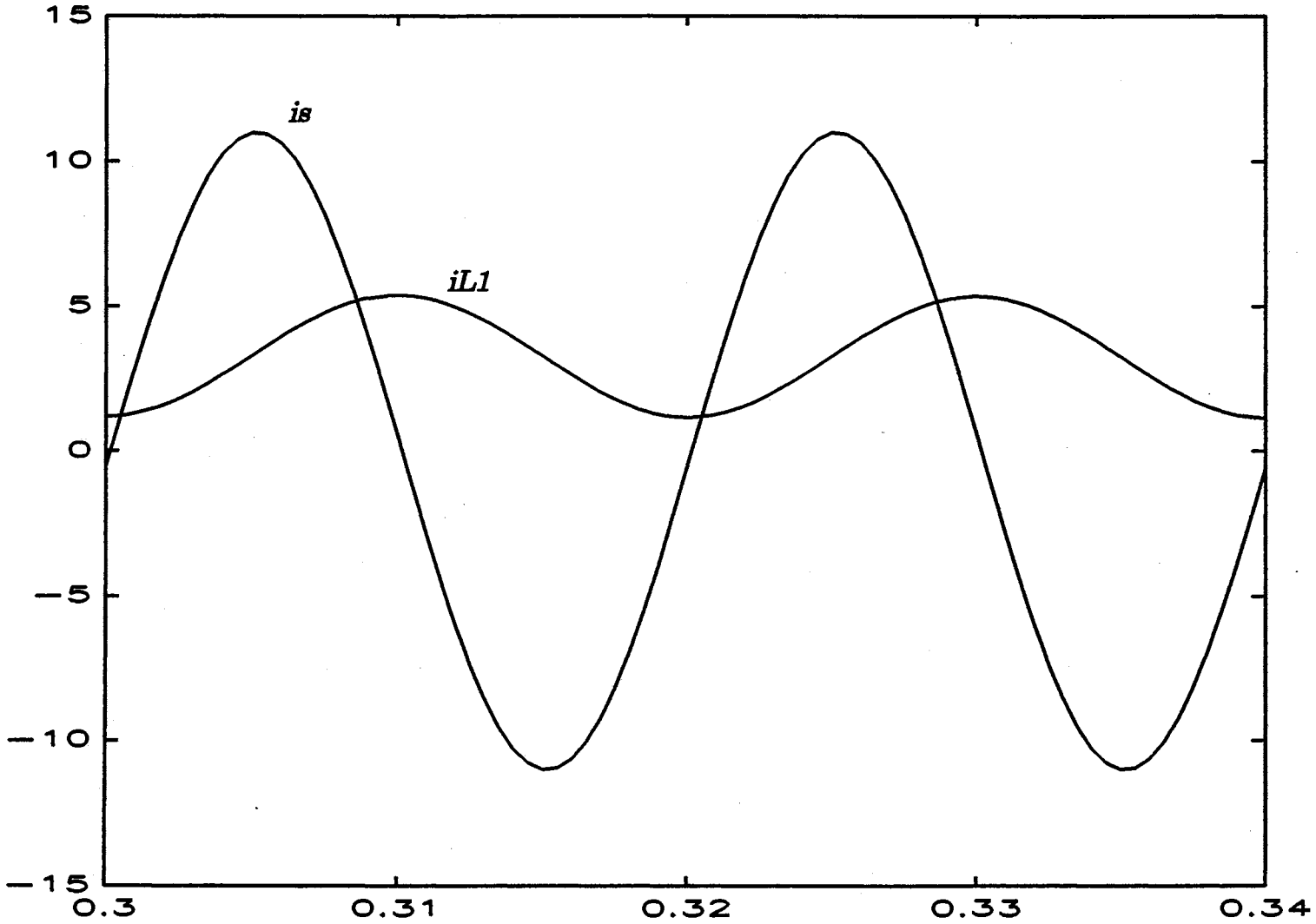

Figure 46 Current waveforms in the inductors Ls and L1 simulated by MATLAB

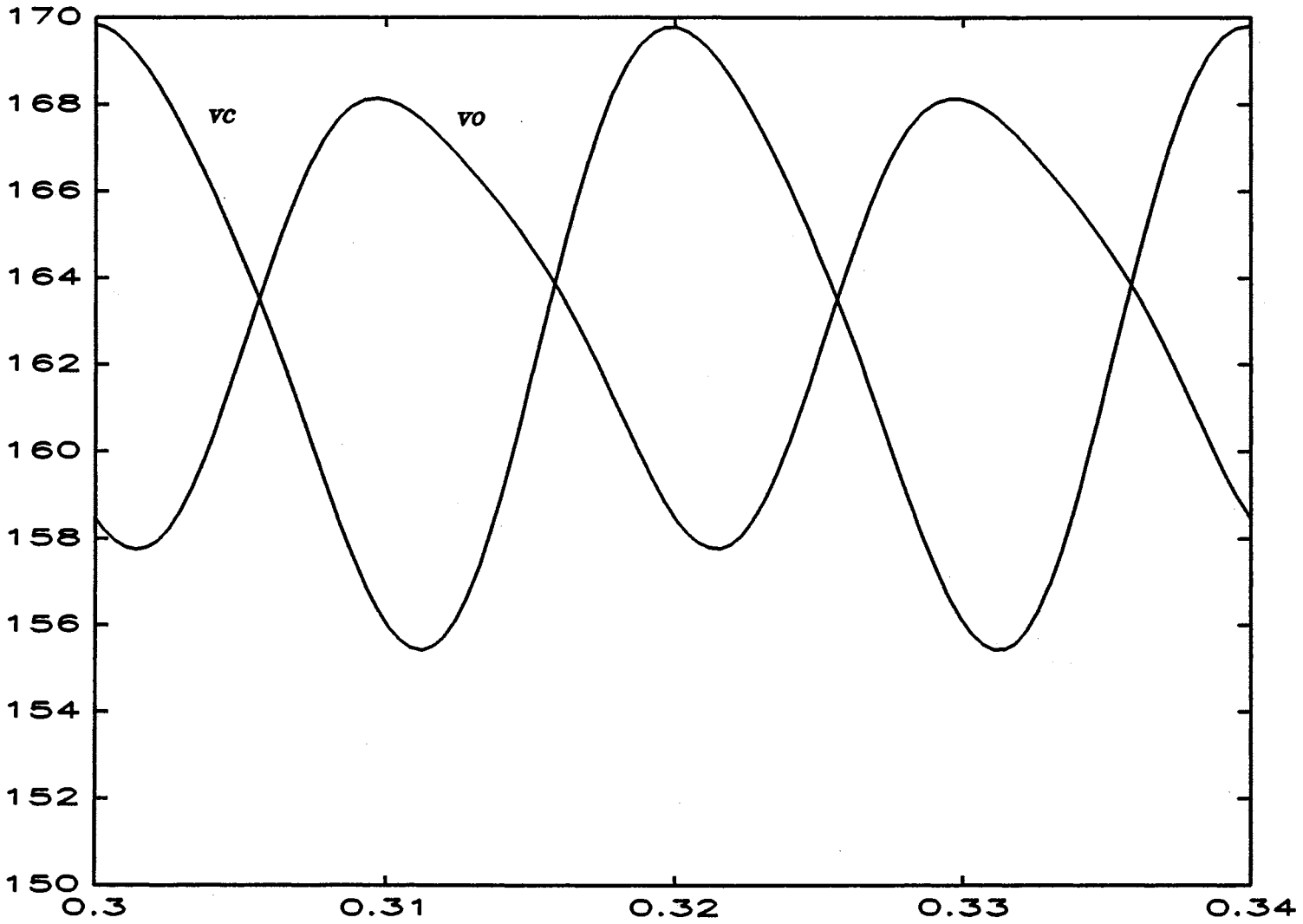

Figure 47 Voltages across the capacitors C1 and C2 simulated by MATLAB

CHAPTER VI

CONTROLLER CONFIGURATION

Stability Considerations

The purpose of applying feedback is to determine the proper magnitude of the input current and to improve the response of the open loop system. In the steady state condition, the magnitude of the input current must agree with the power balance between the input and the output. We directly control the input current to keep the output voltage constant.

The open-loop transfer function of the converter can be approximately obtained by assuming that an average of the duty cycle is 0.5. Consequently, the average state space equation, which we discussed in Chapter V, can be written as

$$\begin{bmatrix} \frac{diL1}{dt} \\ \frac{dvc}{dt} \\ \frac{dvo}{dt} \end{bmatrix} = \begin{bmatrix} 0 & \frac{0.5}{L1} & -\frac{0.5}{L1} \\ -\frac{0.5}{C1} & 0 & 0 \\ \frac{0.5}{C2} & 0 & -\frac{1}{RC2} \end{bmatrix} \begin{bmatrix} iL1 \\ vc \\ vo \end{bmatrix} + \begin{bmatrix} 0 \\ -\frac{0.5}{C2} \\ \frac{0.5}{C2} \end{bmatrix} is \qquad (6\text{-}1)$$

From modern control theory, we know that the transfer function can be found from

$$H(s) = C[sI_n - A]^{-1}B + D \tag{6-2}$$

where $H(s)$ is the transfer function; A, B, C, and D are coefficient matrices of dimensions $n \times n$, $n \times r$, $m \times n$, and $m \times r$, respectively, and I_n is the $n \times n$ identity matrix. Therefore, we obtain

$$H(s) = \frac{2L1C1Rs^2}{4L1C1C2Rs^3+4L1C1s^2+(C1+C2)Rs+1} \tag{6-3}$$

where

$$[sI_n - A]^{-1} = \frac{\begin{bmatrix} 4L1C1s(C2Rs+1) & 2C1(C2Rs+1) & -2C1C2Rs \\ -2L1(C2Rs+1) & C1(4L1s(C2Rs+1)+R) & C2R \\ 2L1C1Rs & C2R & C2R(4L1C1s^2+1) \end{bmatrix}}{4L1C1s^2(C2Rs+1)+(C1+C2)Rs+1}$$

$$B = \begin{bmatrix} 0 \\ -\frac{1}{2C1} \\ \frac{1}{2C2} \end{bmatrix} \qquad C = [0 \;\; 0 \;\; 1] \qquad D = [0]$$

From the transfer function, we can predict the stability of the system. The Bode representation, which provides a convenient method of analyzing the system, is illustrated in Figure 48. The magnitude and phase shift of the open loop function are plotted by using the same parameters as the design example in Chapter V. The plots give two crossover points. The

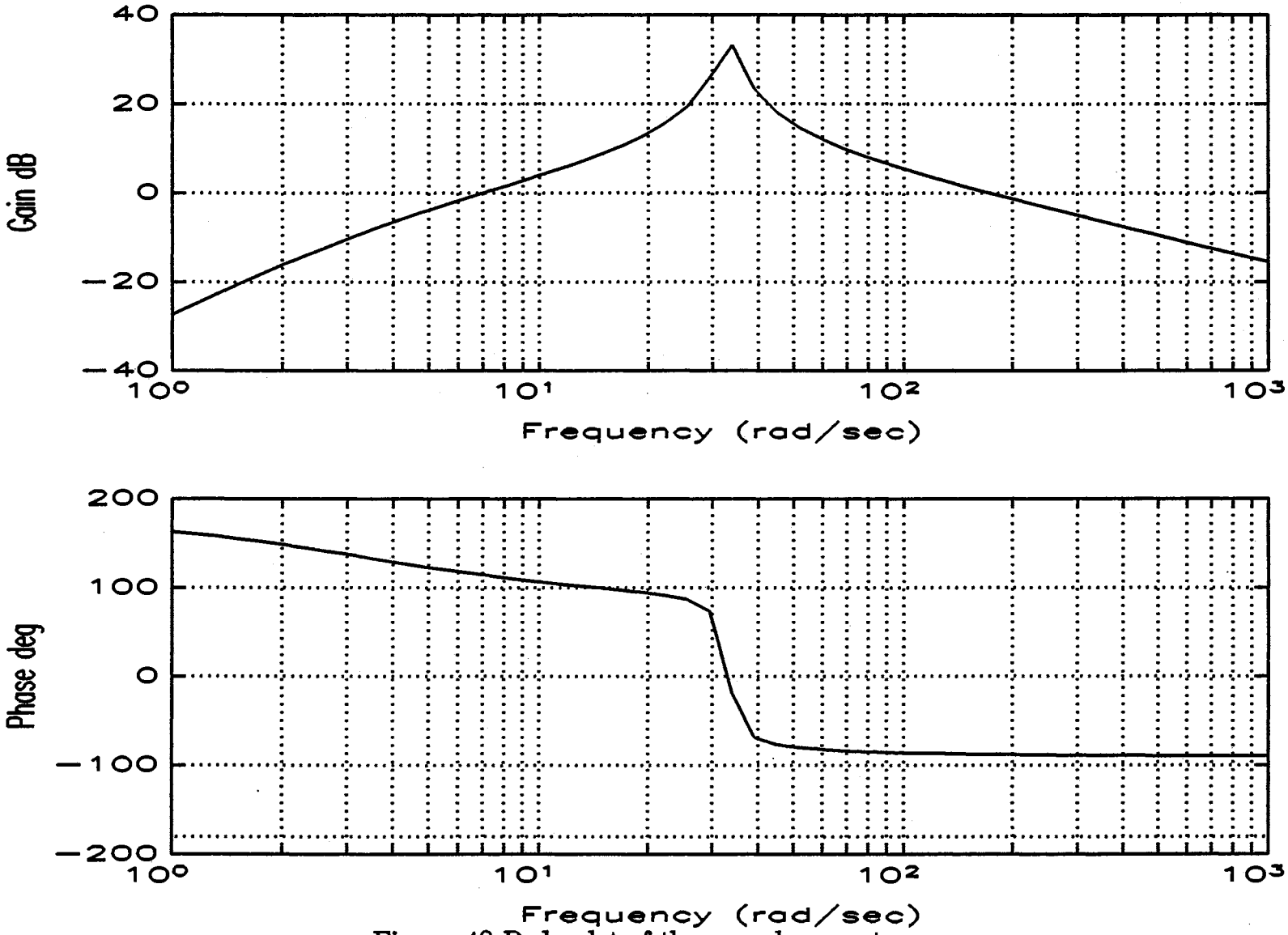

Figure 48 Bode plot of the open-loop system

crossover point is the point that the gain magnitude cross unity gain (0dB). Because the phase lead is less than 180 degrees at the low-frequency crossover point and the phase lag is less than 180 degrees at the high-frequency crossover point, the open-loop system is explicitly stable.

Closed-loop Control

For the closed-loop control, the feedback signal is used to determine the magnitude of the input current. The proper magnitude of the input current is obtained by multiplying the feedback signal and a unit reference waveform. The control configuration is shown in Figure 49. Under the closed-loop system, the output voltage *Vo* is measured and compared to the reference voltage *Vref*. The error is amplified by a gain *K* and used as the amplitude of the reference current. The converter is inherently sluggish. Since the purpose of the converter is to be used as a dc voltage source, we usually want the output voltage to be constant. The output capacitor is in order of thousand micro farads, which causes the system to respond slowly. Thus, the proportional feedback control has been selected for this study.

The proportional controller reacts very rapidly to a change of command or disturbance, in order to reach a steady state. However, there is always an offset error. For our system, we can use a proportional controller and increase the gain until the steady state error is decreased to the value desired. However, we must compromise between the distortion of

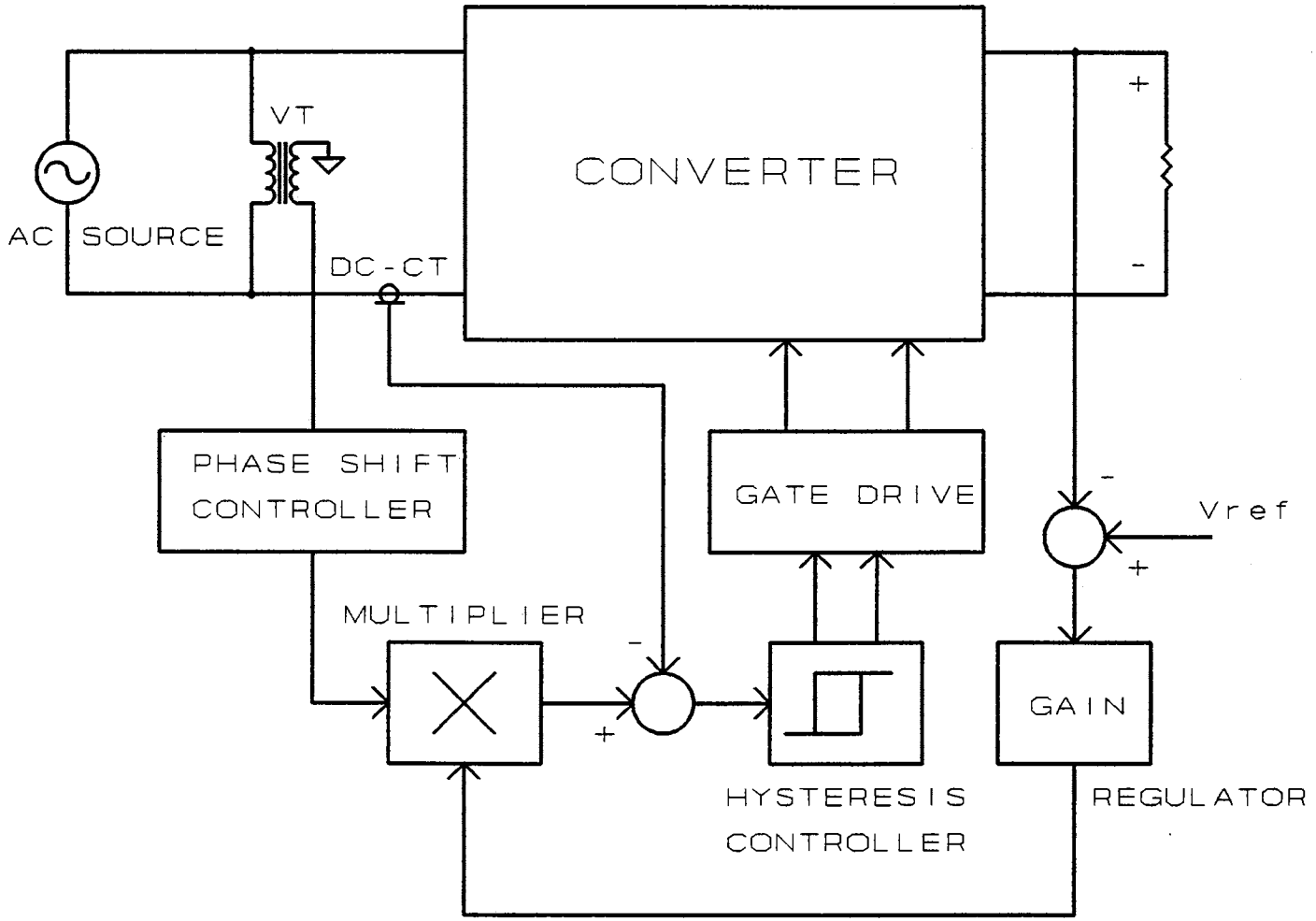

Figure 49 Block diagram of the closed-loop feedback control

the input current waveform and the response time of the system.

The gain influences the input waveform, as shown in Figures 50 to 53. In Figure 50, we adjust the gain to equal 3. Both the positive and negative cycles are approximately the same crests. In contrast, the positive crest becomes larger than the negative crest when the gain equals 6 as shown in Figure 51.

The input current waveform becomes more distorted as the gain increases as shown in Figures 52 and 53.

Three Phase System

For a three phase system, since each phase of an ac-dc converter can be operated independently, three single phase converters can be used with a common dc output. A three phase system configuration is shown in Figure 54. Input current waveforms are shown in Figure 55.

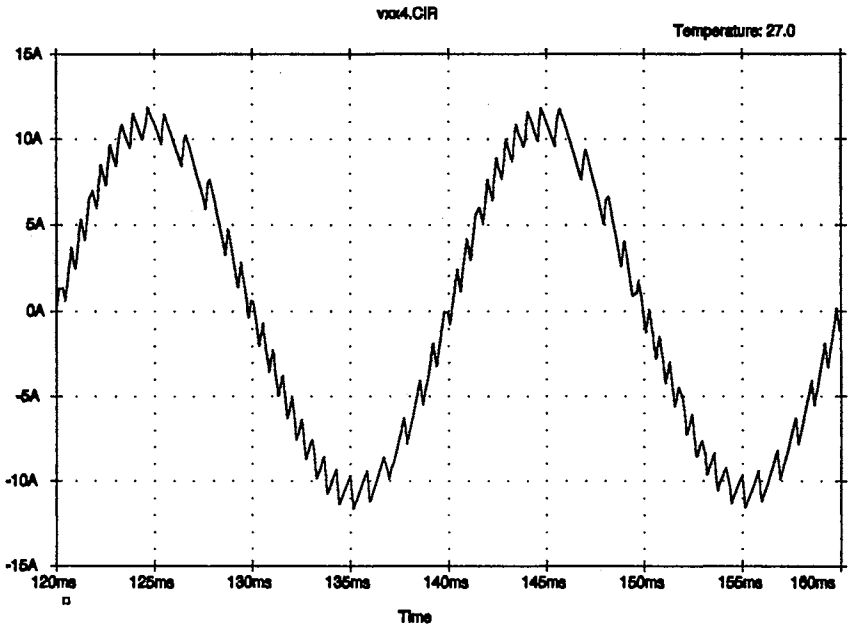

Figure 50 An input current waveform with the feedback gain = 3

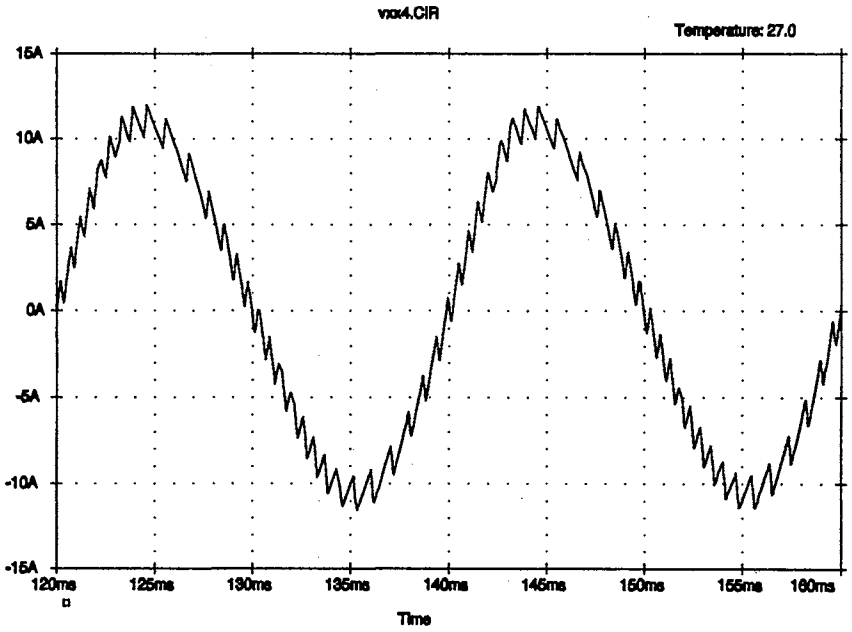

Figure 51 An input current waveform with the feedback gain = 6

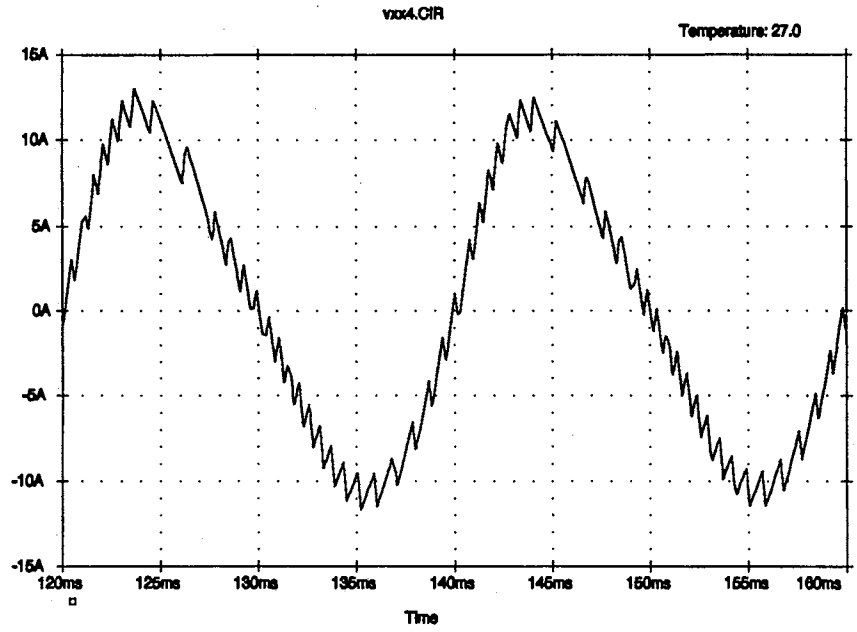

Figure 52 An input current waveform with the feedback gain =12

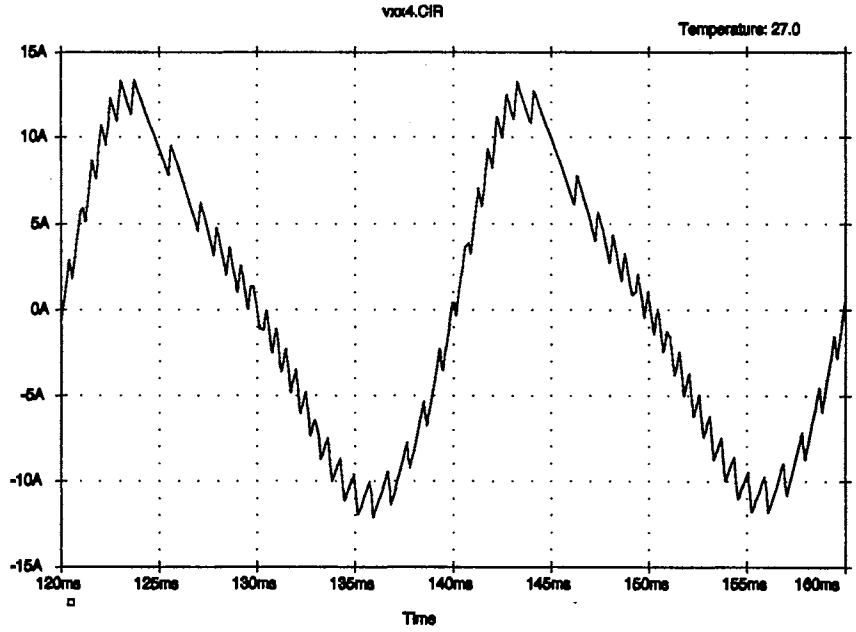

Figure 53 An input current waveform with the feedback gain =18

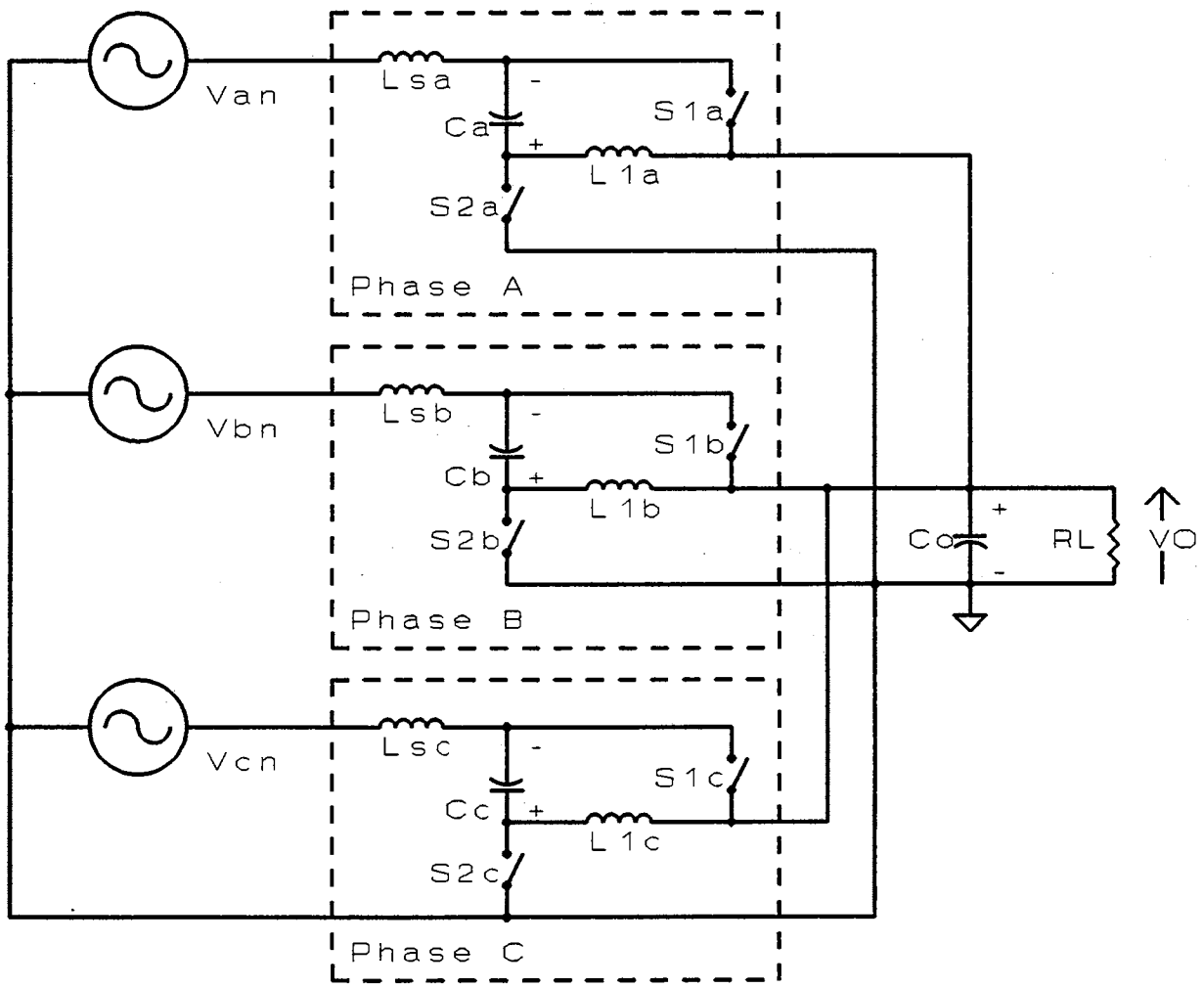

Figure 54 A three phase system configuration

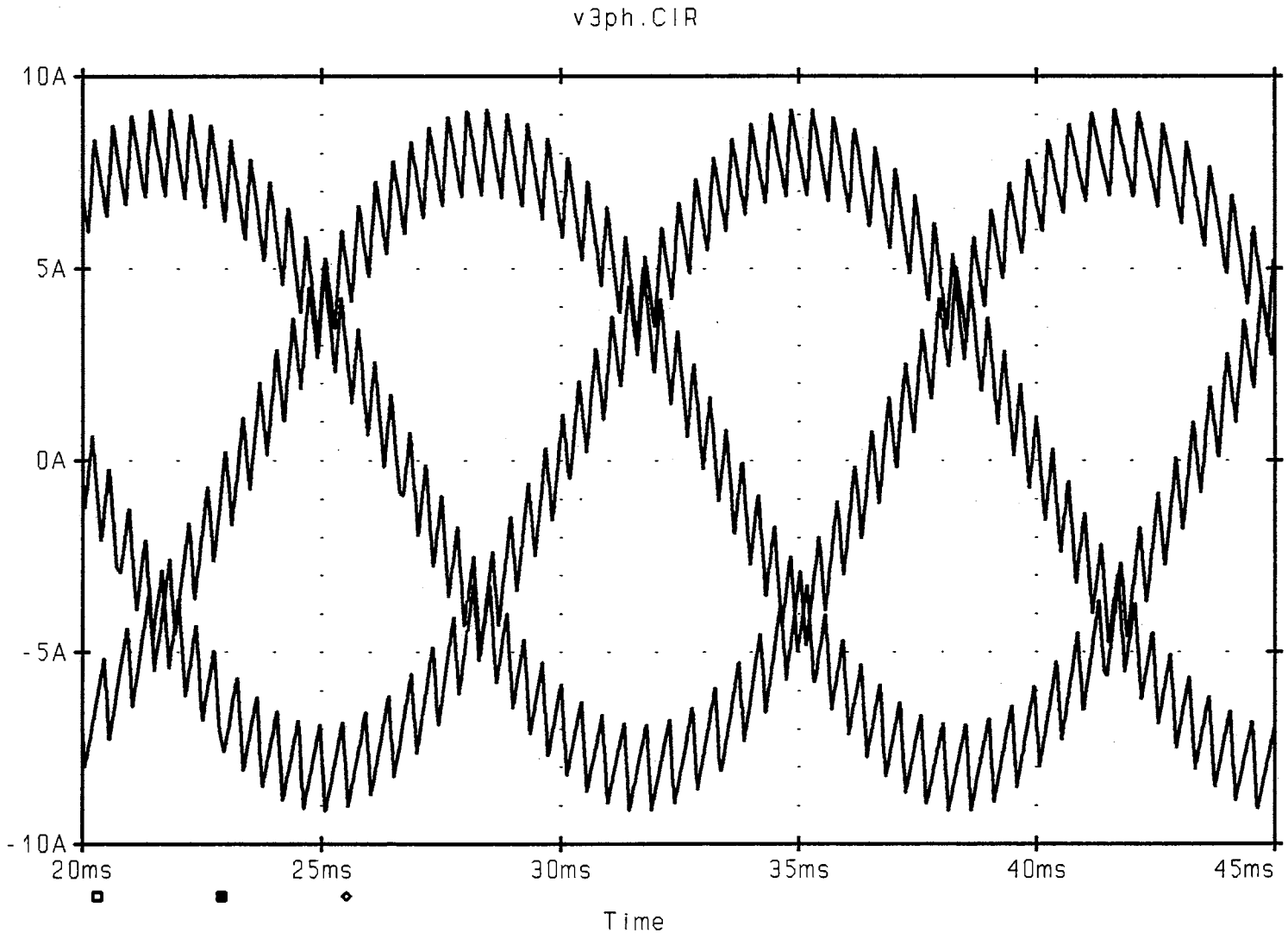

Figure 55 Input current waveforms of a three phase system

CHAPTER VII

APPLICATIONS

Converter Performances

Some applications for the converter presented in this thesis are discussed in this chapter. It provides low harmonic input currents and an adjustable power factor. Moreover, two remarkable characteristics of the converter are a controllable dc output voltage and a bidirectional power flow capability. One of the applications is to replace a diode bridge rectifier circuit in an adjustable ac speed drive. Also, a static var compensator with distortion compensation and an uninterruptible power supply can be developed from the converter.

An Adjustable AC Speed Drive

Replacing the diode bridge rectifier circuit in an adjustable ac speed drive with the converter can bring about three improvements, extremely low harmonic input currents, increased output voltage of the inverter, and regenerative braking capability.

A conventional adjustable ac speed drive is shown in Figure 56. The

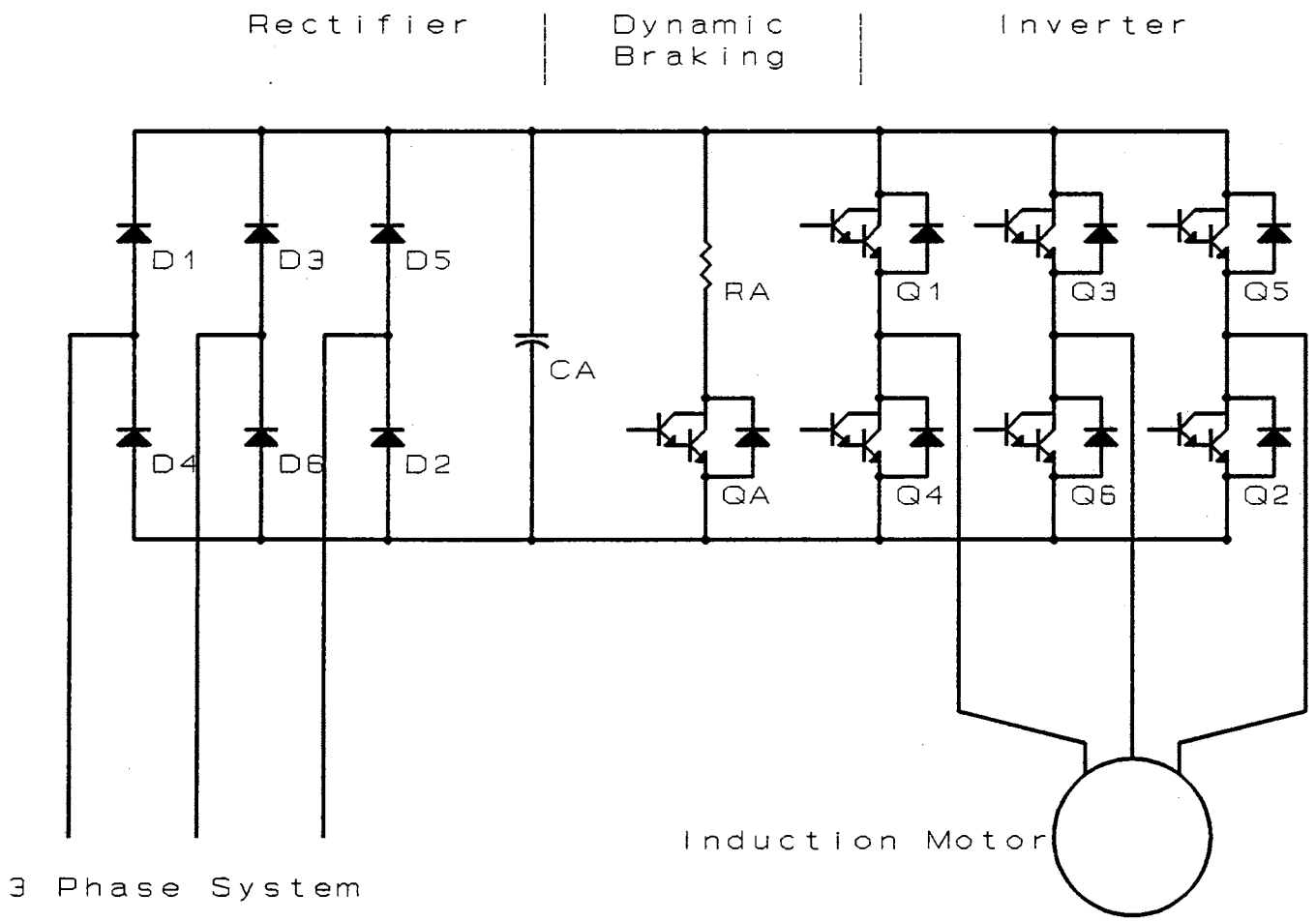

Figure 56 An adjustable ac speed drive circuit diagram

ac to dc conversion from line voltages employs a diode bridge rectifier. The nonlinear input impedance of the diode bridge rectifier causes nonsinusoidal input currents. By replacing the diode bridge rectifier with the converter, the performance characteristics are likely to improve dramatically because not only are the current waveforms substantially sinusoidal, but also the converter is capable of working at a unity power factor.

In a pulse width modulation (PWM) inverter, the encoding is done by admitting two inputs: a triangular carrier signal and a modulating signal. The switching intervals determine that the pulse widths are based on the intersections of the triangular and modulating signals as shown in Figure 57.

A PWM inverter, using sinusoidal modulation, cannot supply a sufficient voltage to enable a standard motor to operate at rated power and rated speed (Houldsworth, 1984). The dc supply for an inverter is usually obtained by rectifying a three phase supply. Let the line-to-line voltage of this supply be V_{in}. The dc link voltage will be approximately equal to the peak voltage of the three phase supply. Therefore,

$$V_{dc} = \sqrt{2}\, V_{in} \tag{7-1}$$

The peak-to-peak output voltage for each phase of the PWM inverter is equal to the dc link voltage. Thus, the RMS output voltage of each phase is given by

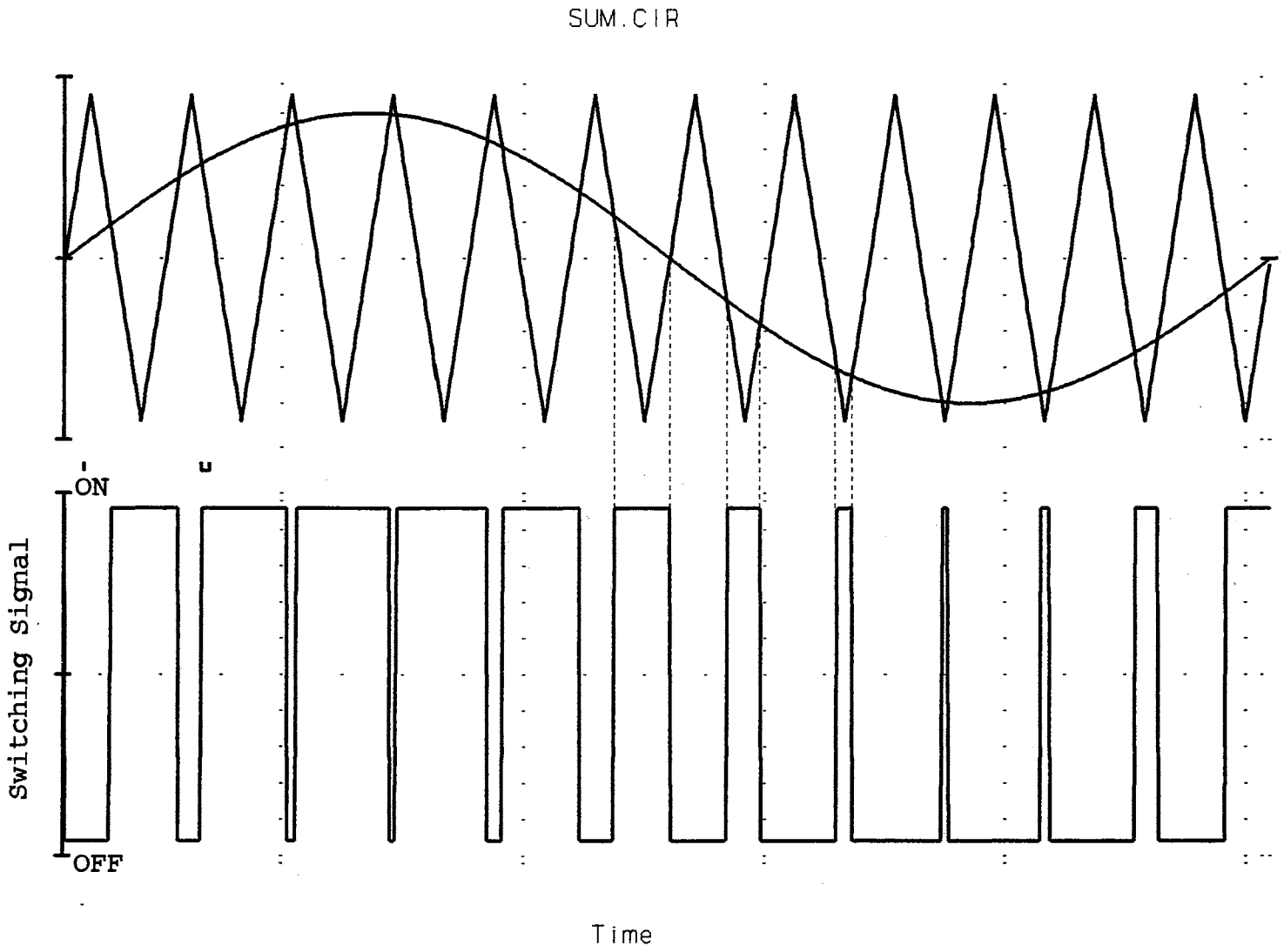

Figure 57 Sinusoidal pulse width modulation

$$V_{out\ (phase)} = \frac{V_{dc}}{2} \cdot \frac{1}{\sqrt{2}} \tag{7-2}$$

Substituting from (7-1), we obtain

$$V_{out\ (phase)} = \frac{\sqrt{2}\ V_{in}}{2} \cdot \frac{1}{\sqrt{2}} = \frac{V_{in}}{2} \tag{7-3}$$

The line-to-line output voltage is therefore given by

$$V_{out} = \sqrt{3}\ \frac{V_{in}}{2} = 0.866\ V_{in} \tag{7-4}$$

As the result, it can be seen that an inverter, which operates from a supply of standard voltage and driving a standard voltage motor, can maintain the correct relationship between output voltage and output frequency only up to 0.866 of the supply frequency (e.g., 52 Hz for 60 Hz mains, and 43 Hz for 50 Hz mains).

However, the fundamental output voltage can be increased beyond the linear range by overmodulation, but this produces distortion of the output waveform. By replacing the diode bridge rectifier with the converter, the dc link voltage can be higher than the peak input voltage. Therefore, the correct relationship between output voltage and the output frequency can maintain up to the base speed of the motor.

Furthermore, in adjustable speed ac drives, the machines may be subjected to electrical braking for reduction of speed. In electrical braking,

the motor is operated as a generator and the kinetic energy stored in the system inertia is converted to electrical energy. For a dynamic braking, the energy is dissipated in a resistor. The loss in the resistor is significant in a middle to large size inverter. However, with the bidirectional power flow capability of the converter the energy can be recovered in the power supply.

Solid-State Var Compensator with Distortion Compensation

The proposed scheme can compensate for a displacement power factor. It can also provide either leading or lagging reactive power. The

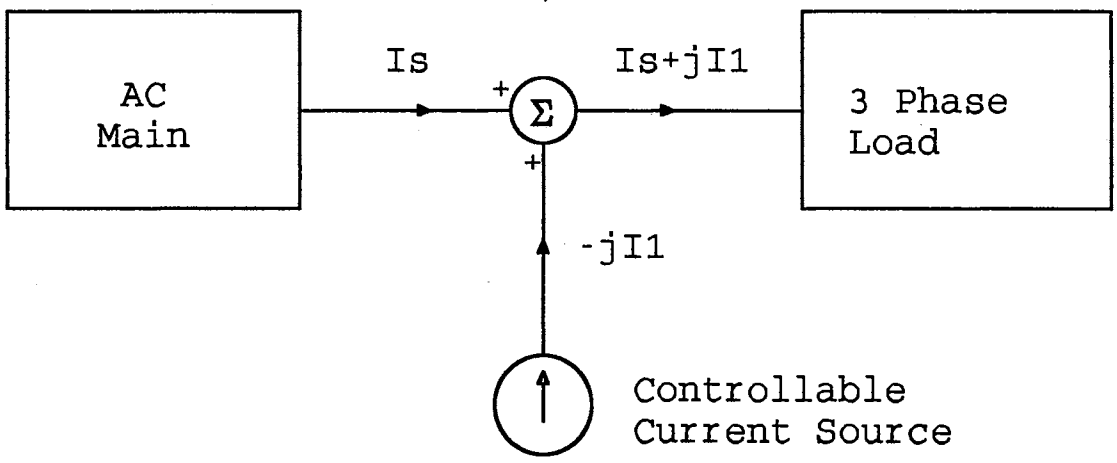

Figure 58 Principle of reactive current compensation

reactive power compensator can be explained by considering a controllable current source connected in parallel with the load as shown in Figure 58. The controllable current source generates a sinusoidal current, leading or lagging by 90 degrees with respect to the corresponding source voltage. This implies that reactive power flows bilaterally, going from the controllable current source to the ac system for leading 90 degrees, and vice-versa for lagging 90 degrees. The amount of reactive power generated or absorbed is controlled by adjusting the amplitude of the current. However, the current must be made to lag or lead the voltage by an angle approximately equal to 90 degrees because of losses in the converter.

Moreover, the converter has a capability to correct network distortion by injecting equal but opposite distortion at carefully selected points in a network. The distorted current waveform flowing through the system impedances creates a distorted voltage waveform, affecting the performance of other equipment connected to the same system bus. A nonsinusoidal voltage waveform at a bus can be corrected to a sinusoid by injecting the proper current magnitude and waveform.

Uninterruptible Power Supply (UPS)

For very critical loads, uninterruptible power supplies (UPS) are used so that the power flow to the load is uninterrupted even in the event of a power outage. With an on-line system, the load is continuously served

from the UPS. The configuration for the on-line system employs back to back connection of the converters as shown in Figure 59 (a). However, with an off-line UPS, which is the load connected directly to the utility supply, one converter is required as shown in Figure 59 (b).

For the UPS function, the converter is controlled to operate as a voltage source, since the reference signal is generated for the output voltage. The simulated output voltage waveform for the UPS is shown in Figure 60.

Summary

In this chapter, some applications are introduced. The new ac-dc converter can be employed in an adjustable ac speed drive to improve its performance. By operating as a current source, the converter can perform as a static var compensator with distortion compensation. Moreover, with a voltage source operation, the converter can be used in an uninterruptible power supply.

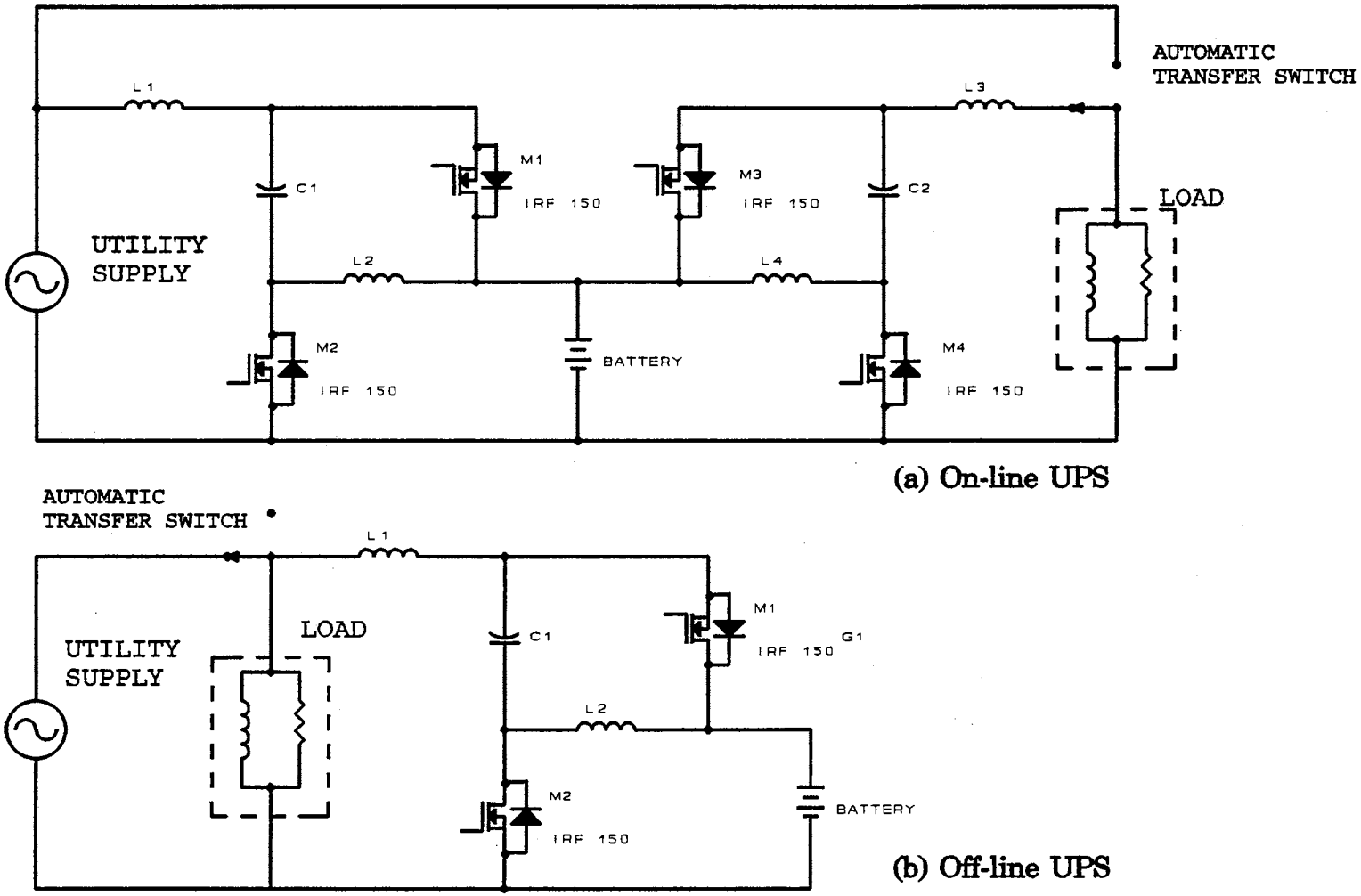

Figure 59 On-line and off-line UPS configurations

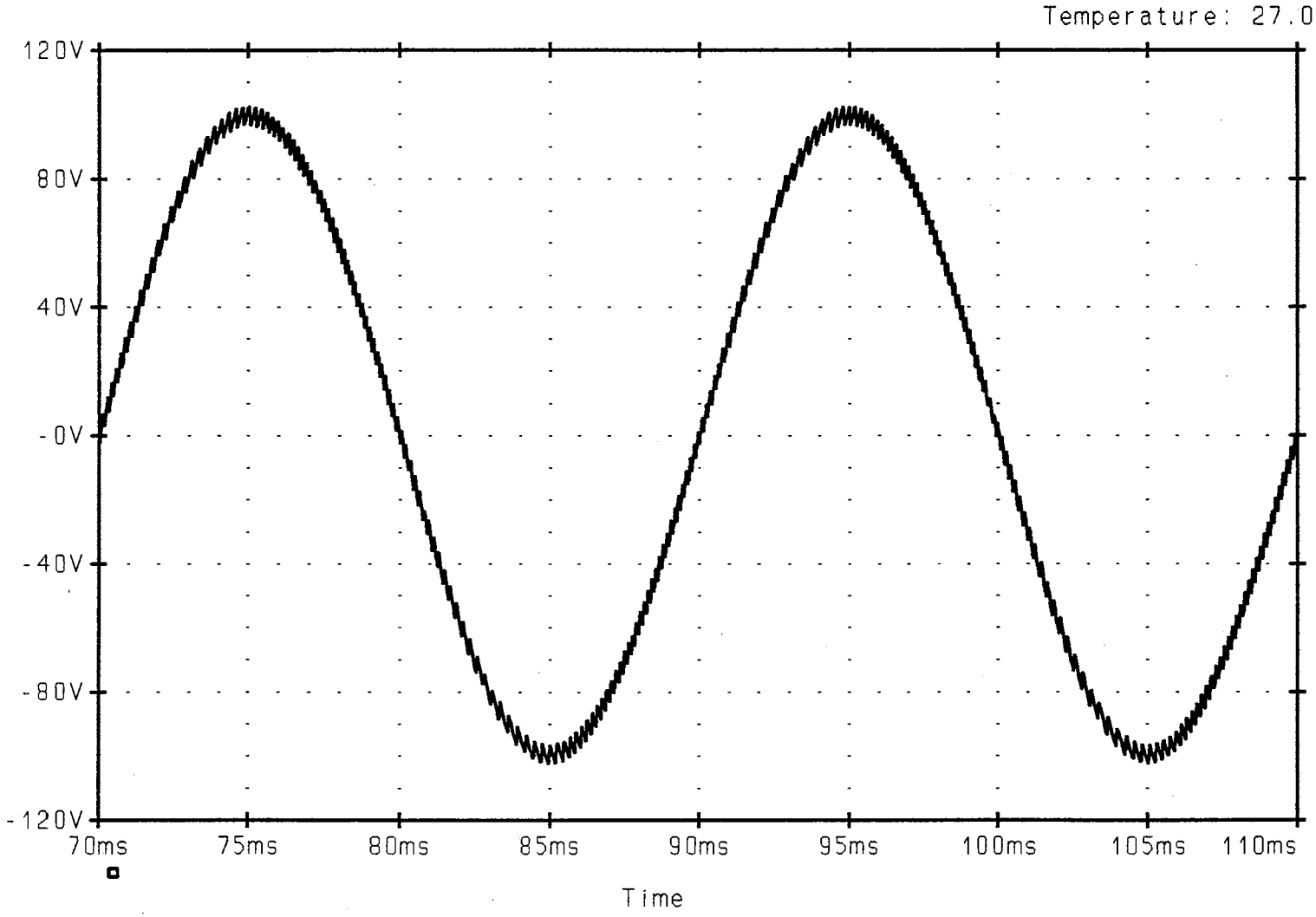

Figure 60 The output voltage waveform from the uninterruptible power supply

CHAPTER VIII

SUMMARY AND CONCLUSIONS

Conclusions

In recent years, the levels of harmonic distortions of the voltage and current waveforms in power systems have steadily increased. A large number of harmonic contents are generated by power electronic equipment. In most power electronic equipment, the power input is in the form of a sinusoidal waveform from the power line. It is first converted to a dc voltage by using a rectifier with a filter capacitor. It changes the sinusoidal nature of the ac power current resulting in the flow of harmonic currents in the system. The harmonics generated by power electronic equipment have been reaching levels that interfere with other power distribution network. Harmonics can be the cause of many undesirable effects. For example, eddy currents and hysteresis losses in iron cores of transformers and motors are increased so that their efficiencies are decreased and may even fail due to additional heat. Power factor correction capacitors may overload and fail because of increasing dielectric losses. Moreover, measuring instruments tend generally to read higher by several percents. Various international

standards and recommended practices are issued to limit on harmonic current injection to maintain a good power line quality.

Ac-dc converters with passive input filters frequently represent a substantial part of their total cost, weight, and size. For this reason, improved types of the converters are constantly being sought. Ac-dc converters with low harmonic currents represent a new approach still in its infancy, about which little has been published. A new bidirectional ac-dc converter with low harmonic input current and an adjustable power factor has been presented in this dissertation.

The new bidirectional ac-dc converter was obtained from modifying a non-inverting buck boost. The duality theory was applied to get the new ac-dc converter. The new ac-dc converter allows a bidirectional power transfer capability. The converter can operate in either the rectifier mode or the inverter mode. Power factors can also be controlled in both modes.

The power circuit consists of two switches, two inductors, and two capacitors. Power MOSFETs are used as switches. They allow bidirectional flows of current while withstanding one voltage polarity in their blocking state. For the control circuit, a hysteresis band current control technique is used to cause the input current to track a reference waveform. A sinusoidal reference waveform with a proper magnitude is compared to the actual input current to generate commands for the switches. Since we directly control the input current, the proper magnitude of the reference signal is

determined by a closed-loop control.

A state space averaging technique was used to develop a mathematical model for the system. The given terminal currents and voltage were substituted in the converter time varying equation to determine the currents and voltages of the converter energy storage elements.

A digital computer simulation was used to examine and verify the operation of the converter. Two different software packages were used. PSPICE was used to analyze the converter circuit. Power transfer modes were carefully examined. Various simulations were scrutinized in both the rectifier mode and the inverter mode. The results of the study indicate both the rectifier mode and the inverter mode are very easy to control. Moreover, the converter configuration allows us to control the power factor in both modes. MATLAB was used to simulate the converter from a mathematical model. The results from both methods were presented and compared.

The study shows that the open-loop converter has good stability. Closed-loop control with proportional controller was applied to determine the proper magnitude of the input current and to improve the response of the open-loop system.

Suggestions for Future Work

The significant loss in the converter discussed in this thesis is the switching loss. The switches are subjected to high switching stress and high switching power loss that increases linearly with the switching frequency. To overcome these problems, the concept of resonant switches can be applied to the converter.

A resonant switch represents a sub-circuit consisting of a semiconductor switch, an inductor, and a capacitor. The inductor and the capacitor constitute a resonant circuit whose oscillation is initiated by the turn-on of the switch. The resonant circuit is used to shape the current waveform through the switch.

Hence, further work can be done by applying the resonant switch concept to the converter.

REFERENCES

Arrillaga, J., Bradley, D. A., and Bodger, P.S. 1985. *Power system harmonics.* New York: John Wiley & Son.

Biswas, S. K., Bask, B., and Swamy, M. M. 1991. A Three-phase half-controlled rectifier with pulse width modulation. *IEEE Transactions on Industrial Electronics.* 38: 121-5.

Bose, B. K. *Power electronics and ac drives.* 1986. Englewood Cliffs. New Jersey: Prentice-Hall.

Brogan, W. L. 1991. *Modern control theory.* Englewood Cliffs, New Jersey: Prentice Hall

Carter, G. W., and Richardson, A. 1972. *Techniques of circuit analysis.* London: Cambridge University Press.

Chen, C. 1970. *Introduction to Linear System Theory.* New York: Holt, Rinehart and Winston, Inc.

Cameron, M. M. 1993 Trends in power factor correction with harmonic filtering. *IEEE Transactions on Industry Applications.* 29: 60-65.

Connelly, J. A., and Choi, P. 1992 *Macromodeling with SPICE.* Englewood Cliffs, New Jersey: Prentice Hall.

Dewan, S. B., and Straughen, A. 1975. Power semiconductor circuits. New York: John Wiley & Sons.

Dai, S., Lujara, N., and Ooi, B. 1992. A unity power factor current-regulated SPWM rectifier with a notch feedback for stabilization and active filtering. *IEEE Transactions on Power Electronics*. 7: 356-63.

Domijan, J. A., and Embriz-Santander, E. 1992. A summary and evaluation of recent developments on harmonic mitigation techniques useful to adjustable speed drives. *IEEE Transactions on Energy Conversion*. 7: 64-71.

Duffey, C. K., and Stratford, R. P. 1989. Update of harmonic standard IEEE-519: IEEE recommended practices and requirements for harmonic control in electric power systems. *IEEE Transactions on Industry Applications*. 25: 1025-34.

Fröhr, F., and Orttenburger, F. 1982. *Introduction to electronic control engineering*. London: Heyden & Son Ltd.

Houldsworth, J. A., and Grant, D. A. 1984. The use of harmonic distortion to increase the output voltage of a three phase PWM inverter. *IEEE Transactions on Industry Applications*. IA-20: 1224-1227.

IEEE Working Group on Power System Harmonics. 1983. Power system harmonics: an overview. *IEEE Transactions on Power Apparatus and Systems*. PAS-102: 2455-9.

Itoh, R., and Ishizaka, K. 1991. Three-phase flyback ac-dc converter with sinusoidal supply currents. *IEE Proceeding-B.* 138: 143-51.

_____ , Steady-state and transient characteristics of a single-way step-down PWM GTO voltage-source converter with sinusoidal supply current. *IEE Proceedings-B.* 136: 168- 74.

Kataoka, T., Mizumachi, K., and Miyairi, S. 1977. In *IEEE/IAS International Semiconductor Power Converter Conference.* pp.334-9 New York: Institute of Electrical and Electronics Engineers, Inc.

Kazerani, M., Ziogas, P. D., and Joos, G. 1991 A novel active current waveshaping technique for solid-state input power factor conditioners. *IEEE Transactions on Industrial Electronics.* 38: 72-8.

Kimbark, E. W. 1971. *Direct current transmission.* New York: John Wiley & Son.

Liaw, C.M., Chen, T. H., Wang, T. C., Cho, G. J., Lee, C. M., and Wang, C. T. 1991. Design and implementation of a single phase current-forced switching mode bilateral convertor. *IEE Proceeding-B.* 138: 129-36.

Mechi, A., and Funabiki, S. 1993 Step-up/down voltage PWM ac to dc convertor with one switching device. *IEE Proceedings-B* 140: 35-43.

Middlebrook, R. D., and Cuk, S. 1976. A general unified approach to modeling switching converter power stages. In *IEEE Power Electronics Specialists Conference.* pp 18-31 New York: Institute of Electrical and Electronics Engineers, Inc.

Mitchell, D. M. 1988. *Dc-dc switching regulator analysis*. New York: McGraw-Hill Book Company.

Mohan, N., Undeland, T. M., and Robbins, W. 1989. *Power electronics: converter, applications, and design*. New York: John Wiley & Son.

Ooi, B. T., Dixon, J. W., Kulkarni, A. B., and Niishimoto, M. 1988 An integrated ac drive system using a controlled-current PWM rectifier/inverter link. *IEEE transactions on power electronics*. 3: 64-70.

Prasad., A. R., and Ziogas, P. D. 1991. An active power factor correction technique for three-phase diode rectifiers. *IEEE Transactions on Power Electronics*. 6: 83-92.

_____ , Manias, S., and Olivier, G. 1989 A high-frequency off-line SMR converter with improved performance characteristics. *IEEE Transactions on Industry Applications*. 25: 1167-75.

Sen, K. K., and Emanuel, A. E. 1984 Voltage distortion at mains supplying quasi sinusoidal current pulses. In *International Conference on Harmonics in Power System*. Worcester, Massachusetts: Worcester Polytechnic Institute.

Severns, R. P., and Bloom, G. 1985 *Modern dc-to-dc switchmode power converter circuits*. New York: Van Nostrand Reinhold Company Inc.

Shepherd, W., and Zakikhani, P. 1973. Power factor correction in nonsinusoidal systems by the use of capacitance. *J. Phys. D: Appl. Phys.* 6: 1850-60.

_____. 1972. Suggested definition of reactive power for nonsinusoidal systems. *Proceedings of the IEE.* 9: 1361-2.

Stihi, O., and Ooi, B. 1988 A single-phase controlled-current PWM rectifier. *IEEE Transactions on Power electronics.* 3:453-9.

Thorborg, K. 1988 *Power electronics.* Englewood Cliffs. New Jersey: Prentice-Hall

APPENDIX

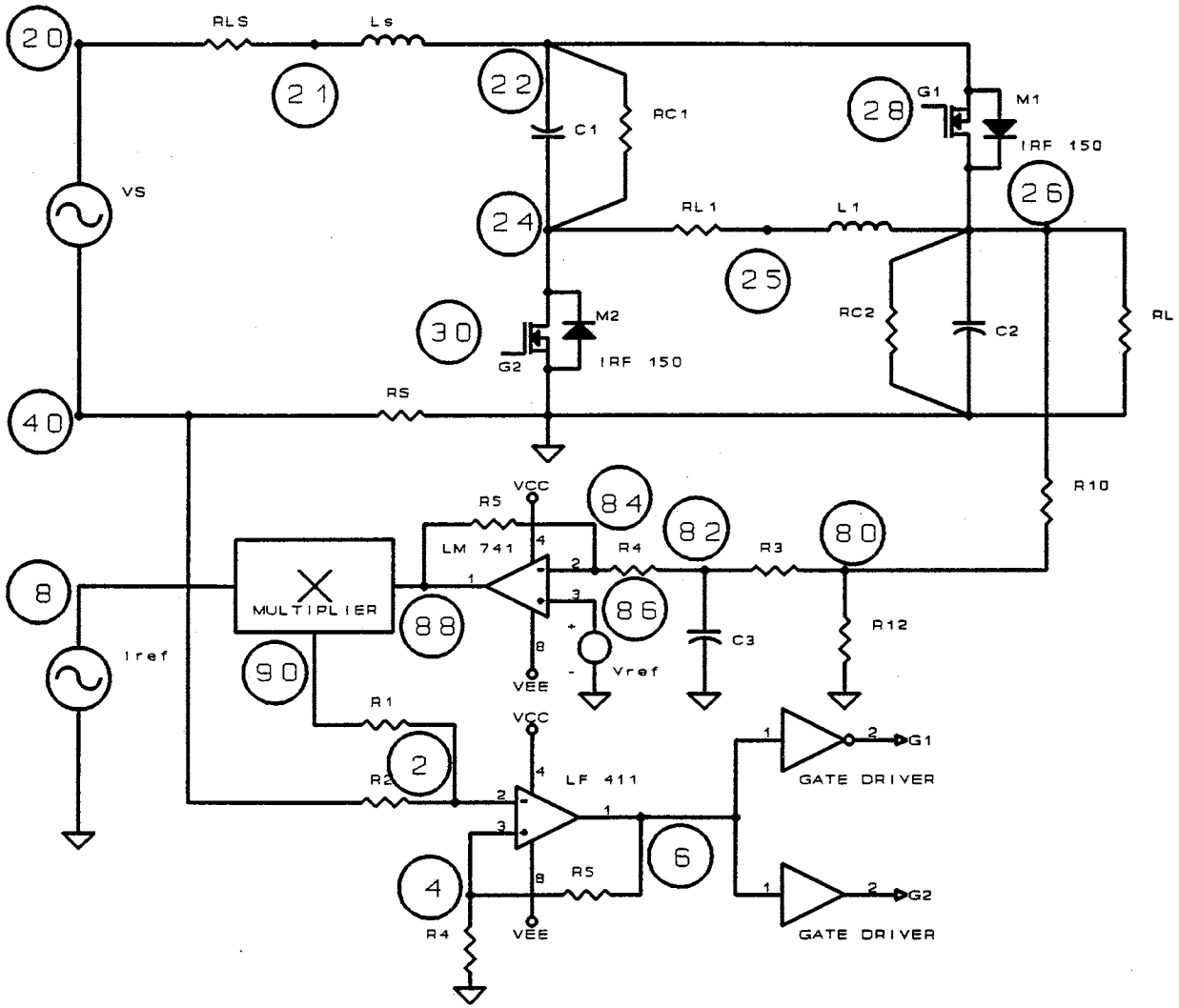

Circuit diagram used in PSPICE simulations

```
PSPICE INPUT FILE
vxx4.CIR
*****POWER CIRCUIT*****
V1    20    40    SIN(0 100 50)
LS    20    21    20MH
RLS   21    22    .125
C1    24    22    3000uF ic=169.45
RC1   24    22    50k
L1    24    25    150mH ic=1
RL1   25    26    .942
C2    26    0     3000uF ic=156.13
RC2   26    0     50k
RL    26    0     50
RS    0     40    .02
M1    24    30    0     0     IRF150
M2    26    28    22    22    IRF150

*****CONTROL CIRCUIT*****
X1    4     2     100   99    6     LF411
R1    90    2     1K
R2    10    2     1K
R3    6     0     10K
R4    4     0     100
R5    4     6     3k
R6    34    30    100
R7    30    0     1K
R8    32    28    100
R9    28    22    1K
VREF  8     0     SIN(0 1 50 0 0 180)
R10   8     0     10K
VCC   100   0     15
VEE   99    0     -15
E1    10    0     0     40    50
E2    32    22    6     0     -.8
E3    34    0     6     0      .8
```

```
*****REGULATOR*****
ER    80    0     26    0     .01
RER   80    0     1K
RR1   80    82    100
CR1   82    0     10uf  IC=1.59
RR2   82    84    1K
RR3   84    88    1.5K
RR4   88    0     10K
VR    86    0     1.6
XR    86    84    100   99    88    UA741
EM    90    0     POLY(2) 88 0 8 0 0 0 0 0 6.9

.LIB D:\PSPICE\LINEAR.LIB
.LIB D:\PSPICE\PWRMOS.LIB

.tran    40.000u  .36     .26     200.000u uic ; *ipsp*

.options itl5 = 0 digmntymx = 0 abstol = 10.000p
+    chgtol = 200.000f reltol = .01 vntol = 20.000u  ; *ipsp*

.probe   V(90)    V(88)    V(82)
+    V(24)    V(22)    V(26)    I(LS)    I(L1)    v(20)
+    I(C1)    I(C2)    ; *ipsp*

.END
```

MATLAB INPUT FILES

SMR.M

```
t0=0;
tf=1;
x0=[1 170 159]';                    % Initial conditions
[t,x]=ode23('vd2',t0,tf,x0, 1.e-4);
plot(t,x)
```

VD2.M

```
function xdot = vd2(t,x)
d1=.5+(0.3*sin(314*t));
d2=1-d1;
xdot(1) = 6.6*(d1.*x(2)-d2.*x(3));
xdot(2) = 333*(-d1.*x(1)-d2.*11.*sin(314*t));
xdot(3) = 333*(d2.*x(1)-.02*x(3)+d1.*11.*sin(314*t));
```

VITA

Veerapol Monyakul

Candidate for the degree of

Doctor of Philosophy

Dissertation: A NEW BIDIRECTIONAL AC-DC CONVERTER WITH LOW HARMONIC INPUT CURRENTS AND AN ADJUSTABLE POWER FACTOR

Major Field: Electrical Engineering

Biographical:

Personal Date: Born in Ubon Ratchatani, Thailand, August 29, 1958, the son of Pravet and Patra Monyakul.

Education: Graduated from Assumption College, Lampang, Thailand, in 1976; received Bachelor of Science from King Mongkut's Institute of technology and Master of Engineering from Kasetsart University, bangkok, Thailand, in 1982 and 1986 respectively; completed requirements for the Doctor of Philosophy at Oklahoma State University in December 1993.

Professional Experiences: Electrical engineer, Castral (Thailand) Co., Ltd., 1982-1986. Head of Department of Electrical Engineering, South-east Asia College, 1986-1988. Managing Director, Novem Power Electronics Co., Ltd., 1988-1990